1-1-1980

Processes in the wall region of a turbulent boundary layer.

Steven Paul Metzler

PROCESSES IN THE WALL REGION OF A TURBULENT BOUNDARY LAYER

by

Steven Paul Metzler

A Thesis

Presented to the Graduate Committee

of Lehigh University

in Candidacy for the Degree of

Master of Science

in

Mechanical Engineering

Lehigh University

1980

This thesis is accepted and approved in partial fulfillment of the requirements for the degree of Master of Science.

10 December 1980
date

Professor in Charge

Chairman of Department

ACKNOWLEDGEMENTS

The author would like to express his thanks to Professor C. R. Smith, Mechanical Engineering Department, Lehigh University, for his many original and helpful thoughts and for his guidance during the experimental work.

Appreciated also is the assistance of coworkers S. P. Schwartz and A. W. Cerra in the conducting of experiments and the taking of data.

Much thanks to Ms. Beverly Diehl for her work in the preparation of the typed manuscript.

Lastly, the patience and support of my wife, Karen, is gratefully acknowledged.

This work was performed under Air Force Contract Number E49620-78-C-0071, Air Force Office of Scientific Research.

TABLE OF CONTENTS

	Page
List of Tables	vi
List of Figures	vii
Abstract	1
Chapter I. Introduction	3
A. Need for Investigation	3
B. Turbulent Boundary Layer Regions	4
C. Overview of Turbulence Structure	5
D. Experimental Areas of Present Investigation	20
Chapter II. Experimental Apparatus	23
A. Flow Facility	23
1. Inlet System	23
2. Channel	26
3. Outlet Tank	26
4. Maintenance of Water Quality	27
B. Moving Reference Platform	27
C. Video Equipment	28
D. Flow Visualization Apparatus	29
E. Hot-Film Anemometry Equipment	31
Chapter III. Results and Discussion	33
A. Mean Streak Spacing	33
B. Spatial Distributions of Streak Spacing	40
C. Split-Screen Side/Plan Views of a Horizontal Bubble-Wire	50
D. Boundary Layer Manipulation	66
CHAPTER IV. Model and Conclusions	75
LIST OF REFERENCES	79
APPENDICES	83
A. Anemometry Results and Operating Procedure	83

B. Calculations of the Mean Wall Shear Stress 89
C. Construction of Hydrogen Bubble-Wire Probe 92
D. Uncertainty Analysis 97
E. Vita 101

LIST OF TABLES

Table		Page
3.1	Mean Streak Spacing and Flow Parameters	36
A.1	Flow Conditions and Obtained Boundary Layer Parameters for Two Experimental Flows	83

LIST OF FIGURES

Figure		Page
1.1	Orientation of coordinate system and classification of turbulent boundary layer regions	4
1.2	End-on view of proposed mechanism of streak perpetuation	8
1.3	Correlation of inflows and outflows with stretching and compression of wall vorticity	9
1.4	Shedding regions behind a sphere in uniform flow	15
1.5	Wake downstream of a hemisphere and analogous boundary layer structure	16
2.1	Schematic and cross-sectional views of channel	24
2.2	Two-dimensionality of flow in channel	25
2.3	Float for displacement/time measurement of velocity	32
3.1	Transparency used for marking streak locations	34
3.2	Graph of λ^+ vs Re_δ	38
3.3	Histograms of nondimensionalized streak spacing	41
3.4	Graph of λ^+ vs y^+	44
3.5	Intermittency of low speed streaks	45
3.6	Streak merging sequence	47
3.7	Streaks visualized by 125 μm glass beads and bubble wire	64
3.8	Diagram of split-screen views on video screen	50
3.9	Streak deformation occurring with passage of loop vortex	60
3.10	Combined side/plan view of loop vortices	53
3.11	Sketch of loop vortex	52

Figure		Page
3.12	"Wavy mode" of streak oscillation	55
3.13	"Branching" behavior of low speed zones	60
3.14	Velocity defect downstream of hemisphere	58
3.15	Convecting loop clearing out bubble-free region	61
3.16	Sketch of convecting loop	62
3.17	Lateral flows due to low speed streaks	64
3.18	End-on view of streak streamlines	65
3.19	Axial vorticity and spanwise variations in velocity in a thin shear flow	68
3.20	Streaks downstream of rods	70
3.21	Histogram of nondimensionalized streak spacing over rods	69
3.22	Streaks downstream of rods	70
3.23	Loop vortex ejection over rods	70
A.1	Logarithmic profile and cross-plot	86
A.2	Logarithmic profile and cross-plot	87
A.3	Profiles nondimensionalized on freestream velocity and boundary layer thickness	88
A.4	Turbulence intensity profile	89
A.5	Bubble-wire probe construction	96
A.6	Bubble-wire probe construction	97
A.7	Bubble-wire probe construction	98
A.8	Bubble-wire probe construction	99

ABSTRACT

Close examination of the behavior occurring in the wall region of a turbulent boundary layer enables the clarification of some structural aspects. Characteristics of the alternating pattern of slow speed regions close to the wall known as the streaky structure are investigated by several approaches. Measurements of the mean transverse spacing of this structure over a wide range of Reynolds numbers show that within the uncertainty of the data the spacing may be a weakly increasing function of Reynolds number at best. Spatial distributions (histograms) of the spacing between low speed streaks are presented that detail streak behavior throughout the wall layers.

Detailed observation of the bursting event is accomplished through an approach incorporating dual orthogonal views (side and plan) of the near-wall region, as visualized by the hydrogen bubble method. Ejections of fluid from the wall are observed to originate from low speed streaks in the form of loop-like vortical structures with a horseshoe configuration. Discrete arrays of typically three to five closely spaced vortex loops are observed to appear at a frequency commensurate with that experimentally established for the bursting cycle. Several such arrays of loops, or "bursts" may be shed from a given low speed streak; this event does not result in the destruction of the streak, but acts rather to perpetuate it by a downstream lengthening that occurs as a manifestation of the axial vorticity contained in the legs of the periodically shed loops. Additional

experimental results are presented which substantiate and support a wake-type interpretation of wall layer behavior.

Also presented is a method based on the above concept of wall layer flow that offers a potential means for the manipulation of boundary layer characteristics. The method employs an arrangement of longitudinal surface elements, uniformly spaced in the spanwise direction, to effect an alteration of the natural spacing between low speed streaks.

CHAPTER I

INTRODUCTION

I.A. GENERAL

Since a degree of turbulence is inherent to almost any real flow, the accurate prediction of turbulent flows is a fundamental concern of fluid mechanics. Many turbulent flows of practical interest are bounded by a solid surface that acts as a source of shear; within this category the simplest possible case is that of a turbulent boundary layer on a flat plate. Because the present physical understanding of the underlying processes responsible for the preservation of a turbulent boundary layer is limited for even this simple case, state-of-the-art prediction techniques rely on a minimum of physical insight and are based upon time-averaged empirical correlations. This approach tends to ignore the actual kinematics and dynamics of a given flow situation, and accuracy and flexibility suffer as a consequence. Thus, a primary goal of present turbulence research is to develop predictive methods of a more deterministic nature that can be effectively extended for a variety of flow situations. Obviously, the success of such approaches is strongly dependent upon how closely they model the governing mechanisms of the flow. The present study seeks to enlarge upon our understanding of the processes by which a turbulent boundary layer sustains itself.

The defining feature of a turbulent flow is the presence of fluctuations in the flow properties. A turbulent boundary layer is characterized by fluctuations that occur normal to the mean flow, attaining their highest intensity immediately adjacent to the surface upon which the boundary layer has formed (wall). The resulting exchange within the

boundary layer of fluid from regions of differing streamwise momentum gives rise to higher (compared to the laminar case) velocities near the wall and a larger mean wall shear stress, and increased heat and mass transfer. This behavior strongly influences the design and performance of many engineered systems; hence the demand for accurate prediction methods.

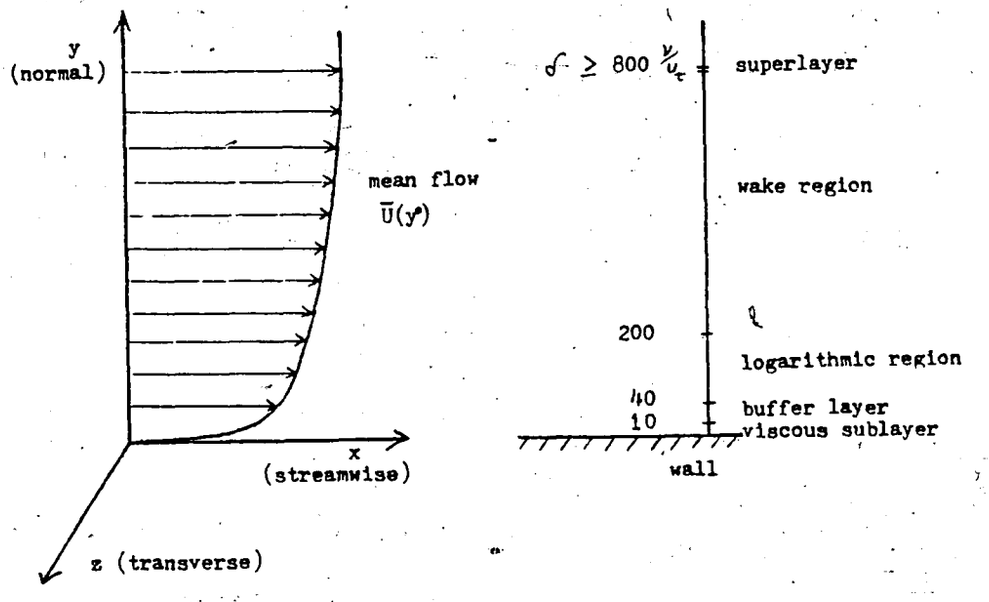

Figure 1.1 Orientation of Coordinate System and Classification of Regions Within a Turbulent Boundary Layer.

I.B. TURBULENT BOUNDARY LAYER REGIONS

A brief digression is now made to identify the conventionally defined regions within the boundary layer. From the wall out to $y^+=8$ - 12*, the mean velocity varies linearly with distance from the wall. Within this "linear sublayer" the mean shear stress is constant and at a maximum.

*A distance nondimensionalized on inner variables may be defined: $y^+ = \frac{yu_\tau}{\nu}$ where $u_\tau=\sqrt{\tau_w/\rho}$. The quantity ν/u_τ corresponds to the scale of the smallest (dissipative) fluctuations.

Within the logarithnic region, approximately $40 \leq y+ \leq 200$, the mean velocity varies as the logarithm of the distance from the wall. These two regions and the transitional buffer layer joining them comprise the "wall layer," where most turbulent mixing takes place. The outer, or wake, region occupies the greater part of the boundary layer. This region is marked by large vortical structures, which at the edge of the boundary layer are evidenced as "bulges" of rotational fluid that protrude out into the potential flow. The resulting intermittency of this interface (termed the superlayer) makes an exact boundary layer thickness hard to define. Adopting the convention $y=\delta$ for $u/U_\infty = .99$, a boundary layer thickness in the time averaged sense of $y^+ \simeq 800$ for $Re_x < 10^6$ may be deduced from empirical correlations. For larger Reynolds numbers δ becomes larger due to turbulent diffusion of low velocity fluid outwards.

The regions or layers just described were originally identified* from time-averaged measurements; however, the subsequent development of improved flow visualization techniques has made it possible to show that instantaneous behavior within these regions may also be differentiated. Lines of demarcation between the zones cannot be drawn too sharply, but close visual inspection reveals characteristic patterns within the flow that change with distance from the wall.

I.C. REVIEW OF TURBULENCE STRUCTURE OF BOUNDARY LAYERS

The identification of characteristic, recurring flow patterns has encouraged investigation into the physical processes of turbulence; a

*Different zones are apparent when observing the changes in slope and deviations from the curve, of data plotted with the Law of the Wall: $u/u_\tau = 1/.41\ (\ln y^+) + 5.0$

phenomenon once regarded as hopelessly random. Evidence is accumulating to show that the fluctuations characteristic of boundary layer turbulence are generated by and appear to be a part of an observed cyclic behavior of the boundary layer structure. In some way not yet fully understood, a recurring sequence of events acts to create the high rate of momentum transfer that characterizes a turbulent boundary layer.

The following sections will discuss different physical features of the boundary layer structure as educed from visual observation, anemometry measurements, and, in some cases, analytical approaches. Most of the literature deals with zero pressure gradient flows; the discussion will generally refer to these flows unless otherwise indicated.

I.C.1 TURBULENT STREAKS

One of the first clues as to the existence of an ordered structure within a turbulent boundary layer was the discovery of an instantaneous spanwise velocity distribution consisting of alternating zones of high and low speed fluid which develops in the viscous sublayer and extends into the logarithmic region. Streamwise filaments of low speed fluid (streaks) with a fairly unfirom transverse spacing were observed in the near wall region by Beatty, Ferrell, and Richardson [11] in 1956. They flushed a turbulent pipe flow of colored water with clear fluid and watched as the dye was swept from the outer portions of the boundary layer, leaving only streamwise traces of dyed fluid close to the wall. This phenomenon was discovered concurrently by Hama [11], who noted that when dye was injected into the sublayer through a small slit cut into the wall, the marking agent became concentrated into narrow regions of low velocity.

Since then, the streaky structure has been recognized and examined in many investigations and under different experimental conditions. It displays a remarkable degree of persistence and regularity, and appears to constitute a universal feature of bounded shear flows.

Schraub and Kline [41] investigated boundary layers exposed to different pressure gradients and noted the presence of the "streaky" structure in all cases, even those in which relaminarization (due to a strongly favorable $\frac{\partial P}{\partial x}$) took place. The dominance of this phenomenon is illustrated by the laminar boundary layer undergoing transition, where one of the first nonuniformities to be observed is a spanwise, sinusoidal variation in the mean velocity which has the appearance of what seems to be a precursor of the streaky structure [17, 40, 21]. Even when disrupted, the streaky pattern quickly reestablishes itself. Its ubiquity has led Kline [22] to propose its presence as a sufficient condition for determining whether or not a given location within a flow is turbulent.

Various researchers have measured the physical characteristics of streak behavior, such as the mean transverse spacing, and its vertical and streamwise extent. For flows of moderate Reynolds number ($Re < 2000$), the mean spacing between slow speed streaks (λ^+) is generally accepted as being close to $\Delta z^+=100$. For more developed flows, a functional dependance upon Reynolds number may exist. Several researchers [16, 18] have measured substantially larger values for λ^+ at Re_θ as high as 10^4. Height and length of the structure is indicated from measurements performed by Blackwelder and Eckelmann [5] using a vertical rake of 10 hot-wire anemometers. They found connected regions of low axial velocity in the region $5 \leq y^+ \leq 100$ that persisted for times corresponding to a streamwise length scale of $300 \leq \Delta x^+ \leq 1000$.

The strength and coherence displayed by the streaky structure invites speculation as to the mechanism by which it originates. In a 1967 investigation, Bakewell and Lumley [2] concluded from hot film space-time correlations that a system of counter-rotating eddy pairs (ω_x) composes the dominant flow structure in the wall region, and that strong outflows of low speed fluid from the wall occur between the pairs. They also determined that the average transverse spacing of the vortex pairs coincided with accepted values for the streak spacing. Subsequent measurements by Blackwelder and Eckelmann [5] using hot film probes, but with a different configuration from Bakewell and Lumley, yielded similar results; that counter-rotating axial vortices of considerable streamwise extent appear to give rise to low speed streaks through the pumping action of each pair (Figure 1.2).

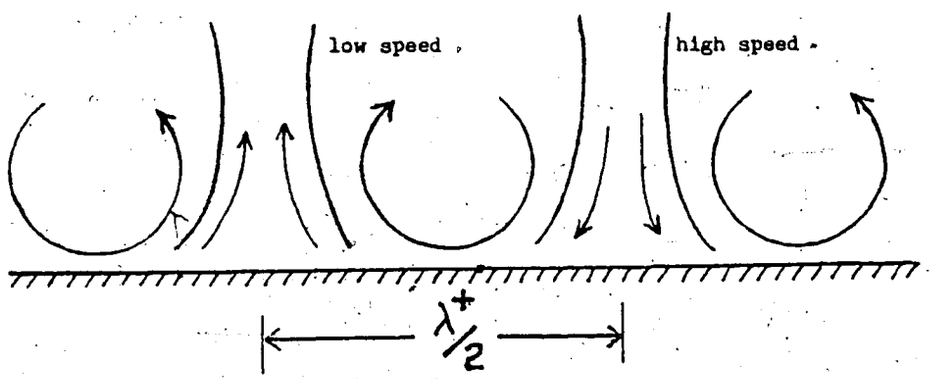

Figure 1.2 End-on View of Proposed Mechanism of Streak Formation; Vortices Act so as to "Pump" Fluid Away From the Wall.

Lighthill [29] discusses a process that can be construed as another possible means of streak generation. In a turbulent boundary layer, and especially in the wall region, there exists strong inflows and outflows of fluid (normal to the wall) coupled with a large mean strain rate. An inflow near the wall has the effect of stretching this vorticity, while

an outflow will compress it (Figure 1.3). Since the vorticity near the

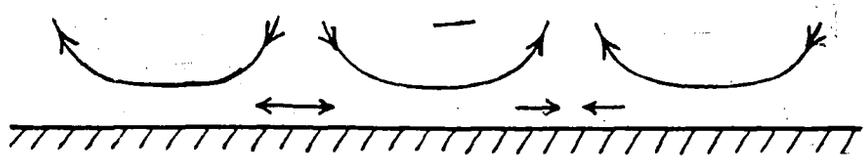

Figure 1.3 Correlation of Inflow With Stretching, and Outflow with Compression, of Wall Vorticity (End-on View).

wall is primarily $\frac{\partial u}{\partial y}$, the decrease in circulation caused by an outflow, for example, results in a smaller normal gradient of the streamwise velocity, and a region of low momentum fluid results. For an inflow the opposite effect occurs, causing a zone of high velocity fluid bounded by two low speed regions. The existence of such inflows has been observed by Falco [13], who in a smoke visualization study of outer layer structure noted the recurrent formation within the logarithmic region of "typical eddies" with a wallwards component of velocity. The transverse scale of these motions was $\Delta z^+ = 100$.

The reasoning involved in the mechanism just discussed is valid, but to the author at least there appears some doubt as to whether this interaction alone can account for the large streamwise extent of the streaky structure; this point will be treated further in Section III.

So far, only one predominant physical feature of turbulent boundary layers has been discussed - the alternating high and low momentum regions observed in the vicinity of the near wall. The following section deals with the processes of momentum transfer within the boundary layer, and the hypothesized interactions by which they occur.

I.C.2 THE BURSTING PROCESS

In 1956 an important series of investigations upon turbulent boundary layer structure was initiated at Stanford University. Although

a wealth of quantitative data was available for the mean flow properties of turbulent boundary layers, relatively little was known as to the time-dependent flow patterns which produced the mean quantities. From motion picture studies employing the newly developed hydrogen bubble technique combined with dye injection, S. J. Kline and his colleagues [25, 40, 41, 24, 21, 36] were able to develop hypotheses for a deterministic cycle of events occurring in the wall region. They confirmed the existence of the streaky structure, and showed that it was a fundamental component of the regularly recurring patterns which they observed. Also significant were two highly correlated fluid motions involving large displacements in the normal direction, which appeared responsible for most of the momentum transfer (and turbulence production) within the wall layers.

The observed cycle of events now known as the bursting sequence starts off with a slow uplifting of a slow speed streak.* A strong influx of fluid from the wake and logarithmic zones (a "sweep" event) then appears to precipitate a more rapid liftoff of the low speed fluid. This stage is accomplished by an apparent three-dimensional oscillation of the marker, and terminates in a strong ejection(s) of fluid from the wall layers. Further tracing of the motion becomes difficult when the uplifting parcel of fluid "breaks up" into finer scales as it mixes with higher speed flow well away from the wall. It is speculated that the conditions for another cycle of events come about through the combined influence of earlier upstream bursts, in a process perhaps involving the phenomenon of vortex pairing [52].

*One should bear in mind that a slow speed streak is composed of momentum-deficient fluid upwelling from the wall; if a fluid marker is present it will be convected upwards.

R. S. Brodkey and his coworkers [10, 35, 38] at Ohio State University have also observed similar processes of a repetitive nature that appear to contribute to momentum transfer within the boundary layer. Their visual approach incorporates selective viewing of a suspension of tiny neutral buoyancy particles throughout the flow, accomplished by illuminating the suspension with a narrowly focused, high intensity sheet of light. Using this technique they have observed a pattern of events inside the wall layers which involves strong inflows and outflows that seem to correspond to the sweep and ejection events of the bursting cycle as described by the Stanford group.

In their cycle, the Brodkey group notes the initial formation of a region of low streamwise momentum occurring in conjunction with a sharp decrease in the wall shear. This is followed by a high speed mass of fluid centered at $y^+ \simeq 15$ which enters their field of view and acts to accelerate the fluid within the low speed zone. Ejections of low speed fluid from this region ($7 \leq y^+ \leq 30$) occur immediately after the onset of acceleration. It is stressed that the transverse (z) location of the high speed front often does not coincide with that of the low speed region; if not, their interaction is somewhat delayed. The sequence is closed by the entry of a high speed influx of fluid often appearing to be a part of the fluid mass involved in the acceleration event. They term this the "sweep" event, since it "sweeps" the low speed fluid from the field of view and replaces it. However, since this sweep terminates the ejection phase rather than initiating it, one should not equate it with the "sweep" described in the Stanford studies. But there are important parallels: First, both patterns of events cyclically repeat themselves,

and secondly, the observed outflows both originate in zones of low streamwise momentum.

The accounts given thus far have only described the fluid motions that yield the characteristically large Reynolds stresses within the wall layers; little mention has been made of the interactions precipitating these events. Lu and Willmarth [32], using a burst detection scheme based on the presence of low velocity fluid at $y^+=15$, found that the conditionally sampled wall pressure is low at the time of burst detection. In a 1975 review, Willmarth [50] notes that a zone of low pressure should occur below a transverse vortex ($-\omega_z$) as it convects downstream; Willmarth and Wooldridge [52] in a subsequent investigation using correlation measurements of R_{pv}* verified that convected large-scale transverse vorticity is capable of impressing a local low pressure fluctuation upon the wall layers. Finally, C. R. Smith [45] notes from his visual observations that initiation of a bursting sequence usually involves the prior passage of concentrations of transverse vorticity in the logarithmic and wake layers.

The foregoing observations indicate the bursting event to be associated with pressure disturbances arising from vortical activity; how fundamental this may be to the phenomenon of bursting is not yet clear. Pertinent to this question is the work of Doligalski and Walker [12], who carried out a numerical prediction of the viscous interaction that occurs when a two-dimensional transverse vortex ($-\omega_z$) convects in a uniform flow over a developing boundary layer. Their

$$*R_{pv}(x,T) = \frac{\overline{p(0,t)\,v(x,t+T)}}{\left[\overline{p^2(0,t)}\;\overline{v^2(x,t+T)}\right]^{1/2}}$$

work indicates that such a vortex tends to "break down" the flow in the near wall region, creating zones of recirculation and upwellings of fluid from the wall.

Other interpretations for a wall layer ejection mechanism exist. From his visual observations using hydrogen bubbles and dye, Kim [21] describes a process in which the ascending region of low velocity fluid (the low speed streak) causes the formation of a point of inflection in the instantaneous velocity profile. He construes this inflection to be the location of maximum instantaneous shear, and suggests that in most cases the breakup stage of the bursting sequence is the result of the growth of an unstable oscillatory disturbance within this shear layer.

Blackwelder [4], from detailed anemometry measurements made by himself and Eckelmann [5], gives an account of turbulent processes within the wall region that refers to a possible Helmholtz-type viscous instability there. One experimental configuration that was employed for these studies used a single hot-film probe measuring streamwise velocity at $y^+=15$, combined with two flush-mounted wall elements sensitive to $\frac{\partial u}{\partial y}$ and $\frac{\partial w}{\partial y}$ located $\Delta z^+=9$ to either side of the velocity probe. The detection at $y^+=15$ of a velocity less than the local mean was found to occur in conjunction with spanwise gradients consistent with a pair of counter-rotating axial vortices. This event is followed by the appearance of a high speed "sweep" of fluid which results in the formation of an inflectional instantaneous profile, with the point of inflection corresponding to the high shear interface between the high and low speed fluid. Although this interface is three-dimensional, Blackwelder demonstrates that an analogous two-dimensional free shear layer of a similar thickness and magnitude is unstable for the

experimentally observed range of wavelengths,* and speculates that the nonlinear stage of a similar instability at the interface constitutes the beginning of the bursting event observed in a boundary layer. The visually obtained results of Kim bear close resemblance to the conclusions presented by Blackwelder from his anemometry measurements; thus, they tend to substantiate each other.

The work of Nychas, Hershey, and Brodkey [35] is a continuation of earlier efforts at Ohio State. It also resembles the nearly parallel sequences of events described by both Kim and Blackwelder which involve a shear layer instability, but places emphasis on the presence of large scale transverse vortices in the outer layers. Unlike Kim and Blackwelder, they hold that a shear layer instability does not directly cause the rapid lifting of slow speed fluid and its breakup, but rather results in the formation of one or more transverse vortices which are capable of causing ejections as they convect downstream in the wake and logarithmic layers.

Levi [28] offers an intriguingly different perspective of the flow processes of the bursting event. Noting that the wake structure behind a spherical obstruction is dominated by streamwise vortical filaments, and that different modes of wake behavior may be observed (Figure 1.4) by varying the characteristic Reynolds number based on diameter [33], he makes a qualitative analogy between this behavior and the fluid motions observed in conjunction with the lift-up of a low speed streak.

*The uncertain nature of the oscillation observed in the boundary layer raises some doubt as to whether its "wavelength" is properly defined. This point is further discussed in Section III.

Treating the low speed streak lift-up as a flow obstruction capable of shedding a wake, he computes a characteristic Reynolds number based on the transverse dimension of a streak, finding that within a turbulent boundary layer the range of Re_D encountered corresponds to a regime in the sphere's wake where the vortical filaments form either an undulating counter-rotating pair or an orderly series of periodically shed loops with counter-rotating legs.

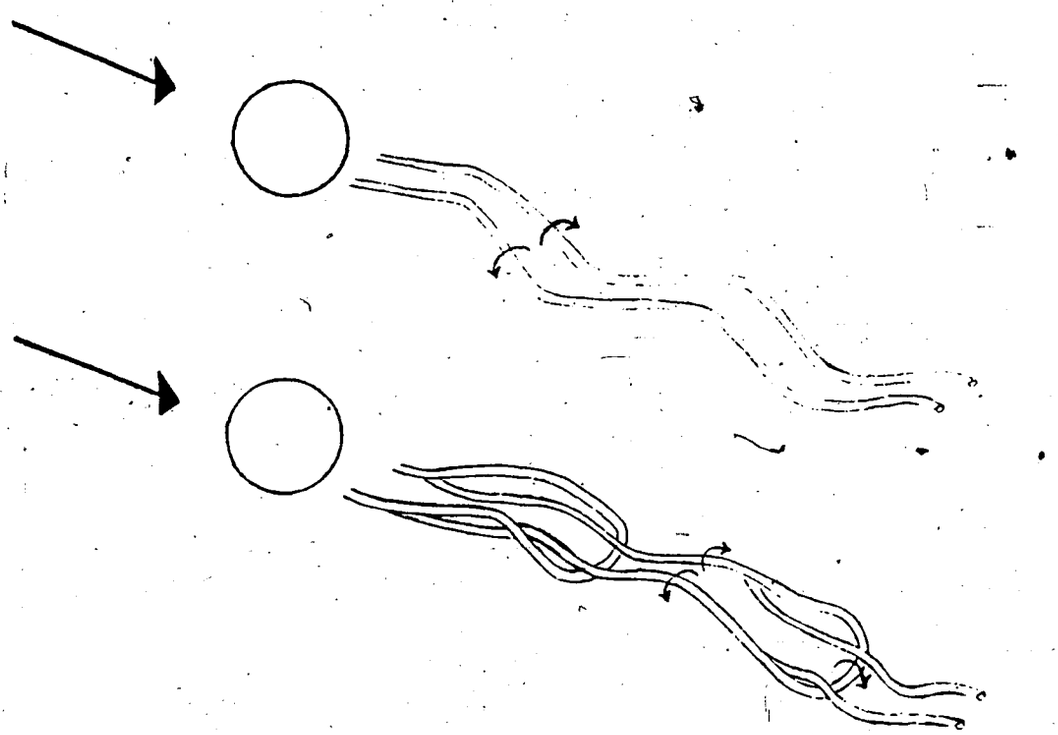

Figure 1.4 Shedding Regimes Behind a Sphere in Uniform Flow.
(a) $270 \leq Re_D \leq 290$
(b) $290 \leq Re_D \leq 410$ (after Magarvey [33])

Similarly, Smith, Metzler, and Schwartz (1979 unpublished) observed a striking visual similarity between the wake of a small (1.1 cm) hemisphere placed in a laminar boundary layer (Figure 1.5 a and b) and the wall layer structure associated with an ejection in a fully turbulent boundary layer (Figure 1.5c and Figure 3.12 abc).

a. hemisphere wake: U_{local}=.12 m/s, $\Delta x \simeq 40$ D downstream, y_{wire}=2.5 mm, scale: 1 cm = 6 $\frac{\nu}{u_\tau}$ (friction velocity based on laminar wall shear stress)

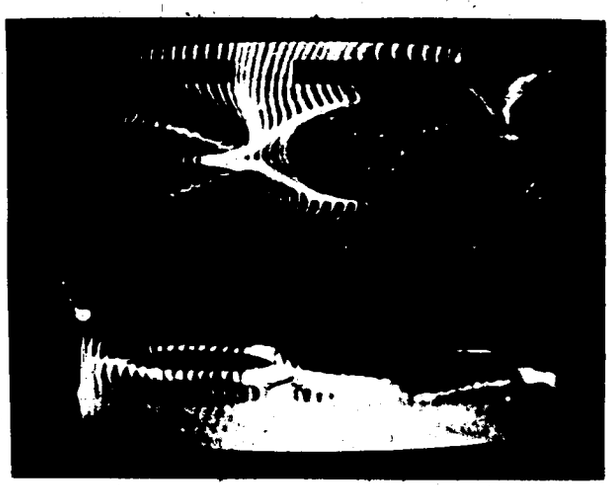

b. hemisphere wake: U_{local}=.12 m/s, $\Delta x \simeq 25$ D downstream, y_{wire}=5.0 mm, scale: 1 cm = 6 $\frac{\nu}{u_\tau}$

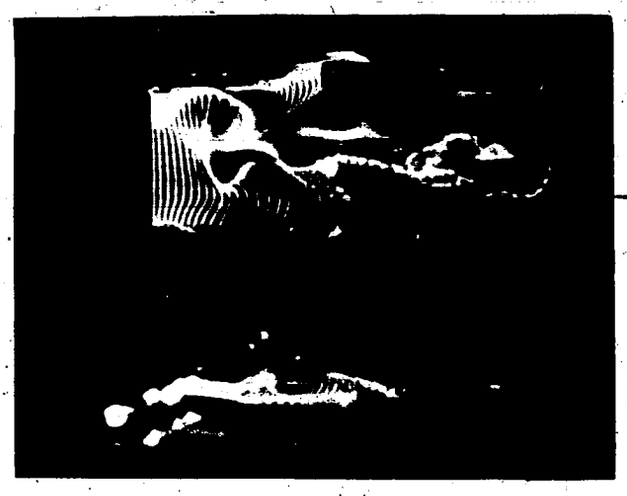

c. turbulent boundary layer: Re =1910, y^+=15, scale: 1 cm = 6 $\frac{\nu}{u_\tau}$

Figure 1.5 Split-screen views (plan and side) of the wake behind a hemisphere in a laminar boundary layer and an analogous structure in a turbulent boundary layer.

Interpretation of the split-screen views shown in Figures 1.5 and 3.12 may be facilitated by referring to Figure 3.8, which diagrams both perspectives.

The idea that wall layer ejections are involved with vortical structures of a loop-like conformation is not new. Postulated by Theodorsen in 1952, "horseshoe vortices" are a key feature in the model of Offen and Kline, and that of Head and Bandyopadhyay (hairpin vortices) [19]. The measurements of Willmarth [et al] suggest such a flow feature, and hypotheses concerning the formation of this structure have been forwarded by Blackwelder [4], based on his measurements.

In a 1963 study of boundary layer transition, Hama and Nutant [17] observed the formation of horseshoe-shaped vortices in a perturbed laminar boundary layer. Introducing a disturbance by means of pulsing a large (10 cm) rubber membrane mounted flush with the wall, they watched the subsequent growth of spanwise nonuniformities in the velocity. The resultant deformation of the wall vorticity gave rise to a loop-shaped vortex filament with upstream-pointing legs containing a streamwise component of vorticity that became intensified through stretching. A strong upflow between the legs caused the formation of a high shear layer which broke down to form a secondary loop vortex, in a process observed to recur for as many as four times with a given initial disturbance.

The discussion has so far dealt primarily with wall layer events; however, the picture would be incomplete without a treatment of the characteristics of the outer region. It has been noted that large scale motions of transversely oriented vorticity within the log and wake regions seem to stimulate bursting activity at the wall. Also, the fronts of high speed fluid which appear to precipitate ejections and shear layer

instabilities (as described by Brodkey [et al], Kim, and Blackwelder) possess convection velocities and length scales that imply a wake layer origin.

Falco [13] has performed extensive studies of the structure of the outer layers, and has been able to discern discrete and recognizable fluid motions within this region. Falco describes the presence of coherent large scale motions of fluid within the outer layers which appear to convect by a given point at a frequency comparable to that of the bursting phenomenon. Smaller structures (typical eddies) are seen to form on the backs, or upstream side, of the large scale motions. In the logarithmic region, these are often observed to have a wallward tendency; Falco hypothesizes that this wallward motion may constitute the sweep event of the wall layers. Another possible source of fluid for the sweep event consists of the fluid entrained between the "bulges" defining the outer edge of the boundary layer; this fluid is nearly irrotational and usually possesses a strong component of downwards velocity [13].

Evidence for a mutual influence bewteen the inner and outer layers is presented by Brown and Thomas [7], who through correlation measurements* showed a correspondence between the passage of large scale structures in the outer region and wall shear stress fluctuations. By varying the delay time and downstream separation distance of their probes they were able to determine that the vertical orientation of the structures, or angle of inclination, was nearly coincident with that of the large motions observed by Falco.

$$^{*}R_{\tau u}(x,T)=\frac{\overline{\tau(0,t)\,u(x,t+T)}}{\left[\overline{\tau^2(0,t)}\;\overline{u^2(x,t+T)}\right]^{\frac{1}{2}}}$$

Because wall layer ejections are events observed to repetitively occur with a statistically definable period, some clues as to the potential role of the outer layer structure in actuating these events may be had by determining the functional dependence of the period upon specific parameters of the flow. Although a description of a bursting period defined in a Lagrangian frame of reference would appear more relevant from a deterministic standpoint, past approaches resort to the measurement of a time interval between bursts (T_B) that occur at a single point in the flow.

In a 1963 investigation using dye visualization, Runstadler [et al] hypothesized a potential dependence of T_B upon the spacing between streaks (λ), but failed to find conclusive evidence for this reasonable assumption. Kim [et al], assuming low speed streak lifting (and ensuing ejection) to be triggered by large disturbances already present within the flow, nondimensionalized T_B upon the outer variables U_∞ and δ (freestream velocity and boundary layer displacement thickness), and successfully correlated the bursting time data of several investigators (Runstadler et al, 1963, Schraub and Kline 1965, Tu and Willmarth 1966, and Rao et al: 1969) for $650 \leq Re_\theta \leq 45100$. Zakkay, Barra, and Wang [14], in a hot-wire study of a high velocity air flow, further extended the range of Re_θ for which T_B was measured to $Re_\theta = 108000$, and found agreement with the nondimensionalized values of Kim ($\frac{T_B U_\infty}{\delta} = 30 - 36$).

Despite the apparent success had in scaling the bursting frequency upon outer layer variables there are reasons to suggest that an inner layer scaling might be more appropriate. The asymptotic behavior of the mean wall shear stress for large Reynolds numbers implies a nearly constant rate of momentum transfer and a bursting frequency that is

likewise unchanged; outer variable scaling would predict a substantial decrease in bursting events to occur for large increases in Reynolds numbers. For a range of Reynolds numbers $1000 \leq Re_\theta \leq 10000$ Blackwelder and Haritonidis [6] have found that the bursting frequency as nondimensionalized on the inner variables ν and u_τ (kinematic viscosity and friction velocity) is a constant ($f^+ = \frac{f\nu}{u_\tau^2} = .005$ where $f = \frac{1}{T_B}$). Because of the rather small range of Reynolds numbers investigated, no firm conclusions can be drawn as to the scaling of the bursting frequency; the question is yet open.

Although it is apparent from the material presented in this survey that the inner and outer regions exert a mutual influence, the nature of their interaction is not yet clear. An answer to the question of their interdependence awaits a better understanding of the mechanism that governs momentum transfer within the boundary layer. A further elucidation of this mechanism is the design of the present study.

I.D. PRESENT INVESTIGATION

The investigation focuses on that part of the boundary layer in close proximity to the wall, extending from the viscous sublayer out to $y^+ = 35 - 40$. It is felt that this region more than any other influences boundary layer behavior, and that a knowledge of its processes would prove to be the most fruitful avenue towards the development of better prediction methods and/or manipulation techniques for the turbulent boundary layer.

Arguing purely from an intuitive standpoint, it is in the near-wall region that the velocity undergoes the greatest adjustment from its free-stream value ($\frac{u}{U_\infty} = .5$ at $y^+ = 10$, $y/\delta = .012$). Thus, it appears justified to suspect that the events taking place in this region to be

the most important and critical to boundary layer development. Furthermore, the structure in this region displays a degree of regularity not to be found elsewhere in the boundary layer; its persistence and apparent universality imply a fundamental role within the mechanism of the boundary layer, with a corresponding potential for manipulation and control. The use of long chain polymers to achieve a decrease in mean wall shear seems to bear this out. Oldaker and Tiederman [37] report that the most apparent change in boundary layer structure observed in conjunction with the reduced momentum transfer is a larger spanwise wavelength within the wall layers - also, that a decrease in mean wall shear can be achieved without the presence of the polymer in the outer region. Finally, the edge of the viscous sublayer marks the zone of greatest production and dissipation of turbulent kinetic energy (Townsend [46]); although rotational flow extends some distance away from the wall, it is the wall layers that extract the most energy from the mean flow.

The present research seeks to quantitatively and qualitatively define the behavior of the near wall region. Experimental areas include:

1) An examination of the average spanwise spacing in the viscous sublayer for a broad range of Re_θ.
2) A spatial distribution that details spanwise spacing of the wall layers as a function of y^+.
3) Simultaneous plan and side views of a horizontal hydrogen bubble wire, from both a stationary and a moving frame of reference.
4) The examination of a rational method for the potential augmentation of transport properties of a turbulent boundary layer, by modification of the wall layer structure.

Subsequent sections will describe the experimental flow facility, experimental apparatus and procedures, the obtained results and a discussion thereof, and conclusions. A section of appendices discusses details not immediately pertinent to the scope of the investigation.

CHAPTER II

EXPERIMENTAL APPARATUS

II.A. FLOW FACILITY

All data presented in this study was obtained in a 4.8 m long open surface water channel located in the Fluid Dynamics Laboratory, Lehigh University. Figure 2.1a is a schematic of the system. The flow is produced by a Peerless centrifugal pump powered by a 7.5 hp variable speed electric motor. A speed controller with a shaft speed feed-back circuit (designed and built in-house) monitors power supply amperage and voltage to the motor and indicates pump speed in revolutions per minute. Maximum flowrate with the existing power supply is 4.0 m^3/min. with a corresponding velocity in the channel of .3 m/s, at a channel depth of 25.4 cm. The flow system has a capacity of 5.0 m^3. Isolation from pump vibration is accomplished by the placement of rubber sleeves at the inlet and exit to the pump, and rubber expansion joints at both ends of the test section.

INLET SYSTEM

The flow enters the inlet tank at the head of the channel via a specially designed distribution manifold in the bottom of the tank. It then must pass vertically through a 5 cm thick plastic sponge before proceeding downstream through a flow straightener consisting of honeycomb (cells 7.5 cm long and .48 cm diameter) followed by 20 mesh stainless steel screen [31]. The 1.75:1 inlet contraction [34] just downstream of the flow straightener further reduces freestream turbulence intensity. The freestream turbulence intensity as measured by a hot-film anemometer 4.0 m downstream of the contraction was .6%

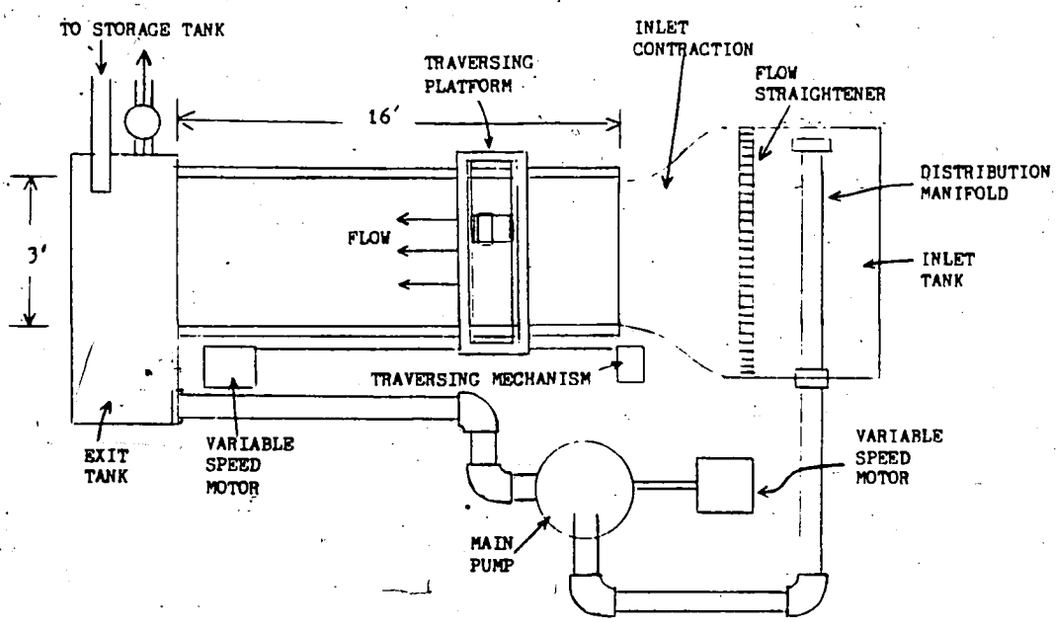

(a)

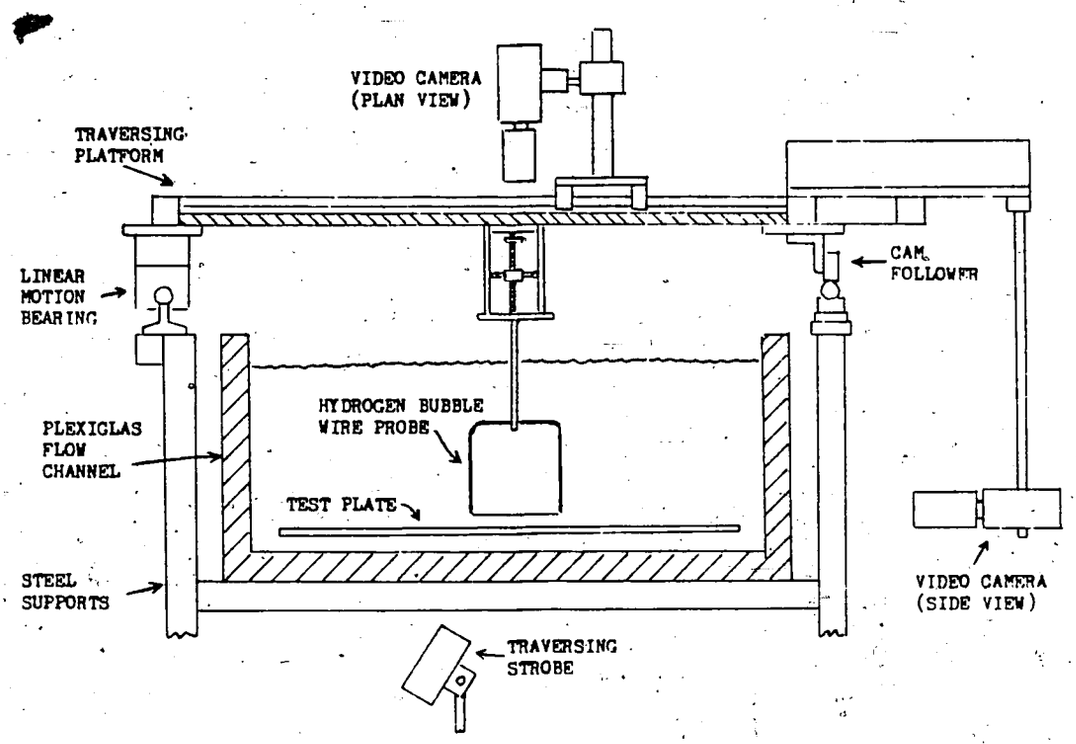

(b)

Figure 2.1 (a) Schematic of Flow Facility

(b) End-on View of Channel (Looking Downstream) and Traversing Platform

of the freestream velocity for U_∞ =.3 m/s, and .4% for U_∞ =.23 m/s.

The inlet contraction is constructed of plywood and covered with fiberglass. The interior surfaces are sanded and polished, and accurately align with the channel sides and bottom. The curvature of the sides is calculated so as to yield a uniform exit velocity [34], but high speed regions close to both walls were found to vary as much as 10% from the centerline velocity. However, subsequent measurements with a hot-film anemometer of the center 10 cm of the channel established the largest excursion within that region to be less than 1% of the mean (Figure 2.2).

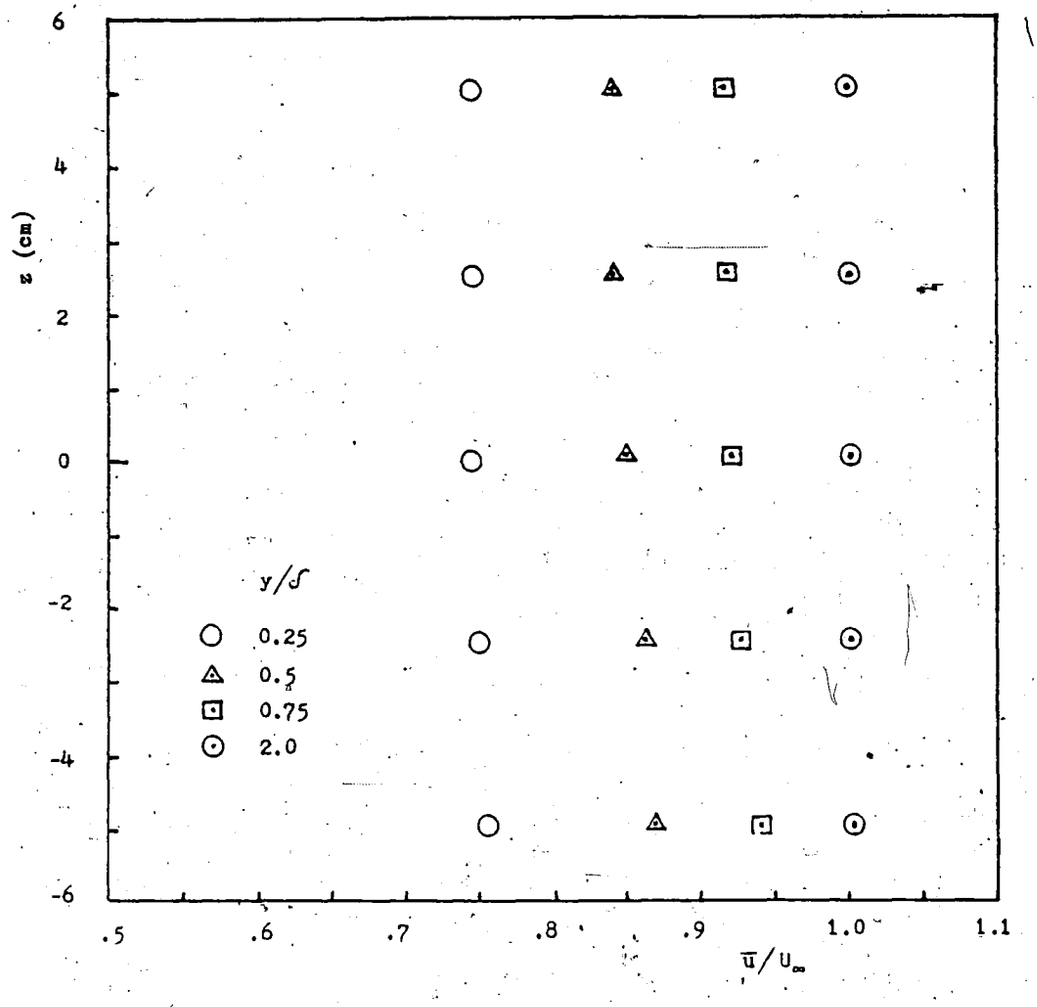

Figure 2.2 Spanwise Variation of the Mean Velocity About Channel Centerline (z=0) for U_∞ =.23 m/s, x=4.0 m, Re_x=.93(10^6).

CHANNEL

The flow channel is 30 cm deep, 87 cm wide, and 4.8 m long. It is constructed of 1.91 cm plexiglass supported on a framework of 5 cm square steel tubing, and rests on a concrete slab. A cross-sectional view appears in Figure 2.1b.

A 3.2 mm diameter rod placed at the channel entrance served as a boundary layer trip. The streamwise distance (x) was measured from thi point using an empirical correlation taken from Schlichting [43] to establish the actual location of turbulent transition.

$$\frac{U_\infty(x_{tr} - x_k)}{\nu} = 2(10^4) \qquad (17.30)$$

Here x_{tr} is the streamwise location of the boundary layer trip, and x_k is the effective location of transition. The channel length allowed Reynolds numbers of $Re_x = 1.5(10^6)$ and $Re_\theta = 2800$ (based on streamwise distance and momentum thickness, respectively) to be attained under normal conditions.*

OUTLET TANK

The large end tank is maintained at the same water level as the channel. A baffle of folded 20 mesh screen placed at the end of the channel inhibits the formation of standing waves and otherwise prevents the upstream propagation of any disturbances originating within the outlet tank. The flow exiting the tank passes through a rubber sleeve which isolates the flow from mechanical pump vibration; it was found necessary to insert a section of honeycomb inside this sleeve to prevent its inward collapse at higher flowrates.

*For several experiments the water was heated to 38 °C and water depth reduced to 10 cm for which a maximum of $Re_x = 3.5(10^6)$ was reached.

MAINTENANCE OF WATER QUALITY

The use of clean water when filling the channel and the maintenance of its clarity are both essential to good visual data. Water used in the channel is passed through two parallel cylindrical filters of wound cotton which remove all particulate matter larger than 1 micron (μm). To prevent the growth of algae and bacteria, copper sulfate in granular form ($CuSO_4 \cdot 5H_20$) and chlorine in the form of common household bleach are added in concentrations per cubic meter (water) of 50 ml and 25 ml, respectively.

Further measures to insure continued water purity include the use of plexiglass covers for the channel and end tanks, and a continuous, 1.1 m^3/hr in-line filtering system.

II.B. MOVING REFERENCE PLATFORM

Flow visualization from a moving frame of reference is accomplished by use of two synchronized platforms which move at the same velocity, one above and one below the channel. The upper platform has provisions for the mounting of video cameras for side, plan, and end-on views, and also carries hydrogen bubble-wire visualization probes. The lower platform carries the lighting equipment for the video system.

To permit a continuous traverse with a hydrogen bubble-wire probe held at a very small distance above the channel floor, a high degree of precision is required in the traverse mechanism for the upper platform. This platform rides on a track consisting of two hardened steel shafts 3.8 cm in diameter and 4.1 m long, and is accurately guided by two Thompson linear motion bearings on one shaft, and two heavy ball bearing cam followers on the other. The shafts are supported at 0.3 m intervals by mounts adjustable in the side and vertical directions. Vertical

deviation of the upper platform that occurs over a continous 3.5 m long traverse is limited to $\pm$0.8 mm ($\Delta y^+ \sim 10$) by this arrangement. Most of the error results from a deflection of the 1.91 cm thick plexiglass channel floor in the 0.61 m spans between support members; a glass channel planned for the future will reduce this deviation substantially.

Such precision is not required for the lower, light-carrying platform, and it rolls on plastic ball bearing wheels along a wooden track beneath the channel. Two separate cable drives (6 mm steel cable running on pulleys) move the platforms. Linkage between the two systems is a chain and sprocket assembly with a 1:1 drive ratio, so that the two platforms move synchronously and at equal velocities. Power input to the entire system is through the cable drive for the top, camera-bearing platform, so that minute fluctuations present in the output of the chain and sprocket linkage are transmitted to the lower platform only. A 1 hp variable speed electric motor, reversible and with dynamic braking, provides translational velocities of 0 - .5 m/s.

II.C. VIDEO EQUIPMENT

The video viewing and recording system is a two-camera, high-speed closed circuit system (manufactured by the Video Logic Corp.) which incorporates synchronized strobe lights to provide 120 frames/s with effective frame exposure times of 10^{-5}s. An exceptionally clear picture is obtained from the high-resolution screen using 250 horizontal, direct overlay rasters with a sweeping frequency of 25.2 kHz. Using conventional lenses, fields of view as small as 6 X 6 mm can be obtained at distances of 0.5 m. A split-screen capability allows two different fields of view to be simultaneously displayed and recorded. All recorded data can be played in flicker-free motion (both forward and reverse), as well as

single-framed for detailed data analysis. Once a video sequence is recorded, conventional still photographs of individual stop-action frames can be taken directly from the video screen. In addition, a video digitizing system which interfaces the video information directly with a mini-computer can be employed to obtain detailed quantitative data from the flow visualization pictures.

III.D. FLOW VISUALIZATION APPARATUS

Marking techniques for flow visualization included the hydrogen bubble method [9], dye injection with a syringe, and, in one case, use of 125 μm glass beads (γ =2.48).

Flow visualization by the hydrogen bubble method involves the placement of a fine metallic wire within the flow to serve as the cathode of a DC circuit. An anode (also submerged) consists of any suitable conducting object, and is placed nearby. Supplying voltage to the circuit causes the liberation of hydrogen at the cathode (wire) through electrolysis, with oxygen being released at the anode. Hydrogen bubbles forming on the wire are swept off by the flow to form a continuous sheet; if the voltage is supplied in the form of square-wave pulses, discrete lines of bubbles are formed. (Since the volume of hydrogen released in electrolysis of water is twice that of oxygen, superior flow visualization is obtained using the ware as a cathode). The size of the bubbles released from the wire is of the order of one half the wire diameter; the use of an extremely fine wire (.025 - .05 mm) renders buoyancy effects negligible [42]. Bubble lines are made visible by illuminating the flow with a light source of high intensity directed at an oblique angle to the line of sight. The addition of a small amount of an electrolyte such as sodium sulfate (.15 g/liter of Na_2SO_4

works well) greatly enhances bubble generation, producing denser bubble lines with a consequent increase in clarity and contrast of the visual data obtained.

For the present investigation, platinum wire .025 mm in diameter was used. Alumel wire of the same diameter was also tried, but produced bubble lines of inferior quality, was harder to solder, and was subject to frequent breakage caused by a reaction of the aluminum with ions in the water. Placement and orientation of the bubble wire within a flow was accomplished by a bubble-wire probe consisting of two conducting, insulated metal prongs between which the platinum wire was stretched, with the ends secured by soldering. The probe is constructed of brass, and insulated with heat shrink tubing and red glyptol. Design requirements for the probe were that it be nonstationary, and provide interference-free side, plan, and end-on views of the wire and bubble sheet. Appendix C details its construction. The probe was mounted to a calibrated traversing mechanism that could be adjusted in .05 mm increments.

The bubble wire is energized by square wave voltage pulses supplied by a specially designed and constructed voltage generator with a range of 0- 90 Volts and a maximum output of 2.5 Amps. The pulse duration is continuously adjustable, and the pulsing frequency may be varied from 0 - 340 Hz. The pulsing frequency is monitored by a multifunction counter manufactured by Data Precision Corp., which can measure frequencies from 5 Hz to 100 MHz.

After about a minute of operation, the quality of bubble lines shed from the wire begins to degenerate. This is due to a buildup on the wire of positively charged ions which may be removed by switching the polarity

of the voltage supply for a few seconds, then switching it back. However, abrupt changes in the voltage output can damage the pulse generator, and/or cause a breakage of the bubble wire. A residual capacitance present in the voltage leads and the generator causes the voltage signal to persist for a few seconds after the generator has been shut down; therefore, to avoid potential damage to the equipment it is necessary to wait for the residual pulses to fade away before switching the polarity in either direction.

II.E. HOT-FILM ANEMOMETRY EQUIPMENT

Hot-film anemometry studies were undertaken to determine the basic parameters of the turbulent boundary layer produced. Details of the technique and the obtained results are covered in Appendix A.

All anemometry measurements were carried out using DISA type 55F hot-film single-fiber probes. The fiber diameter is 70 μm, and the sensitive length is 1.25 mm (about $\Delta z^+=10$ for the flows measured). An overheat ratio of 10% was used. The probes were driven by a DISA 55 D01 anemometer unit in a constant temperature mode. The voltage signal was linearized using a DISA Type M25 linearizer. Time-averaged mean and RMS voltages were monitored by a TSI Model 1076 voltmeter.

The linearized signal was calibrated to the freestream velocity, which in turn was accurately determined by timing the downstream progress of a float through a pre-measured distance. Errors in this method due to inertia of the float and surface tension effects were minimized through the construction of a lightweight float (Figure 2.3), consisting of submerged vanes attached to a slender stem breaking the surface. Comparison of the float technique to time-line measurements using a hydrogen bubble-wire probe yielded a comparison within $\pm$2%.

The section that follows is a presentation and discussion of the visual and quantitative data obtained in the present investigation.

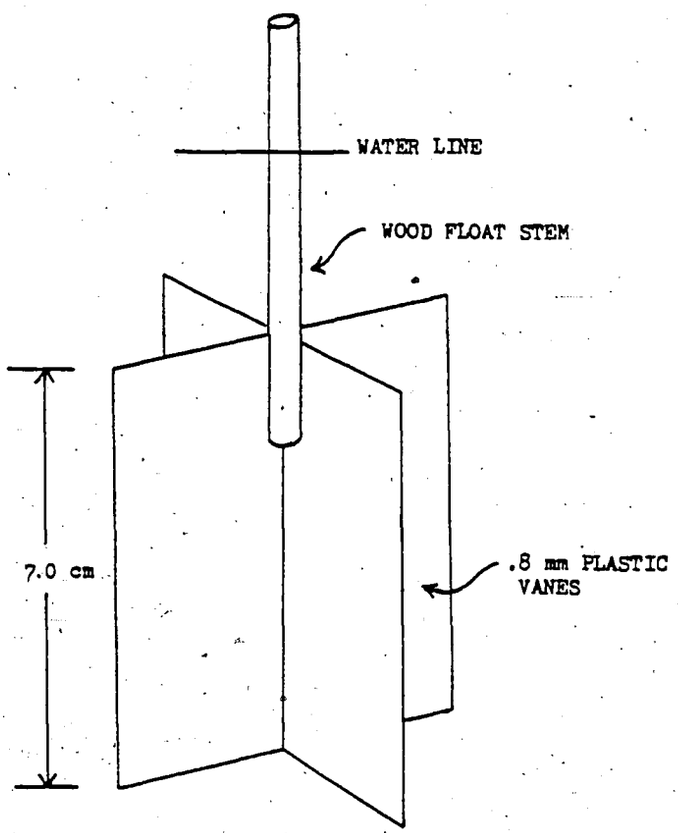

Figure 2.3 Velocity Float Used for Displacement-Time Measurement of Freestream Velocity.

CHAPTER III

RESULTS AND DISCUSSION

This chapter presents the findings of several different experiments, each designed to focus on a different aspect of the wall layer turbulent structure. The presentation takes the form of a recounting of experimental technique together with the obtained data, followed by a discussion of the results.

III.A. MEAN STREAK SPACING

The average spacing between low speed streaks was measured for Reynolds numbers based on momentum thickness $1430 \leq Re_\theta \leq 5831$. It is believed that this extends the upper range of Re beyond that for which visually obtained values were previously available [41, 37]. An additional facet of this study was the measurement of the mean spacing for flows at the same Re_θ, but with differing freestream velocity, viscosity, and downstream distance.

The streak spacing values presented are in the form $\lambda^+ = \frac{\lambda u_\tau}{\nu}$, where λ is the physical distance between streaks, nondimensionalized on the viscous length $\frac{\nu}{u_\tau}$. All values were obtained by visual counting from a video recording of a horizontal hydrogen bubble wire located at $y^+=5$.

The method for counting involved stopping the video system on a single frame, and marking the location of each streak on a transparency (Figure 3.1). Each vertical line on the transparency corresponds to one marked frame, and the small cross marks denote the location of a streak. To ensure a random sampling, frames to be counted were separated by a uniform time interval of 5/6 seconds (100 frames), and a

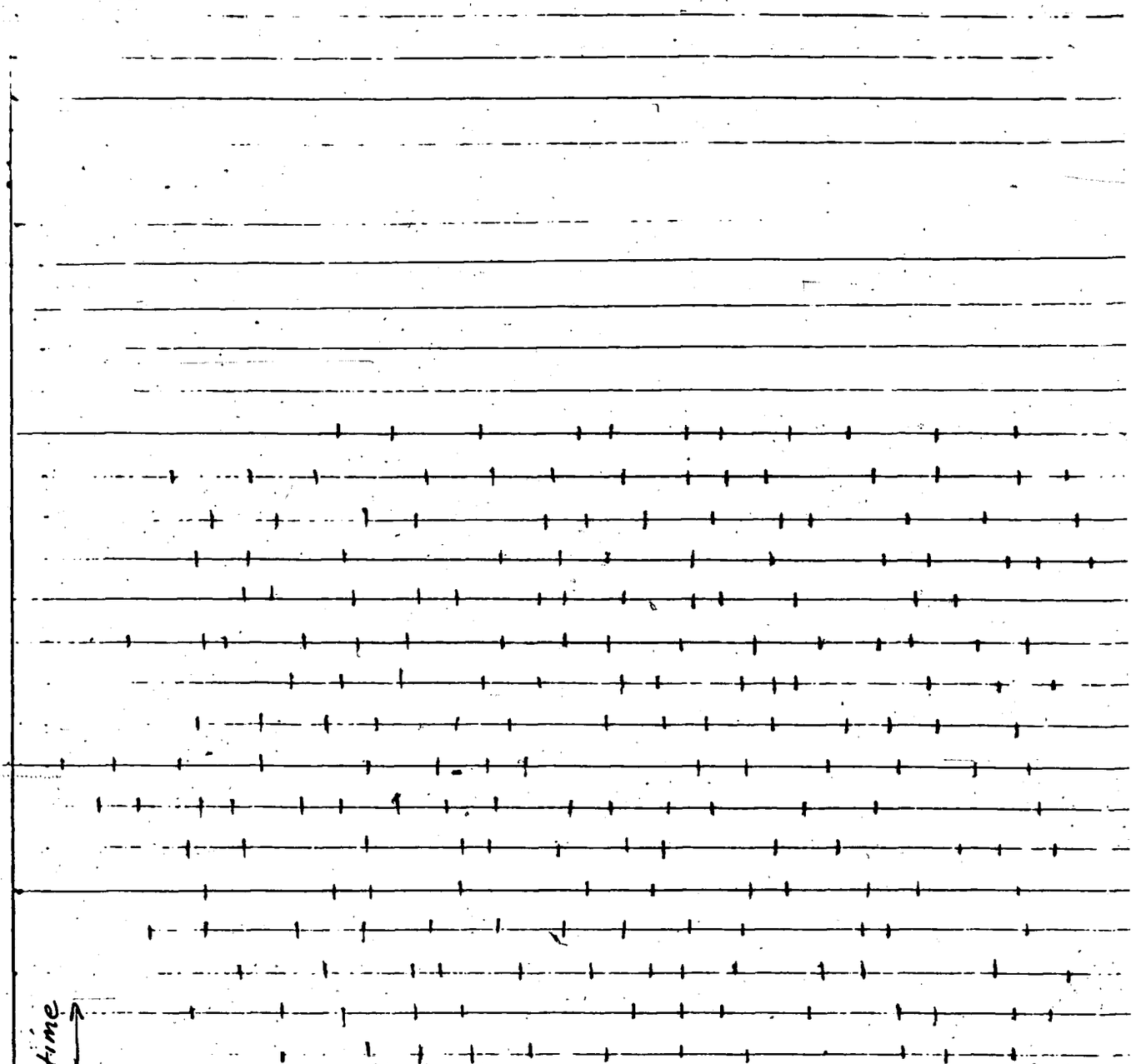

Figure 3.1 A Copy of a Transparency Used in Marking the Locations of Low Speed Streaks.

Scene 049

single sample typically contained 25 or more counted frames. This corresponded to a total sample duration in terms of the time between bursts of approximately 12 T_B for the lowest velocity flow, and 42 T_B for the high velocity. Lens magnification was set to give a field of view of $\Delta x^+ \simeq 900$ and $\Delta z^+ \simeq 700$; the degree of magnification and the corresponding ratio of length scales were determined by recording a short scene with a calibrated rule placed next to the bubble wire. At least 110 streaks were counted in each sample, giving an accuracy of $\pm$10% with 95% confidence.*

The identification of a low speed streak was done using the following criteria. A streamwise concentration of bubbles indicating a region of low axial velocity (closely spaced bubble lines) had to be present, well defined and with a streamwise extent of at least $\Delta x^+=100$. If a streak appeared to end, and its upstream end was more than $\Delta x^+=50$ downstream of the wire, it was not counted. There was no restriction on a minimum spanwise spacing; only if it appeared that two streaks had completely merged would they be counted as one. The location marked on the transparency was the transverse position of the streak $\Delta x^+=50$ downstream of the bubble wire.

Table 3.1 presents values obtained for the mean streak spacing by this investigation; values obtained by other researchers in previous investigations are also shown for comparison. The parameters of the flows for which the counts were made are also listed, when available. (The classical streak spacing study of Runstadler [40] is not included. The streak identification rules used in that study resulted in a larger number of streaks counted, giving rise to smaller mean spacings than those obtained by Schraub and Kline [41]). For the present

*See Appendix D for the uncertainty analysis.

investigation, no marked change in the nondimensionalized spacing (λ^+) was found to occur either with variations in the flow parameters or over the range of Re_θ studied. The results indicate that within the uncertainty of the data λ^+ is either constant or a slightly increasing function of Re_θ at best.

However, taking λ^+=constant does not imply that the physical spacing between streaks (λ) undergoes no change within a given flow.

Table 3.1 Mean Streak Spacing and Flow Parameters.

investigator(s)	Re_θ	U_∞ (m/s)	$\hat{u}_\tau$ (m/s)	x (m)	ν (m^2/s) X 10^6.	λ^+
Metzler	1430	.166	.0074	4.27	1.030	104
(flat plate, water)	1430	.282	.0126	2.51	1.030	105
	1973	.221	.0097	4.24	0.920	87
	2007	.256	.0111	3.87	0.975	85
	2153	.189	.0081	4.27	0.728	100
	2176	.274	.0118	4.27	1.044	92
	2176	.314	.0135	2.51	0.705	98
	3266	.305	.0125	4.27	0.716	100
	4164	.387	.0155	4.27	0.690	93
	4944	.475	.0188	4.27	0.696	100
	5831	.582	.0226	4.27	0.702	112
Oldaker and	298	.169	.0118	-	1.08	93
Tiederman	373	.180	.0106	-	0.92	89
(channel flow, water)	404	.174	.0102	-	0.82	99
	480	.335	.0186	-	1.33	105
	644	.311	.0170	-	0.92	116
	745	.360	.0190	-	0.92	116
Gupta, Laufer,	2200	-	.1402	-	14.7	97.5
and Kaplan	3300	-	.2256	-	14.8	89
(flat plate, air)	4700	-	.3277	-	14.8	110
	6500	-	.4511	-	14.8	151
Schraub and Kline	1080	.152	.0070	3.14	-	98
(flat plate, water)	1325	.152	.0069	4.11	-	108
Achia and Thompson	327	.249	.0152	-	1.0	88
(pipe flow, water)	545	.415	.0245	-	1.0	79
	725	.553	.0325	-	1.0	93

It is easily seen from the definition of λ^+ that as distance downstream from the point of turbulent transition is increased, λ will also increase (u_τ is a weak function of Reynolds number).

Intuitively this is what one would expect. It is an experimentally established fact that the zones of low speed flow representing the streaky structure are intimately involved in the bursting cycle [41], and that the momentum transfer induced through bursting is responsible for a large percentage of the mean wall shear stress in a turbulent boundary layer [21]. A larger spacing between streaks implies a lower incidence of bursting events per unit area, with a consequent decrease in wall shear. This is indeed the case; for a given flow, the mean shear stress decreases to an asymptotic value as downstream distance is increased. Also, a decrease in bursting frequency with higher Reynolds number has been observed (Kline, et al). This implies that as the mean wall shear stress asymptotically approaches a lower bound, the physical spacing between streaks similarly approaches an upper bound.

This may be illustrated through the definitions of λ^+ and u_τ:

$$\lambda^+ = \frac{\lambda u_\tau}{\nu} = 100$$

$$\lambda = \frac{100\nu}{u_\tau} = \frac{\text{const}}{u_\tau}$$

Incorporating White's [49] equation 6-134 for c_f:

$$\lambda = \frac{100\nu}{u_\tau} = \frac{100\,\nu}{.477U_\infty} \ln(.06Re_x)$$

These expressions are of course only valid as long as λ^+ is taken to be a constant independent of Reynolds number. This is at odds with the findings of Haritonidis [18], and also Gupta, Laufer, and Kaplan [16],

whose hot wire anemometry measurements at high Re_θ have indicated larger values for the mean streak spacing than the commonly accepted value of $\lambda^+=100$ (Figure 4.2). The experimental technique used by these researchers employs a transverse array of closely spaced probe elements to yield information about the spanwise scale associated with variations in the axial velocity. A possible source of error that the author sees with these probe results is that the high velocity air flows necessary to attain high Re_θ also possess small length scales - some of which may not have been resolvable with the probe spacing used.

The probe array of Haritonidis incorporates 12 separate hot wire elements with an individual on-center spacing of only 1.5 mm, but at

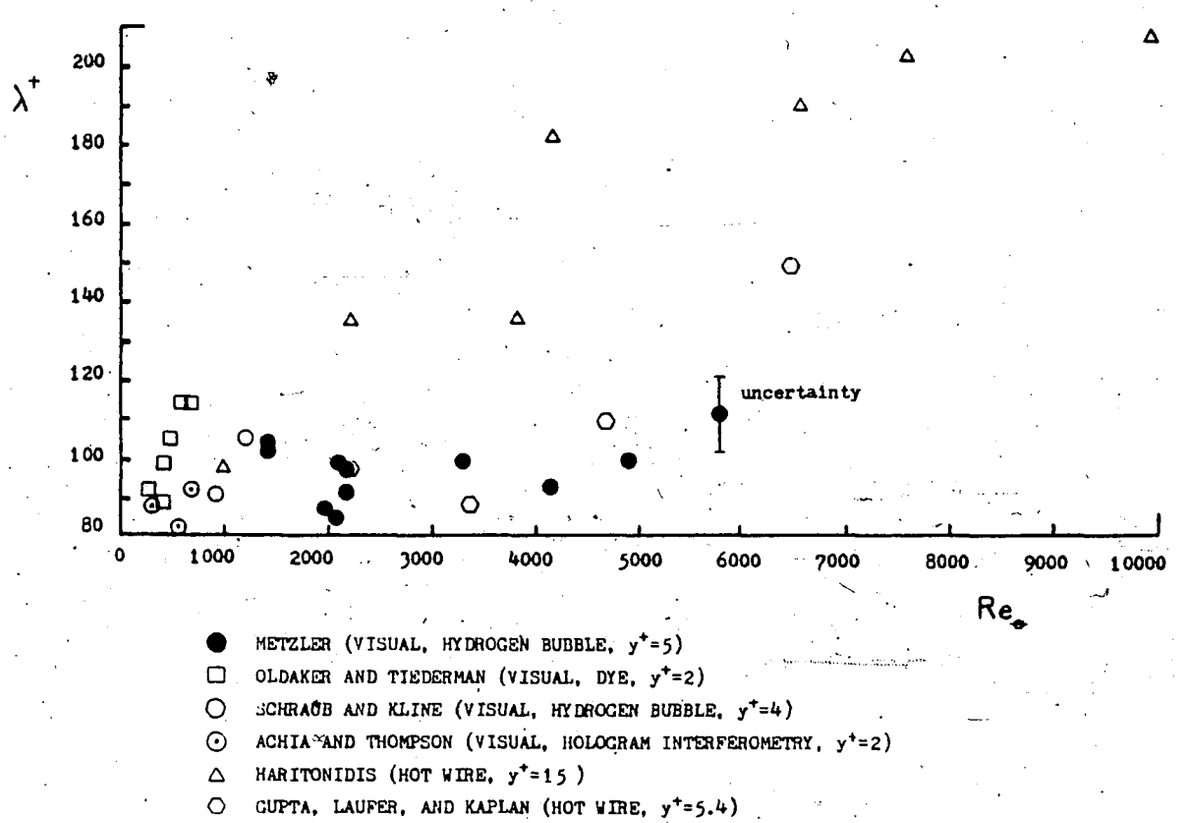

Figure 3.2 Graph of λ^+ vs. Re_θ For Six Separate Investigations.

Re_θ =10000 (his highest velocity flow) this spacing corresponds to a nondimensionalized distance Δz^+=55. This would result in a truncated streak spacing distribution containing no wavelengths less than λ^+_z=110 [3], which in turn would lead to the calculation of a larger mean spacing between streaks. This difficulty was recognized and commented on by Gupta [16], who measured λ^+=151 for Re_θ =6500 using a method similar to that of Haritonidis.

A prior discussion argued the existence of a close relationship between wall shear stress and the spacing between low speed streaks, and speculated that for large Reynolds numbers an asymptotic convergence of the mean streak spacing to an upper bound might occur. An additional hypothesis upon the streaky structure concerns the process described by Lighthill [29] for the generation of spanwise variations in axial velocity at the wall. As discussed in Chapter I, the stretching of the vorticity at the wall caused by an inflow or an outflow (Figure 1.3) gives rise to alternating zones of high and low speed fluid. The scale of these zones is necessarily dependent upon the scale of the fluid movements that cause the stretching.

In a turbulent boundary layer, the transverse extent of the low speed streaks is small compared to that of the high speed regions between them, implying Lighthill's process to be most pronounced for the inflows that create the high speed regions. Assuming that the inflows have a wake layer origin [13], an increase in streak spacing would accompany the increase in scale of outer layer structure that occurs at high Re_θ. However, this implies that a continual and virtually unbounded increase in the streak spacing occurs as the Reynolds number increases; an observation clearly at odds with the former conclusion of

an asymptotic upper limit for λ arrived at through shear stress considerations. The apparent contradiction leads to one further (perhaps tenuous) deduction upon the outer layer structure: That as Re_θ becomes large the outer layer structure consists not of a single zone containing scales of motion the order of the boundary layer thickness, but rather consists of several zones that exhibit graduated scales of motion, including an "inner wake" region that possesses length scales typical of the wake layer for Reynolds numbers far smaller.

III.B. VARIATIONS IN THE STREAKY STRUCTURE WITH DISTANCE FROM A SURFACE

This experiment was designed to examine changes in the spanwise structure with distance from the wall, and to investiage the possible implications of these changes with regard to the bursting event.

Histograms of the nondimensional streak spacing were compiled at six different distances from the wall, for Re_θ =2007. Data was obtained from plan view video footage of a horizontal hydrogen bubble wire. The locations of individual streaks were marked on a transparency, using the same procedure as for the mean spacing. The identification and marking of a streak followed the same constraints as outlined in section III.A. Six different scenes were recorded, starting with the bubble wire located as close to the wall as possible ($y^+ \simeq 1$), then in increments of $5\frac{\nu}{u_\tau}$ out to y^+=25. To allow better resolution of closely spaced streaks, and to obtain a finer "mesh" histogram, the lens magnification used was somewhat higher than for the mean spacing study, with about 5 - 7 streaks appearing in the field of view. The sample for each distribution consisted of $\sim$170 low speed streaks. The mean streak spacing as calculated from the histograms yielded values for λ^+ within 1 - 2% of the values obtained directly from the transparencies.

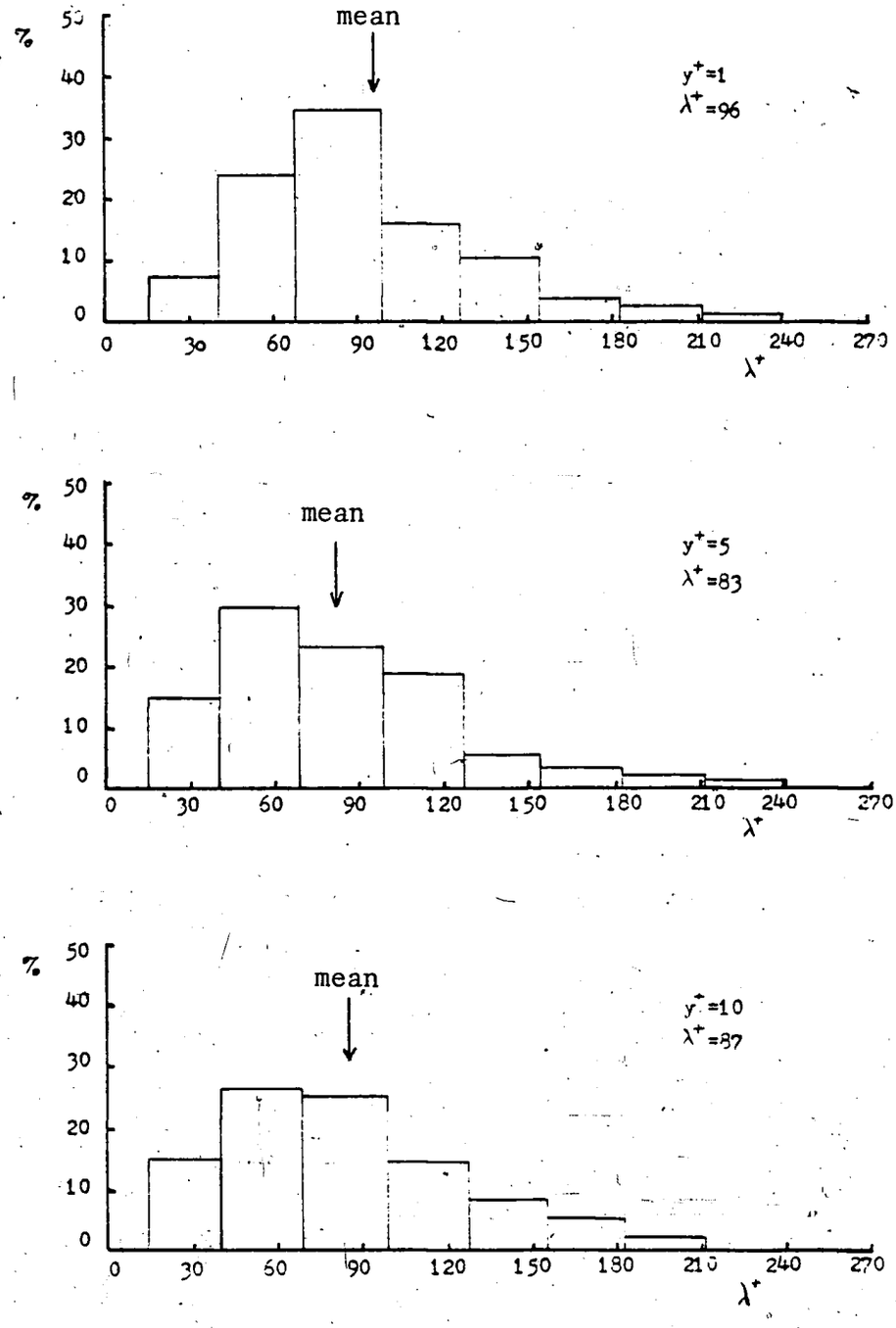

Figure 3.3 Distribution of Streak Spacing at Different Levels Within the Wall Layers, Re_τ =2007.

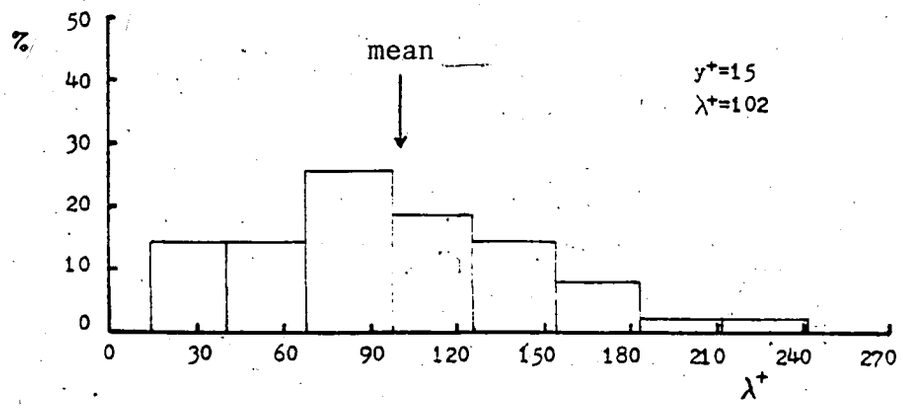
%
50
40
30
20
10
0
mean
y^+=15
λ^+=102
0
30
60
90
120
150
180
210
240
270
λ^+

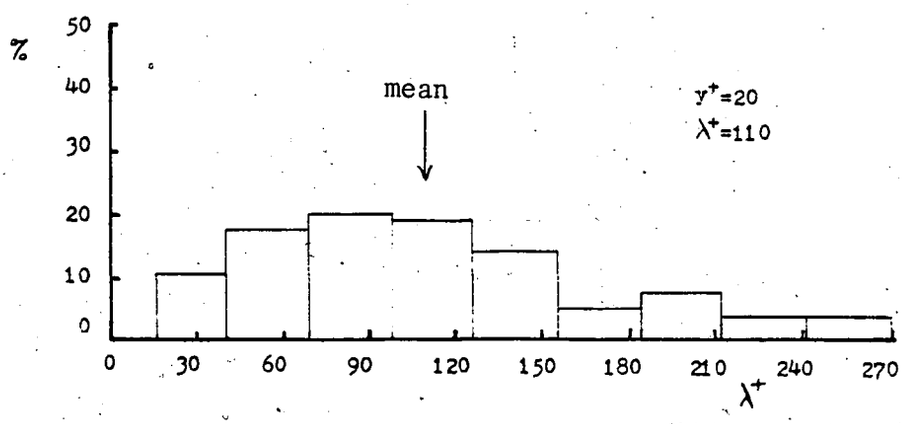
%
50
40
30
20
10
0
mean
y^+=20
λ^+=110
0
30
60
90
120
150
180
210
240
270
λ^+

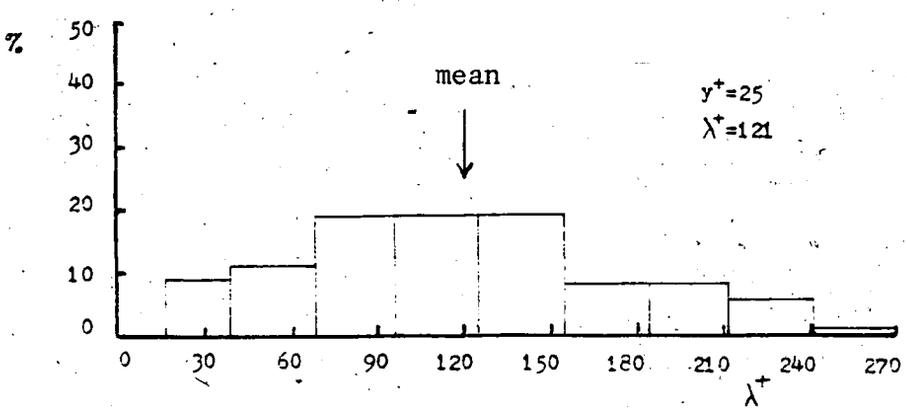
%
50
40
30
20
10
0
mean
y^+=25
λ^+=121
0
30
60
90
120
150
180
210
240
270
λ^+

The two most apparent trends to be observed from the histograms (Figure 3.3) are (1) a broadening of the streak distribution with increased distance from the wall, and (2) a skewness toward values lower than the mean which is particularly pronounced at y^+=5, 10, and 15.

A fairly uniform spanwise spacing close to the wall results in a distribution peaked about the mean; transverse movement, merging, and the apparent disappearance of slow speed streaks all contribute to the subsequent broadening of the distribution to both smaller and larger scales as the distance from the wall increases.* In the region of $5 \leq y^+ \leq 15$, the somewhat skewed appearance of the distribution reflects a tendency for two or more streaks to assume a small transverse spacing, an event that for $y^+ > 10$ often resulted in a temporary merging of the streaks. This aspect will be discussed subsequently.

Variations in the mean streak spacing with distance from the wall (Figure 3.4) were found. At y^+=5 and 10, the values for λ^+ are depressed from that at the wall (y^+=1), while at y^+=15 λ^+ increases back to the wall value. The small mean spacing obtained at y^+=5 and 10 appeared to result from the presence of transient streaks of a short streamwise length which existed in addition to the "established" pattern evident throughout the region $0 \leq y^+ \leq 25$. Further increases in λ^+ are observed at y^+=20 and 25. These variations do not necessarily imply a larger physical spacing, but may be accounted for by differences in streak behavior observed at different levels.

*Calculated from the histogram data, the ratio of the standard deviation to the average streak spacing is σ/λ =.44 at y^+=1, and σ/λ =.59 at y^+=15. For comparison, Oldaker and Tiederman [35] measured σ/λ =.36 at $y^+ \simeq 2$ using dye injection.

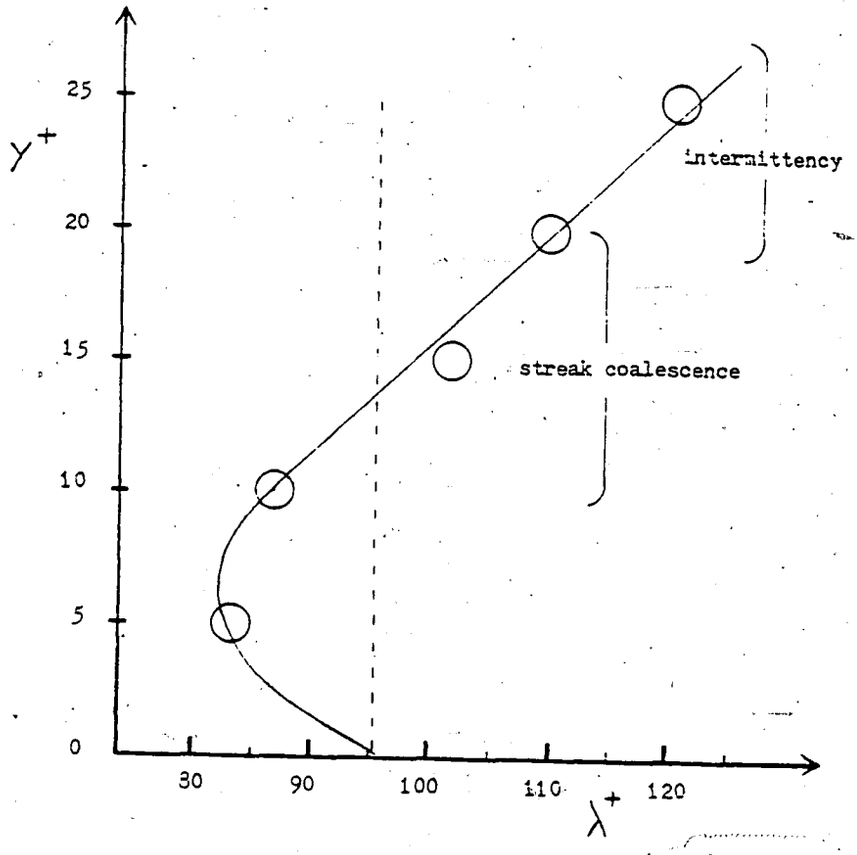

Figure 3.4 Variation of λ^+ With y^+, and Observed Streak Behavior

A larger relative streak spacing results from a lower number of streaks being counted per unit width. Contributing to this effect is the merging of two or more streaks, a phenomenon that was observed to occur more frequently in the region $10 \leq y^+ \leq 20$ than elsewhere. Another phenomenon which resulted in a lower number of streaks being counted was the apparent disappearance and reappearance of single streaks. This intermittency was most often observed for $y^+ \geq 20$ and appeared to result from "humps," or undulations, in the upper edge of the region of low speed fluid defining a streak (Figure 3.5). While sharply defined

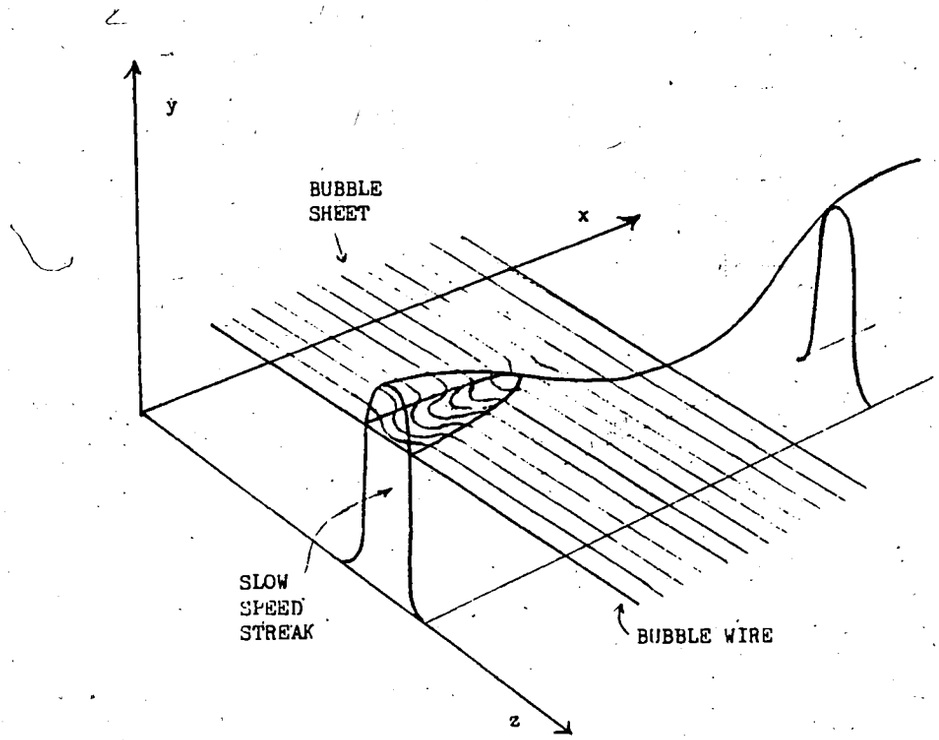

Figure 3.5 "Undulations" of a Streak Giving the Effect of Intermittency When Visualized With a Fixed (Horizontal) Hydrogen Bubble-Wire.

filaments of low speed fluid with a typical streamwise extent of $\Delta x^+ > 1000$ appear for $y^+ < 5$ (measured both from the video screen and from direct observation of dye traces at the wall); for $y^+ > 5$ this pattern becomes increasingly disrupted and intermittent as distance from the wall increases. At $y^+ \simeq 20$ the length of the low speed streaks visualized by the bubble wire is only of the order of their spanwise spacing, i.e. $\Delta x^+ \simeq 100$. The shorter streamwise length did not appear to be the result of the actual destruction or elimination of the streaks, but seemed to be a manifestation of a rapid transverse shifting of the low speed fluid, and the intermittency resulting from vertical undulations of the interface defining the "top" of a streak.

An observation regarding the transverse shifting of streaks is that in a stationary frame of reference, abrupt transverse motion appears more pronounced for slow speed streaks than for the wider high speed regions between them. Regardless of the source or nature of the disturbance causing the transverse movement, lateral velocities resulting from that disturbance will be comparable for adjacent low and high speed regions, but because of the smaller axial velocity of the low speed streaks, their displacement as seen from an Eulerian frame will involve larger angles of deviation from the streamwise direction. Through continuity this behavior has the effect of forcing high speed fluid to ride up and over, or around and otherwise through, the low speed zones representing the streaks, giving rise to potentially unstable configurations. Attention will be called to this effect later in Section III.C., in reference to the bursting phenomenon.

Though fragmented in appearance, the streaky structure at $y^+ \geq 15$ displays signs of continuity. As viewed in the (stationary) reference frame of the hydrogen bubble wire probe, a coalescence or merging of several streaks was a temporary event, the termination of which was often marked by what seemed to be a reappearance of the old constituent streaks in their original locations prior to the coalescence. Thus, only part of the streamwise length of a given streak appeared to be involved in the merging. Figure 3.6a-c is a picture sequence of such an event; it shows three low speed streaks in the process of coming together and merging, then resuming their former positions. It is hypothesized that the streaks, appearing as manifestations of the mechanism that produces them, are perhaps not as long-lived and continous as that mechanism.

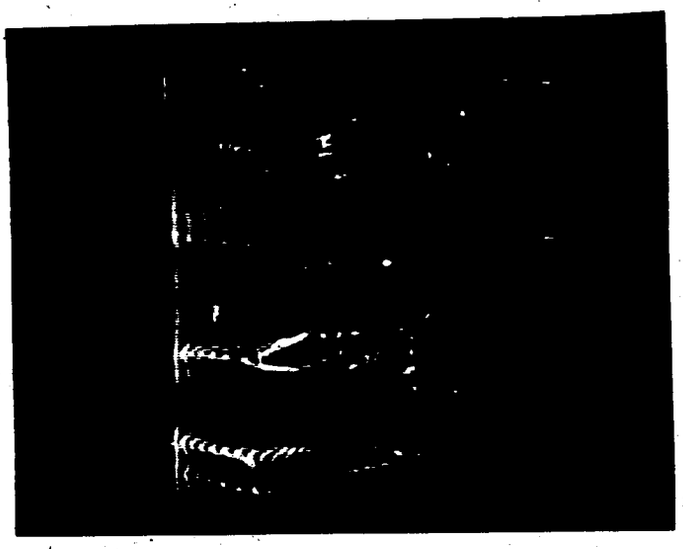

(a)

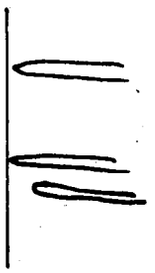

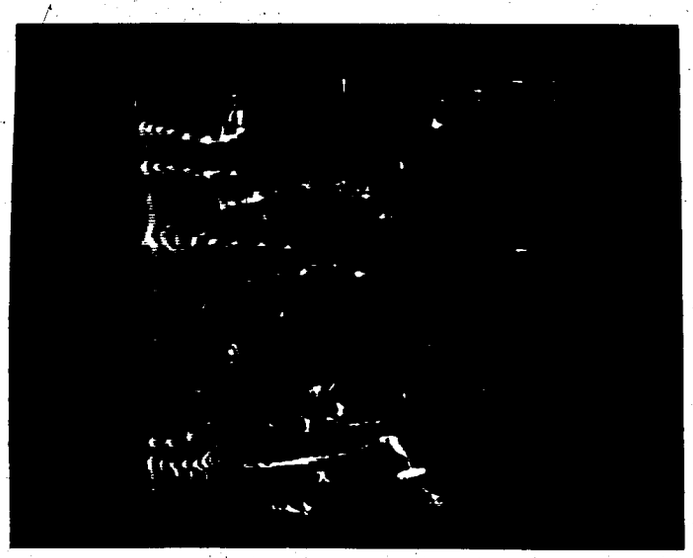

(b)

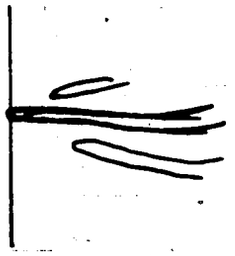

(c)

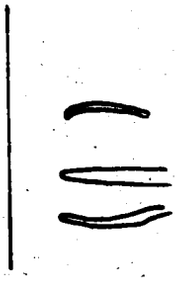

Figure 3.6 Merging sequence for $y^+=20$, $Re_\theta=1973$. Scale: 1 cm=90 $\frac{\nu}{u_\tau}$

(a) three separate streaks about to merge
(b) merging has occurred
(c) streaks are separating

The existence of a continuous streak generation mechanism is further evidenced by the repetition to be found in the marked transparencies used for determination of the streak spacing distributions. In Figure 3.1 it may be observed that individual marks denoting the spanwise location of a streak are often unchanged for four or even more consecutive scenes, which implies that the low speed region persisted for that entire time period. Using the expression $\frac{T_B U_\infty}{\delta} = 5$ for the bursting frequency based on outer variables, this corresponds to a time duration $\Delta t = 4\text{-}5T_B$.

A further investigation of streak longevity was carried out through an experiment that capitalized upon the observation that stray particulate matter on the channel bottom appeared to resolve itself into long streamwise aggergations. A formal approach involved the injection via syringe of a thin slurry of 125 μm glass beads* into the boundary layer, similar to a procedure used by Grass [15].

Within a few seconds after injection the beads collected into streamwise concentrations of width $\Delta z^+ \simeq 35$, that extended essentially uninterrupted the length of the channel with a nearly uniform spanwise spacing of $\Delta z^+ = 80$. This pattern appeared stable and stationary, with the only movement being a quasi-periodic buffeting and a gradual downstream migration of the beads. Further investigation with a horizontal hydrogen bubble wire disclosed that the bead concentrations coincided with the zones of low velocity, or streaks (Figure 3.7ab), and

p. 64

*Specific gravity $\gamma = 2.48$, with 125 μm corresponding to an approximate diameter of $1.8 \frac{\nu}{u_\tau}$.

that bead movement occurred principally in response to localized "sweeps" of high speed fluid which had a buffeting effect on the bead concentration.

Grass, using particles of a slightly smaller diameter and lower specific gravity (100 μm sand), reported similar sweep-type events, but his pictures do not suggest the stationarity of the streaky structure observed in the present experiment. Since the beads used were not light enough to move freely with small velocity fluctuations, the results of this experiment should be interpreted with some caution. While it is possible that the bead concentrations tended to give the "mean" locations of very long, naturally occurring slow speed streaks, it is more probable that the wakes induced by the streamwise aggregations of the beads acted to cause their further concentration downstream. The coherent streamwise length of the patterns thus formed carries important implications for the model of wall layer flow to be presented in Section IV. These results also have a direct bearing on the nature of an experiment that is described in Section III.D.

The overall picture to be had of the streaky structure is of narrow, verical bands of upwelling low speed fluid that occupy the zone of highest shear within the boundary layer. The interface between high and low speed fluid that defines the "side" of a streak constitutes a vertical, convoluted sheet of strong vorticity ($\tau_{yx} \simeq .21 \tau_{wall}$)* that becomes increasingly subject to deformation as distance from the wall is increased. The outer parts ($15 \leq y^+ \leq 25$) of this structure appear

*The strain rate $\frac{\partial u}{\partial z}$ was determined from the video screen by noting the streamwise deformation of horizontal hydrogen bubble lines, and the time and transverse distance over which it occurred.

intermittent, but are in fact the fragmented traces of a remarkably persistent and continuous structure below.

III.C. SPLIT-SCREEN ORTHOGONAL VIEWS OF A HORIZONTAL BUBBLE WIRE IN BOTH STATIONARY AND CONVECTED FRAMES OF REFERENCE

To gain insight into the three-dimensional aspects of the wall layer flow, an approach utilizing the split-screen capabilities of the video system was employed, with cameras recording simultaneous side and plan views of a horizontal hydrogen bubble-wire (Figure 3.8). A slightly oblique positioning of the side view camera at a small downwards angle (7° - 9°) yielded a perspective of the horizontal

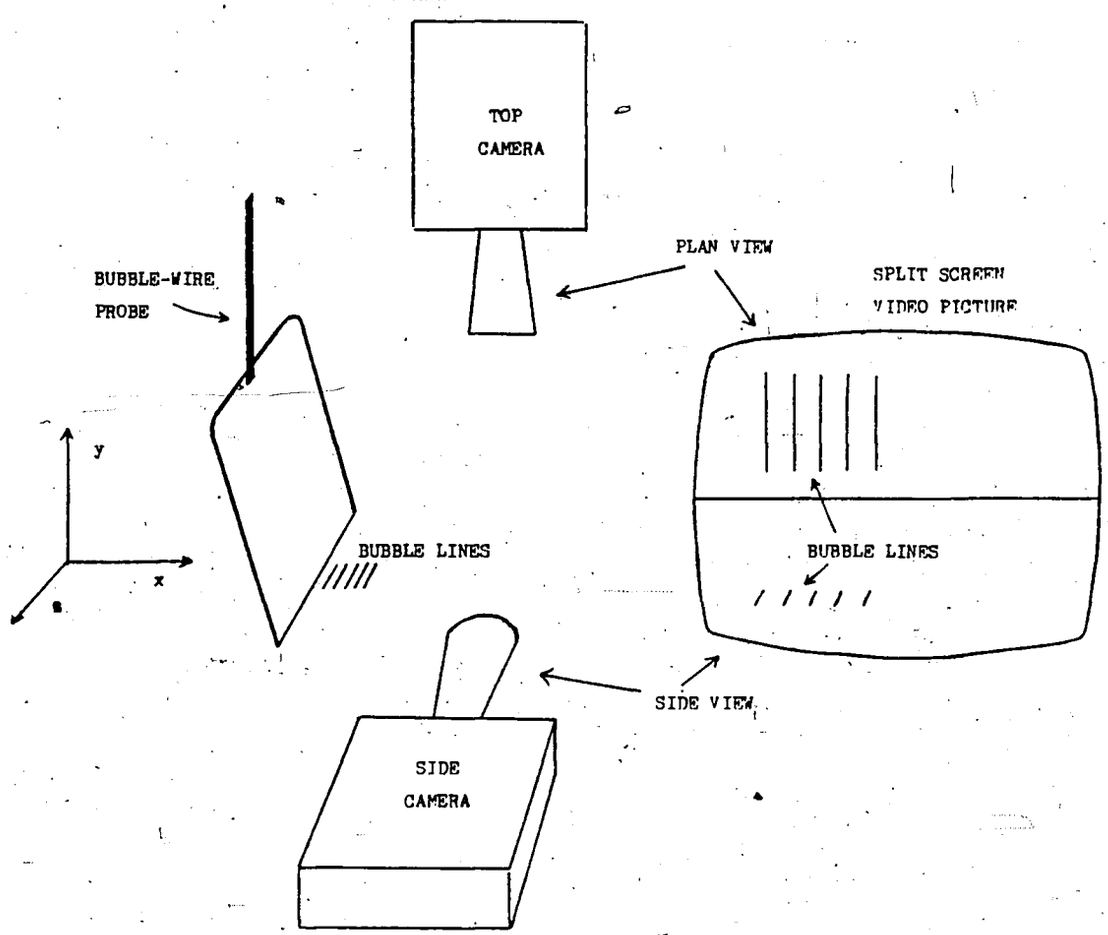

Figure 3.8 Diagram of the Views Obtained With the Video System in a Split-Screen Mode.

bubble wire improved over that which would be obtained if the line of sight was parallel to the wire. A moving frame of reference was utilized in some instances to allow a given convected flow structure to be kept within the field of view for a longer time - this approach emphasizes the presence of fluctuations normal to the mean flow.

As pictured in Figure 2.1, both cameras and the bubble wire probe were mounted to a traversing platform above the flow channel. The cameras were carefully adjusted to obtain equal magnification scales and coincident streamwise fields of view. The recording of a short sequence with a calibrated scale placed in the field of view served as verification of a good scene "match-up."

A problem that inevitably accompanies use of the split screen is the difficulty in identifying the same spanwise location in the side and plan views. One approach to this problem involved knotting the bubble wire at one point, which produced a bubble trace that could be followed in both views. However, in practice this technique was difficult to apply since the limited depth of field of the video cameras results in a side view of the horizontal bubble sheet that is mostly blurred. The present technique eliminates this problem by insulating all but a one centimeter span of the bubble wire, thus producing a narrow bubble sheet that is entirely within the viewing depth of field. For the flows examined, the width of this bubble sheet was of the order of one streak spacing ($\Delta z^+ \simeq 110$). This approach permits (1) a direct association to be made between the plan and side views, and (2) all bubble lines produced to be kept in focus.

Convection velocities of the wire were varied from $U_c = .35 - .46U_\infty$, with U_c increasing as distance from the wall was increased. Due to the

decreased flow velocity over the wire and the increased thickness of the insulated portion, some vibration through vortex shedding was encountered when using a moving reference frame. This caused the quality of individual bubble lines to suffer, but for the results presented this was not crucial.

From the side view, the most important flow feature appeared as a loop-like concentration of vorticity being shed from a low speed streak (Figures 3.9, p. 60, and 3.10 abc). This was observed at all bubble wire locations from $y^+=1$ to $y^+=35$. Figure 3.11 is a sketched representation of this flow structure. The vorticity associated with the upstream-pointing legs is oriented similarly to that of the counter-rotating vortices discussed earlier in conjunction with streak formation. The head of the loop appears as a transverse vortex aligned with the mean strain.

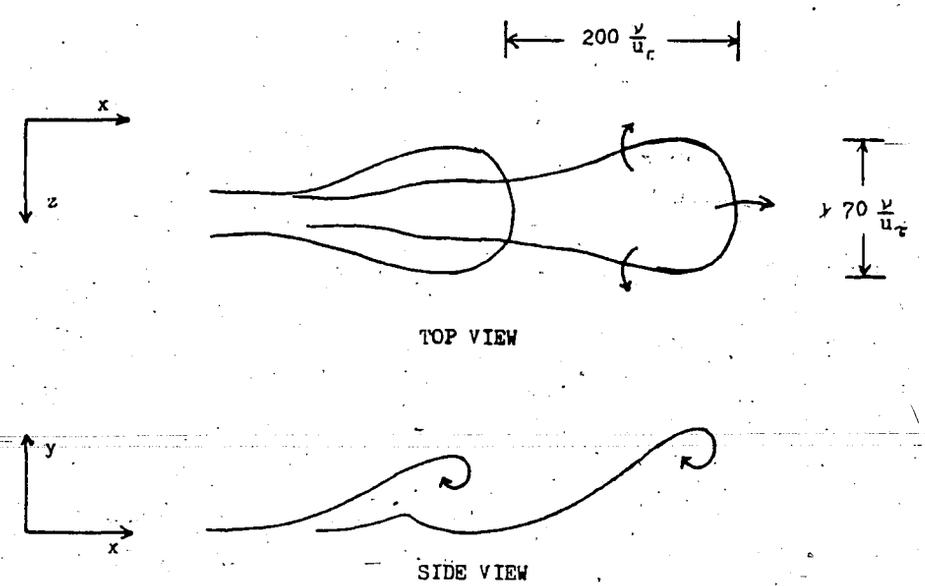

Figure 3.11 Sketch of Loop Vortex, and Average Dimensions.

Velocity characteristics of the loops were measured from video footage of a horizontal bubble wire in a stationary frame of reference.

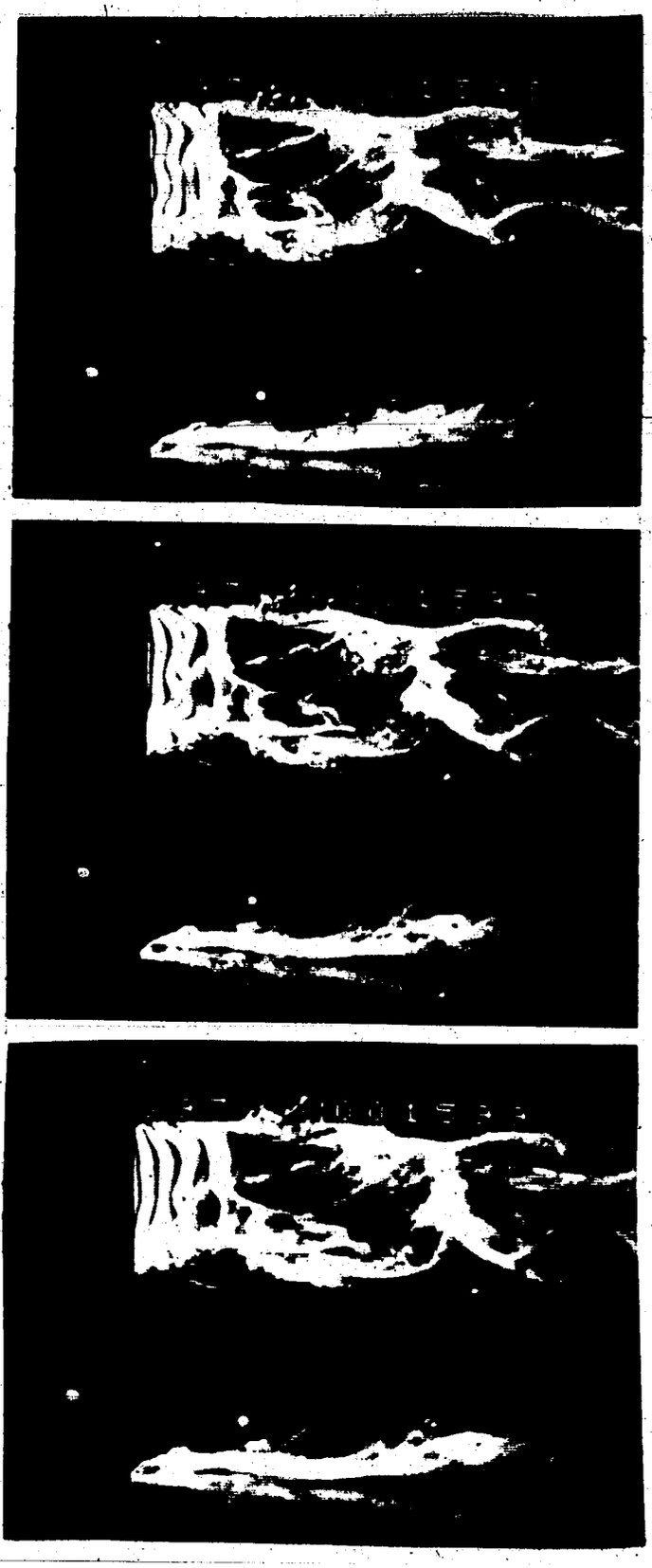

(a) $t^+=0$

(b) $t^+=2$

(c) $t^+=4$

Figure 3.10 Combined side/plan view of vortex loops
$y^+=5$ $Re_\theta=1910$ scale 1 cm=58 $\frac{\nu}{u_\tau}$

The split-screen view of a narrow sheet of bubbles permitted the accurate observation of individual structures. As described in Section III.A., physical distances were taken from the screen using a scale factor, and time intervals were obtained using the camera framing rate. The trajectories of individual loop "heads" typically did not contain a substantial upwards component until reaching $y^+ \simeq 15$. Locating the bubble wire at $y^+=15$ resulted in loop head trajectories that attained an average height of $y^+=78$ after travelling a distance $\Delta x^+=377$ downstream. At $y^+ \simeq 40$, the streamwise convection velocity was $U_c=13.1\ u_\tau$, and the upwards normal component was $v'=2.2\ u_\tau$. The former value (U_c) is close to that measured by Kline et. al [24] for the convection velocity associated with the ejection phase of his bursting cycle - $13.8\ u_\tau$ at $y^+ \simeq 40$.

As observed in plan view, loop formation invariably seemed to originate as a slow speed streak was deformed through transverse movement into an elongated "S" shape. Figure 3.12 is an illustration from Kim [21] of what he terms the "wavy mode" of streak oscillation, and a comparison of his sketch with Figure 3.9 reveals that it is essentially the same phenomenon. (The more symmetrical appearance in plan view of the loop shedding sequence in Figure 3.10 was a far less frequent occurrence; a possible relationship between the two modes will be explored subsequently).

A similar phenomenon may be observed in Figure 1.5 ab (Page 16) in which vortex loops are periodically shed from a small (1.1 cm) hemisphere placed in a laminar boundary layer. This periodicity is also observed in the turbulent boundary layer, where discrete arrays of typically 3-5 loop-like ejections are observed, with an average spacing

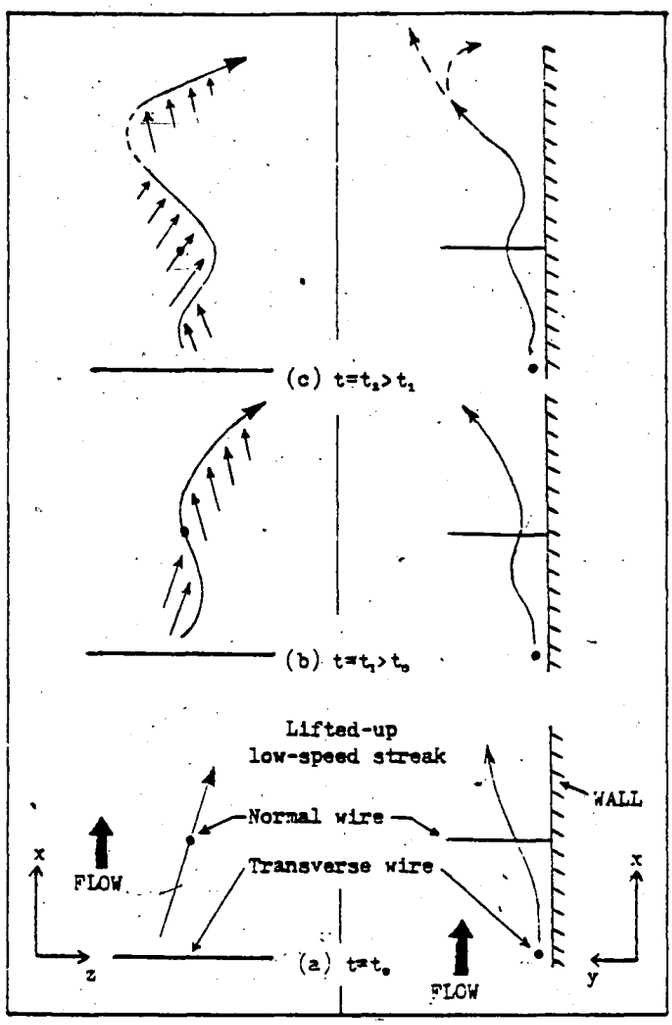

Figure 3.12 Streak Oscillation Occurring in Conjunction With Loop Formation (after Kim [19]).

between loops of $\Delta x^+ \simeq 200$. Large loops are separated by spacings larger than the mean. Separate arrays of loops appear at time intervals between the arrays commensurate with the empirical expressions for the bursting frequency based on inner variables ($f^+ = \frac{fy}{u_\tau^2} = .005$), or outer variables ($\frac{U_\infty T_B}{\delta} = 5$), which for moderate Reynolds numbers are nearly coincident.

An interpretation of what is taking place begins with the observation made in Section III.B., of the low speed streaks being more prone than the high speed flow between them to respond to disturbances producing transverse movement. When deformation of a streak occurs, it has the effect of obstructing the adjacent high speed flow, which must ride up and over the slow speed fluid. It is hypothesized that discrete flow structures (vortex loops) are formed when concentrations of vorticity are shed from the shear layer existing between high speed fluid and a slow speed streak undergoing lateral deformation. The zones of concentrated vorticity thus shed may result from a Kelvin - Helmholtz type instability of the high/low speed interface, the wavelength of which would be the distance between the individual vortex loops of an array. This is probably the wavelength discussed by Blackwelder [4] and mentioned in Section I in reference to a potential bursting mechanism.

It was observed in the present investigation that the structures associated with the ejection event displayed a wide variation in their appearance. Although this is in part due to the stochastic nature of the flow, it was also observed that small changes in the height at which the bubble wire intersected a given structure had a large bearing on the features emphasized. For example, to be well defined and discernible in both side and plan views, it was necessary for a loop vortex to begin its formation essentially at or slightly downstream of the bubble wire. Loops formed upstream of the wire usually preserved their characteristic appearance in side view, but because the heads of the loops lift away from the wall and convect over the bubble wire, the transverse vorticity defining the heads is unmarked.

A good example of how similar flow structures can appear quite different, even when visualized by the same means, can be had by comparing Figure 3.9 with Figure 3.10, which are both pictures taken from stationary reference frames of vortex loops convecting downstream. Figure 3.9 is of a loop formed upstream of the wire, and, as just described, the plan view does very little to suggest the presence of a loop vortex. This picture is typical of most of the events observed involving the passage of loop-like ejections, which without the side view would have been undetectable. (This possibly explains the failure of previous investigations to observe the presence of arrays of loops, as their identification without two simultaneous perspectives is at best difficult). Figure 3.10 also depicts the passage of a loop vortex, but unlike the former picture, structures of a loop-like form are clearly evident in the plan view. It is believed that this is due to the bubble wire being (fortuitously) located just upstream of where loop formation occurred, so that the complete structure is marked. This comes about because the nascent structure is initially at or below the level of the bubble wire; the head of the loop in Figure 3.9 has already lifted away from the wall and above the wire, and therefore only a lower horizontal cross-section of the structure is visualized. A previous observation should be recalled at this point; that a substantial upwards component of velocity of the loop heads was not evident for $y^+ < 15$. The ejection of structures as visualized by a wire located at $y^+ = 1$, 5, and 10 was typically preceded by a gradual outwards drifting of the marked fluid. With the horizontal wire located at $y^+ = 15$, substantial displacements occurred immediately downstream of the wire.

Recalling from Section III.B., that a streak as viewed from a stationary frame of reference may persist for times as long as $4\text{-}5T_B$, it is apparent that a given streak may involve the generation of several loop arrays. As discussed below, this observation may explain the great streamwise length of the streaky structure.

The upstream-pointing legs of a vortex loop involve streamwise vorticity which tends to be stretched as the loop is ejected from the wall and accelerated. An augmentation of the streamwise extent of the streak may occur when fluid is pumped up between the legs of the vortex as it convects downstream. The passage of more than one loop, as in the arrays of loops observed, merely enhances the process. Substantiation for this hypothesis may be found in the similar flow patterns observed downstream of a hemisphere in the experiment just mentioned. Figure 3.13a is a picture taken 40 diameters downstream of the hemisphere, of a horizontal bubble wire. The wire is located at a height (y=0.1 mm) that intersects the legs of the periodically shed loops, as sketched in Figure 3.14. The streamwise location of the wire

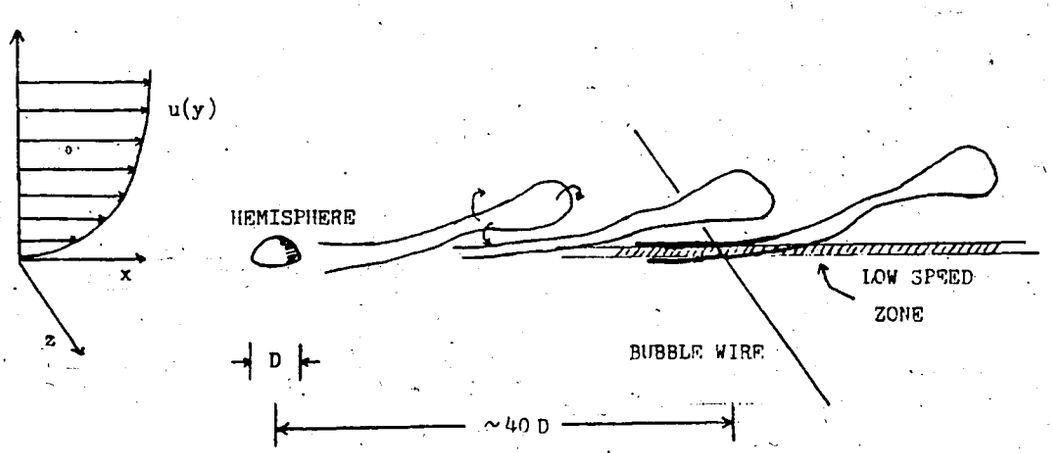

Figure 3.14 Prolonged Region of Velocity Defect Downstream of Hemisphere.

is beyond the point where wake effects should be significant, yet a narrow zone of low speed fluid exists. It appears that the streamwise vorticity contained in the legs of the loops acts to pump low speed fluid up from the wall, thereby extending the region of velocity defect downstream. The bifurcations branching off from the low speed zone appear to be manifestations of the vortical legs of the loops - in a turbulent boundary layer, similar bifurcations with a spacing comparable to that between individual loops may be seen on the sides of low speed streaks (Figure 3.13b). It is believed that the above mechanism constitutes the process by which the streaky structure is perpetuated in a turbulent boundary layer: Loops shed from a low speed streak undergo streamwise acceleration as they rise from the wall, with a consequent stretching and intensification of the axial vorticity contained in their legs. A reinforcement and continuation of a low speed streak results when fluid is pumped up between the stretched, counter-rotating legs of the shed vortex loops.

Evidence for such an effect may be seen in the split screen sequence of Figure 3.15, which shows a horizontal bubble wire located at $y^+=15$ in a moving frame of reference. The interior of the bubble sheet produced is being lifted up and to either side to form a clear, bubble-free region. This formation process is observed to be the result of a revolving motion that embodies counter-rotating streamwise vorticity of the same orientation as the legs of a vortex loop. The vortical appearance ($+\omega_z$) of the bubble concentration defining the upstream edge of the bubble-free region is a result of the convection velocity of the bubble wire being greater than the streamwise velocity of the upwelling, unmarked fluid.

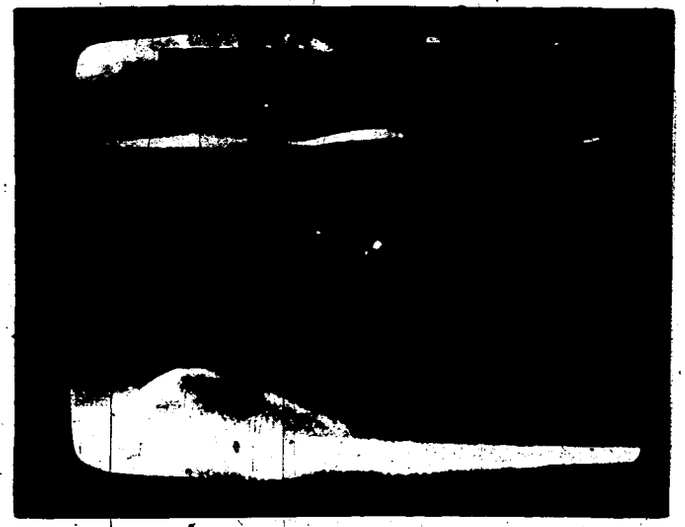

(a)

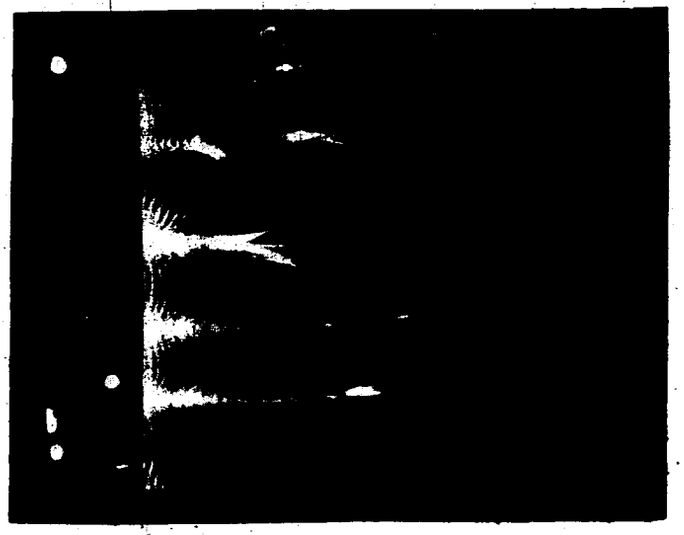

(b)

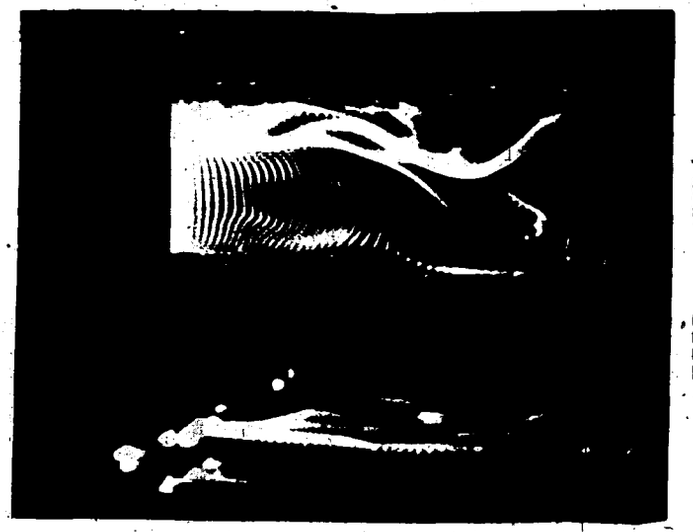

Fig. 3.12 Streak deformation occurring with passage of loop vortex.

$y^+=15$ $Re_\theta=1910$ scale 1 cm=68 $\frac{\nu}{u_\tau}$

Fig. 3.13a Zone of velocity defect $\Delta x \sim 40$ D downstream of hemisphere.

$y_{wire}=1$ mm $U_{local}=.12$ m/s 1 cm=68 $\frac{\nu}{u_\tau}$

b "Branching" of low speed streaks.

$y^+=6$ $Re_\theta=1430$ scale 1 cm=150 $\frac{\nu}{u_\tau}$

(a) $t^+=0$

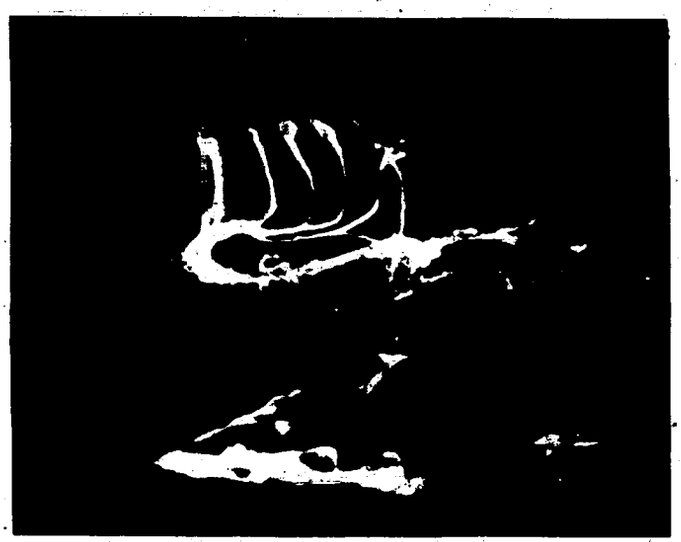

(b) $t^+=9$

(c) $t^+=17$

Figure 3.18 Sequence from a convected frame of reference showing upflow between the legs of a vortex loop. $U_c=.36\ U_\infty$ $y^+=15$ $Re_\theta \simeq 1900$ scale 1 cm=64 $\frac{\nu}{u_\tau}$

It is speculated that the flow pattern shown in Figure 3.15 is the visual evidence produced by a vortex loop already formed and convecting downstream, as sketched in Figure 3.16. Upstream of the

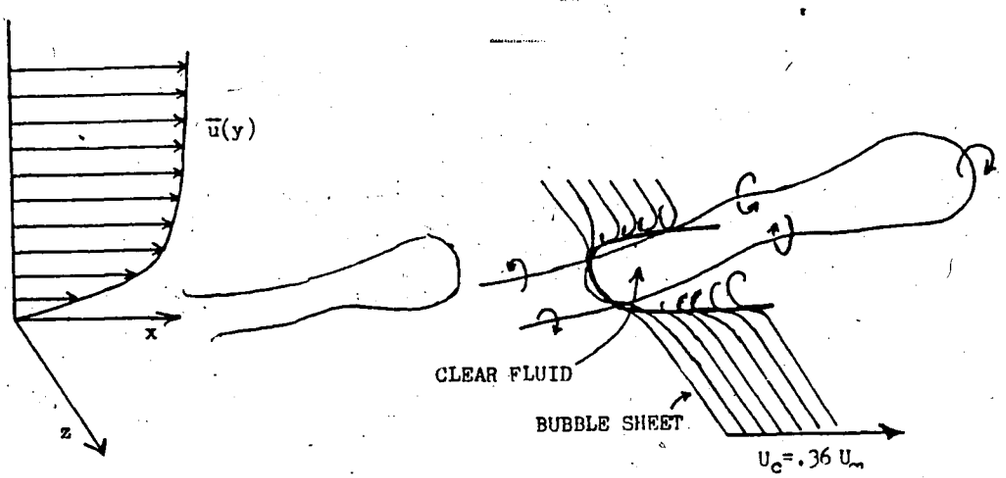

Figure 3.16 Bubble-Free Region Created by Passage of Vortex Loop. Trailing Legs of Loop Clear Out U-Shaped Region in Bubble Sheet.

bubble wire, a vortex loop is shed from a low speed streak. The head of the loop rises from the wall as it convects downstream, and the ensuing acceleration results in an intensification of the vorticity contained in the legs through stretching. This has the effect of increasing the upward flow of fluid between the legs of the loop, so that shortly after they intersect the horizontal bubble sheet the fluid between them has been replaced by clear, unmarked fluid from below the sheet. This is essentially a recapitulation of the process just described that was hypothesized to give rise to the great streamwise length of the streaky structure; the upwelling of fluid that occurs between the legs of the loops as they convect downstream results in the reinforcement and continuation of the low speed streak from which the loops were shed.

An interesting effect was made observable in this experiment because of the short spanwise length of the uninsulated portion of the bubble wire. Lateral velocities in the z direction could be detected by noting movement of the edges of the narrow (horizontal) bubble sheet produced; an effect similar to that obtained when using the combined-time-streak marking method employed by Schraub and Kline [41].

The presence of a low speed streak within the bubble sheet was accompanied by an inwards spanwise movement of the edges of the sheet, signifying inflows from either side (Figure 3.17a). Similarly, when the bubble sheet revealed a high speed "streak," or region, an outwards spanwise movement of the edges indicated a flow towards a low speed region (Figure 3.17b). Because the spanwise displacements were small, exact values for the transverse velocity (w') were not obtained, but in relative terms the effect illustrated in Figure 3.17 seemed most pronounced for $y^+ < 15$. Since the low speed streaks constitute regions of outflow, continuity demands the presence of such cross flows, especially in the vicinity of the wall.

The foregoing observations on the streaky structure are in essential agreement with work done by Bakewell and Lumley [2], who carried out hot-film space-time correlation measurements of the streamwise fluctuating velocity. From their measurements they were able to construct a qualitative picture of the streamlines associated with a low speed streak; Figure 3.18 is a depiction of the streamlines as viewed from an end-on perspective. The diagrammed streamlines appear consistent with the flow patterns revealed in the picture of Figure 3.17ab taken at $y^+=10$; readily apparent in both pictures is the presence of cross flows.

Fig. 3.7a $y^+=13$ $Re_\theta=2257$ scale 1 cm=80 $\frac{\nu}{u_\tau}$

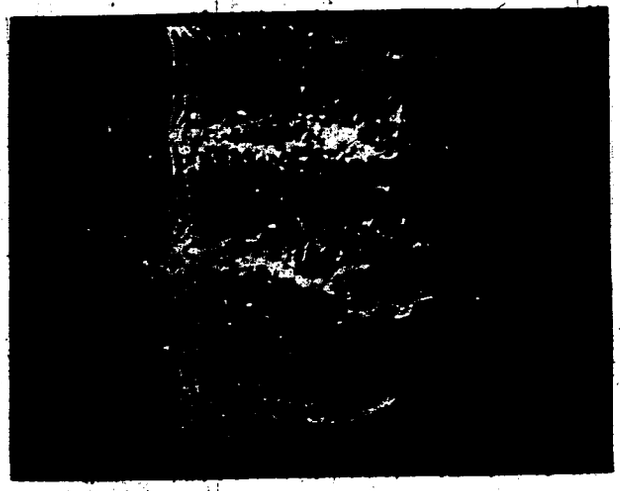

Fig 3.7b $y^+=7$ $Re_\theta=2074$ scale 1 cm=86 $\frac{\nu}{u_\tau}$

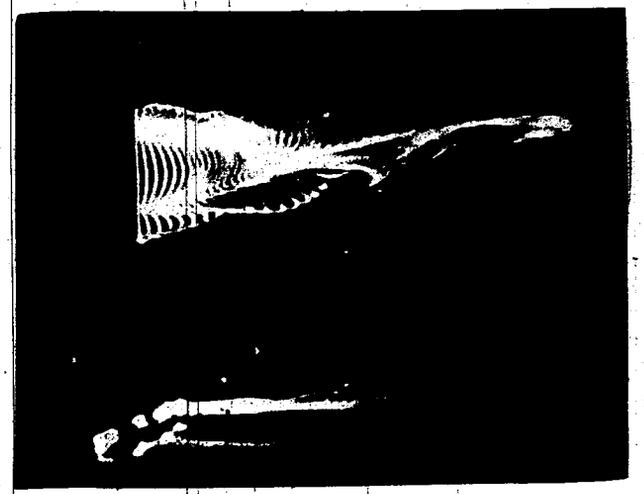

Fig. 3.8a Low speed streak within bubble sheet, $y^+=10$, $Re_\theta=1910$, scale 1 cm=68 $\frac{\nu}{u_\tau}$.

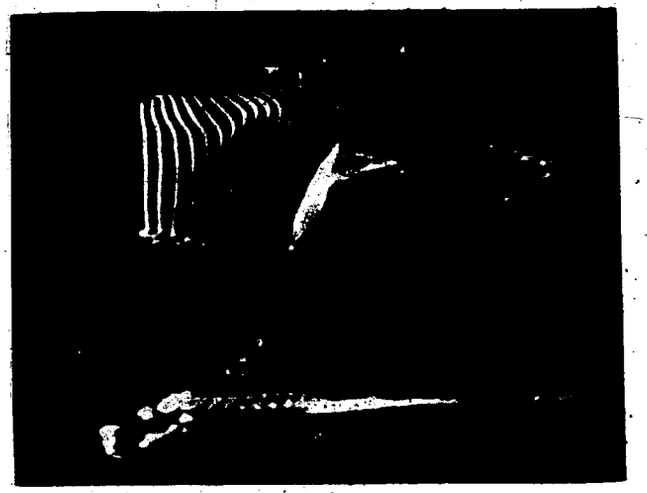

Fig. 3.8b High speed region within bubble sheet, $y^+=10$, $Re_\theta=1910$, scale 1 cm=68 $\frac{\nu}{u_\tau}$.

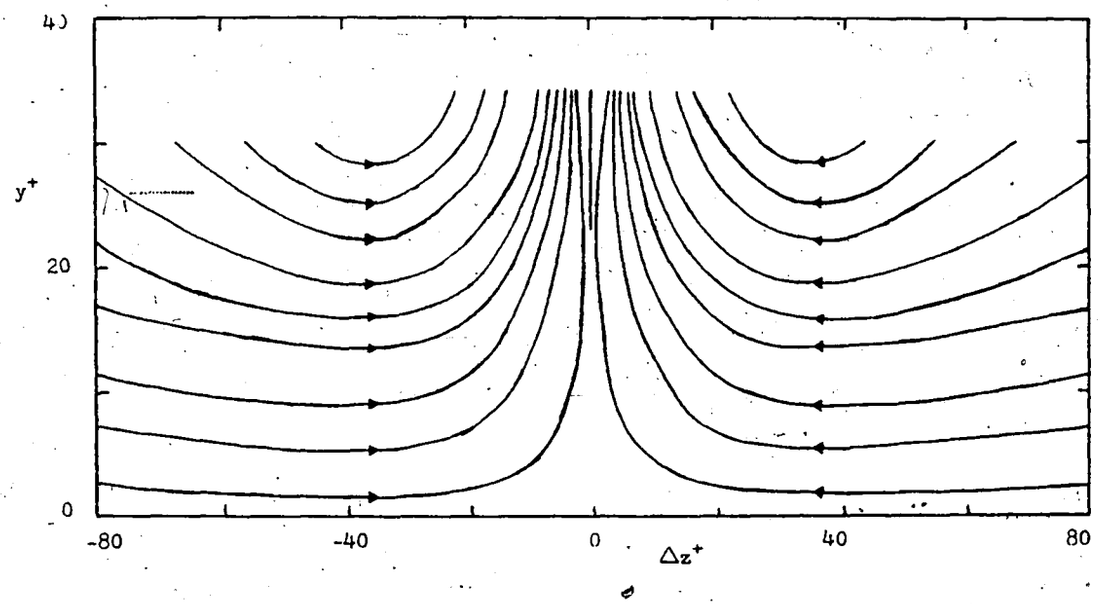

Figure 3.18 Cross-Sectional View of the Streamlines Occurring With a Low Speed Streak (after Bakewell and Lumley [2]).

An additional point of similarity is a vertical component of velocity more pronounced for Figure 3.17a (upwards) than for 3.17b (downwards), consistent with the streamline mapping that shows suppressed downflow close to the wall for $y^+ < 15$.

Comparisons may also be made with Figure 3.15abc. The moving frame of reference that was utilized for the picture sequence gave time for marked fluid between the counter-rotating legs of the vortex loop to be entirely replaced with clear fluid, creating a bubble-free region. Had a stationary reference frame been used, the clear region would have appeared as an ordinary low speed streak.

This discussion serves to underscore the point that caution must be exercised in the analysis and interpretation of visualized flow patterns, as the visual evidence produced by a given structure is

strongly dependent upon which part of the structure is being visualized, its stage of development or age, and also the reference frame used.

III.D. BOUNDARY LAYER MANIPULATION

In this experiment an attempt was made to alter the rate of momentum transfer within the boundary layer by artificially producing a change in the wall layer structure. Efforts to control turbulence levels through the use of various surface modifications have been made in the past. Liu, Kline, and Johnston [30] attempted to achieve a decrease in drag through the deployment of longitudinal strips of a varying height and transverse spacing. In the water flow used for their investigation, the height $(k^+)^*$ of the roughness elements was varied from $k^+=11$ to $k^+=112$, while their transverse thickness was $\Delta z^+=22$ and the streamwise length $\Delta x=1$ m. They measured the frequency of wall layer bursting events, and found that the effect of the longitudinal strips was to slightly decrease the bursting frequency (and mean wall shear) when the spacing between strips was greater than $2\lambda_{streak}$. The opposite effect occurred for transverse spacings of the order of the streak spacing and was most pronounced for $k^+=45$. As their primary concern was to achieve a decrease in the wall shear stress, they did not appear to attach any significance to the higher bursting frequencies observed in conjunction with the smaller transverse spacing, nor did they attempt to interpret in physical terms the changes in bursting frequency.

*Roughness height k nondimensionalized on the viscous length $\frac{\nu}{u_\tau}$.

Bushnell [8] conducted experiments in drag reduction that were concerned chiefly with creating changes in the outer layer structure. Some of the experimental configurations resulted in a small decrease in the wall shear while others resulted in a net increase; however, the surface projections used were of a large physical size (one exception will be discussed later).

In an approach similar to that of Liu, Kline, and Johnston, the present investigation is based on the premise that it is the wall layers that play the dominant role in the creation and maintenance of the turbulent boundary layer (see Section I.D.). Because of the small vertical extent of this region, the surface projections or roughness elements needed to effect a change within it are of a correspondingly small size.

A possible mechanism giving rise to the regularity and streamwise coherence observed in the wall layers has been discussed in the preceding parts of this chapter. Manifestations of such a mechanism are to be seen in experiments already reported in this investigation - for example, the long streamwise aggregations that occurred when small glass beads were injected into the flow, and the prolonged region of velocity defect observed downstream of the hemisphere. Accordingly, the form of surface modification employed in this experiment attempts to capitalize upon the processes believed to occur in conjunction with these phenomena.

Thin brass rods were secured to the channel bottom, uniformly spaced and with their axes oriented parallel to the flow. The nondimensional diameter of the rods was $k^+=9.5$, and their streamwise length was $\Delta x^+=3600$. Two spanwise spacings were examined; initially

set at $\Delta z^+=60$, the separation between rods was increased to $\Delta z^+=120$ by removal of half the rods.

The effect of the rods was to reinforce the formation of low speed streaks close to the wall. The conventional processes by which streaks are maintained in a turbulent boundary layer seemed to be enhanced by the presence of the stable and stationary series of low speed regions induced by the boundary layers on the rods, which acted as nuclei for their formation.

A related effect has been observed by Utami, et. al [47], in a shallow (4-5 cm) open channel flow. They noted the presence of an organized pattern of low speed regions which appeared in conjunction with secondary flows consisting of longitudinal vortex motions ($\pm w_x$), and found also that a stabilization of the pattern occurred when longitudinal roughness elements (3 x 3 mm cross-section) were placed on the channel floor. The transverse spacing of the roughness elements was equal to the water depth, and the transverse scale of the secondary flows produced was comparable to the rod spacing (Figure 3.19).

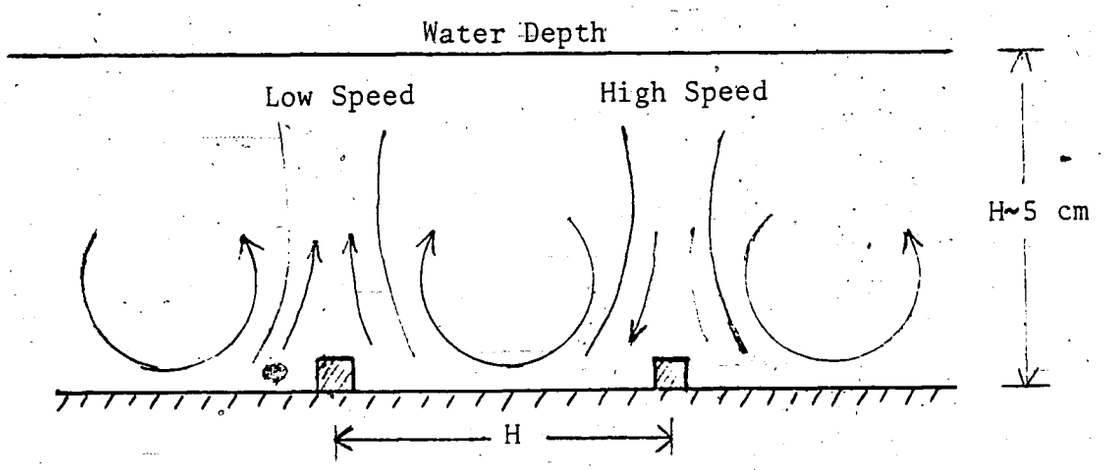

Figure 3.19 Spanwise Variations in Velocity and Axial Vorticity Occurring in a Thin Shear Flow. Longitudinal Surface Elements Accentuate the Effect. $Re_H \sim 3000$

Although the general scale of this structure is therefore much larger than the flow patterns involved with low speed streaks in a turbulent boundary layer (see Figure 1.2), geometrically the phenomena appear quite similar.

III.D.1. OBSERVED BEHAVIOR FOR $\Delta z^+_{rod}=60$

Observations made with a horizontal bubble wire placed at $y^+=10$, directly above the rods, revealed a distinct pattern of low speed regions coincident with the positioning of the rods. The lower than average spacing between low speed regions ($\lambda^+=60$) enforced by the rods persisted to $y^+\simeq 15$ and for a distance downstream of the rods $\Delta x^+\simeq 120$. It can be seen in Figure 3.20a that the spacing of the streaky structure at $y^+=20$ above the rods has begun to revert to a larger, more typical value, as has the structure shown in Figure 3.20b, at $y^+=10$ and $\Delta x^+=120$ downstream of the rods. Above the rods at $y^+=10$, 15, and 20 the mean spacing was $\lambda^+=60$, 81, and 94, respectively, while at distances downstream of the rods $\Delta x^+=120$ and 360, the mean spacing was $\lambda^+=75$ and 95, both measured at $y^+=10$. Figure 3.21 is a distribution of the

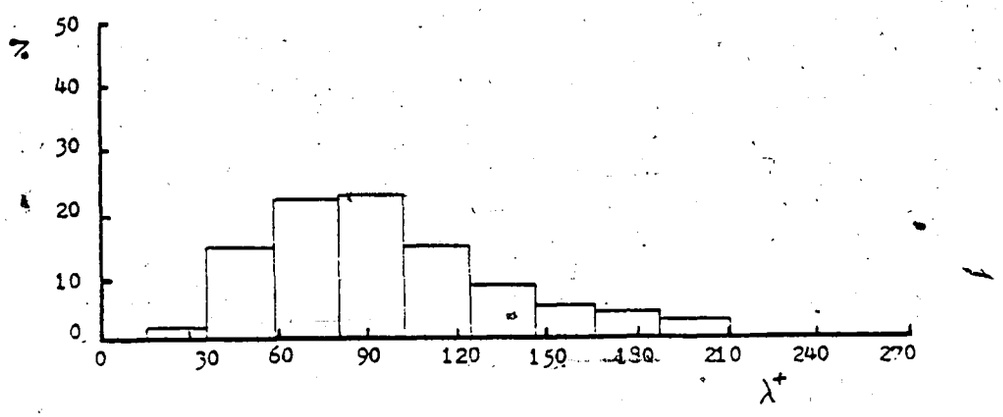

Figure 3.21 Streak Spacing Distribution for Rods Spaced $\Delta z^+=60$, Taken $\Delta x^+=360$ Downstream of Rods, at $y^+=10$.

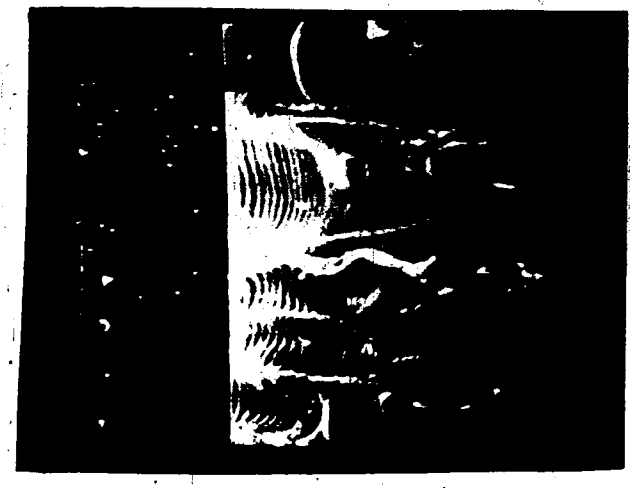

Fig. 3.20b $\lambda_{rod}=60\frac{\nu}{u_\tau}$ $y^+=10$.
$x=120\frac{\nu}{u_\tau}$ downstream

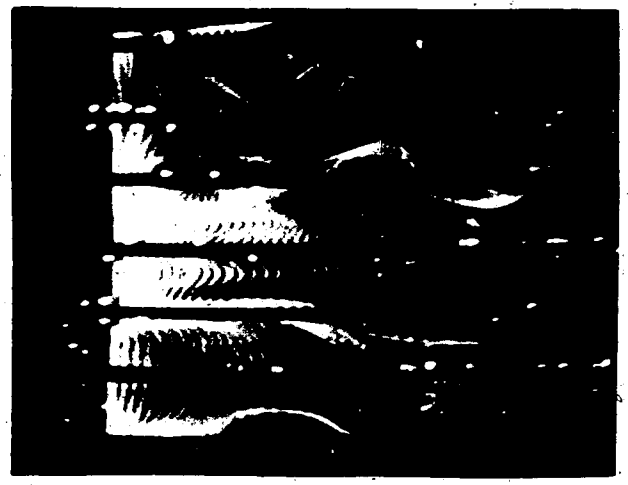

Fig. 3.20a $\lambda_{rod}=60\frac{\nu}{u_\tau}$ $y^+=20$
over the rods

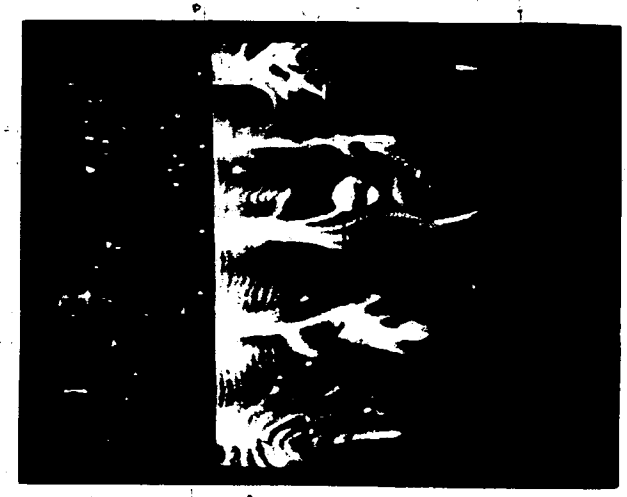

Fig. 3.22 $\lambda_{rod}=120\frac{\nu}{u_\tau}$ $y^+=10$
$x=120\frac{\nu}{u_\tau}$ downstream

Fig. 3.23 $\lambda_{rod}=120\frac{\nu}{u_\tau}$ $y^+=12$
ejection of vortex
loop over rods

spacing between streaks for $y^+=10$ at a distance downstream of the rods $\Delta x^+=360$. This histogram was constructed using the same procedure as for those presented in Section III.B., and is quantitatively very similar to the analogous histogram in Figure 3.3c compiled for an unaltered boundary layer. Evident in the distribution for the rods is a lower percentage of small streak spacings, and a slightly smaller standard deviation ($\frac{\sigma}{\lambda}=42\%$ vs. $\frac{\sigma}{\lambda}=51\%$), due presumably to a residual influence of the rods in maintaining a regular spacing pattern.

In short, the smaller streak spacing enforced by the rods for this particular experiment was limited to the immediate vicinity of the rods. If this form of surface modification is capable of causing a change of scale within the wake region, the streamwise length of the altered wall surface used (rods 3600 $\frac{\nu}{u_\tau}$ long) was probably too short to effect the change. Given that the influence of the rods in maintaining a small streak spacing was localized, an interdependence is thus implied between length scales (and events) in the wake and inner regions. An extension of this experiment that could prove fruitful would be to start the surface modifications at the point of turbulent transition, and to investigate the length scales that result.

A second study of surface modification was done using the same configuration as before, but with a spacing between rods of $\Delta z^+_{rod}=120$. Since this is closer to the streak spacing that naturally occurs, the disparity between wall and wake layer scales is avoided.

III.D.2. OBSERVED BEHAVIOR FOR $\Delta z^+_{rod}=120$

As with the previous experiment, the effect of the rods was to enforce their spacing upon that of the streaky structure. Since the

spacing of the rods was somewhat larger than the typical value established for the streak spacing (120 vs. 100 $\frac{\nu}{u_\tau}$), a "zone of influence" for the rods in enforcing their spacing could be observed. It appeared that the zone in which the enforced streak spacing persisted before reverting back to its unaltered value extended farther in both the streamwise and vertical directions than that observed for the smaller rod spacing. The mean streak spacing measured over the rods at $y^+=16$ was $\lambda^+=120$. At a distance $\Delta x^+=120$ downstream of the rods and at $y^+=10$ a nearly identical value of $\lambda^+=118$ was measured (Figure 3.22).

It was observed that despite the larger streak spacing enforced by the rods, events that occurred in the wall region of the modified boundary layer appeared to parallel those that take place in an unaltered boundary layer. An important structural feature was the presence of discrete arrays of typically 3 - 5 loop-like ejections (Figure 3.23). Measurement techniques similar to those employed to obtain the data for comparison. The results now presented are followed by their corresponding values measured for an unaltered boundary layer, which appear in parentheses.

The mean time interval between separate arrays of vortex loops (bursting time) as nondimensionalized on freestream velocity and boundary layer thickness was $\frac{U_\infty T_B}{\delta}=3.9$ (5.0). The average streamwise distance between the individual loops of an array was $\Delta x^+\simeq 180$ (200). The horizontal convection velocity of the loop heads was $U_c=13.2u_\tau$ (13.1), and perhaps more significantly, their vertical component was $v'=2.6u_\tau$ (2.2), both for $y^+\simeq 40$. Thus it would appear that for the form of surface modification used the processes of momentum transfer are enhanced, since

the bursting event both occurs more frequently and is associated with larger vertical (ejection) velocities.

The method of surface modification utilizes the boundary layers formed upon longitudinally arranged surface elements to reinforce the pattern of low speed regions close to the wall that represent the streaky structure. The transverse spacing of these roughness elements appears to have a pronounced influence upon the net effect observed in the rest of the boundary layer. When the transverse spacing of the roughness elements is comparable to that which naturally occurs in the wall region, the results of the present study and also Liu, Kline, and Johnston show that bursting activity is stimulated. The results of the latter investigation also show that the transverse spacing of the roughness elements need only be increased to twice the normal streak spacing to achieve a slight decrease in bursting activity. Just as remarkable is the observation made by Bushnell using a similar method incorporating a transverse spacing of $\Delta z^+=15$; an 8% reduction in wall shear was measured. That such a wide range of behavior may be observed to occur for such a narrow range of transverse spacings is a surprising result that invites speculation as to the cause. It is possible that the smaller transverse scales enforced upon the streaky structure by the configuration of Bushnell gave rise to bursting events of a similar scale and magnitude with a correspondingly small rate of momentum transfer. Perhaps the roughness elements themselves inhibited the formation of "normal," large scale streaks by interfering with the mechanism proposed in Section III.C. for the initiation of low speed regions at the wall (Lighthill's process). This would come about if the closely spaced surface elements were able to suppress the lateral flows

at the wall which are a key link in this process (see Figure 1.3).

These are questions which can only be resolved through further experimentation. An investigation is presently underway at Lehigh University that will examine a wide variety of surface modifications with a greater streamwise length than those used for the present study. This is an area that holds promise for an improved physical understanding of turbulent processes, and a potential for numerous practical applications as well.

CHAPTER IV

MODEL AND CONCLUSIONS

The following section is a summary and a synthesis of the major conclusions of this study. Taken in its entirety it constitutes a structural model of the mechanism giving rise to momentum transfer within the wall region of a turbulent boundary layer.

A dominant feature of turbulent boundary layers is the alternating pattern of high and low speed regions observed close to the wall known as the streaky structure. The narrow regions of low velocity, or low speed "streaks," exhibit a regularity and an apparent continuity that mark them as an important manifestation of the deterministic processes taking place in the near wall region.

Congruent with past description, "bursting" events involving vigorous outwards ejections of sublayer fluid were observed to invariably originate from low speed streaks, however; a new facet is that a given streak as viewed from a stationary frame of reference typically gives rise to at least 2 - 3 bursts. The existence of a streak is not terminated by a bursting event; as discussed shortly, the effect of a burst is to reinforce the low speed streak from which it originated.

The term "streak" accurately describes the appearance of this structure as visualized by bubble or dye traces, but unfortunately gives only a superficial conception of the three-dimensional aspects of the structure. The results of the present study show the low speed streaks to be zones of strong outflow which extend well beyond the viscous

sublayer out to $y^+ \simeq 25$ or more. In an undisrupted state, a low speed streak would appear as a narrow and continuous vertical band of upwelling fluid (Figure 3.5). However, a streak in a turbulent boundary layer is rarely undisrupted; convolution and deformation of the vertically oriented region occurs and appears to become more pronounced as distance from the wall increases. An apparent intermittency of the streaks at larger y^+ (visually evidenced as a shorter streamwise length scale) results from vertical undulations of the uppermost extent of a streak, and can also occur in response to disturbances that produce lateral dislocations of the constituent low speed fluid defining the streak (seen as a transverse waviness of the streak). It is hypothesized that it is the disruption and consequent irregularity of the streaks, most pronounced above the sublayer, that gives rise to the bursting event.

Separate bursting events were observed to consist of discrete arrays of loop-like concentrations of vorticity shed in a quasi-periodic fashion from a low speed streak; analogous structures are observed to issue from the wake downstream of a hemispherical wall element placed in a laminar boundary layer (Figure 3.16). It is believed that the localized zones of low speed fluid induced away from the wall by the streak mechanism give rise to the same phenomenon as that observed downstream of the hemispherical obstruction; ie, individual vortical structures of a loop configuration. The heads of the loops ($-\omega_z$) possess a strong upwards component of velocity (an ejection), and the upstream-pointing legs of a loop represent paired concentrations of counter-rotating streamwise vorticity ($\pm\omega_x$). The vorticity contained in the legs of the loops is intensified as the loop heads lift away from the wall and accelerate downstream.

An additional facet of the bursting phenomenon is that individual bursting events were observed to be associated with the formation and ejection of typically 3 - 5 loop vortices. It was noted also that a given streak can give rise to multiple bursts. Thus, given that successive loops are roughly "lined up" in the streamwise directions, as is the case, the presence of significant amounts of streamwise vorticity on either side of a low speed streak is implied. This provides a means by which the streak could be both reinforced and perpetuated, in accordance with a current hypothesis that suggests that counter-rotating streamwise vorticity acts to "pump" low speed fluid out from the wall to form a streak. Substantiation for such an effect is presented by Schwartz [44], who in a related investigation observed low speed streaks through an end-on view obtained with a fiber optic lens.

Thus, a mutual relationship between low speed streaks and the bursting pehnomenon is established; separate vortex loops composing a burst are shed from a low speed streak, and the streamwise vorticity defining the legs of the loops acts so as to reinforce the region of low velocity fluid that is the streak.

The method of boundary layer manipulation described in Section III.D. attempts to capitalize upon the salient role the low speed streaks appear to have in the generation of wall layer ejections. Longitudinal surface elements vertically no larger than the viscous sublayer ($y^+ \simeq 10$) but of a considerable streamwise length were arranged on the channel floor. They appeared to act as nuclei for the continuous formation of low speed streaks, with the consequence that the transverse spacing of the elements was enforced upon that of the streaky structure.

What influence various enforced streak spacings may have on the increase or reduction of mean wall shear stress, or other boundary layer characteristics, is as yet undetermined; however, the present study noted apparent increases in momentum transfer for an enforced spacing of $\lambda^+=120$.

BIBLIOGRAPHY

1 Achia, B. U. and Thompson, D. W. (1976). "Structure of the Turbulent Boundary Layer in Drag-Reducing Flow," J. Fluid Mech., 81, part 3, 439.

2 Bakewell, H. P. and Lumley, J. L. (1967). "Viscous Sublayer and Adjacent Wall Region in Turbulent Pipe Flow," Physics of Fluids, 10, 9.

3 Bendat, J. S. and Piersol, A. G. (1966). Measurement and Analysis of Random Data, Wiley.

4 Blackwelder, R. F. (1979). "The Bursting Process in Turbulent Boundary Layers," in Coherent Structure of Turbulent Boundary Layers, ed. by C. R. Smith and D. E. Abbott, AFOSR/Lehigh.

5 Blackwelder, R. F. and Eckelmann, H. (1979). "Streamwise Vortices Associated With the Bursting Phenomenon," J. Fluid Mech., 94, 577.

6 Blackwelder, R. F. and Haritonidis, J. H. (1980). "Reynolds Number Dependence of the Bursting Frequency in Turbulent Boundary Layers," Bulletin of the American Physical Society, 25, 9, 1094.

7 Brown, G. L. and Thomas, A. S. W. (1977). "Large Structure in a Turbulent Boundary Layer," Physics of Fluids, 20, 10, part II, S43.

8 Bushnell, D. (1978). Panel Discussion appearing in Coherent Structure of Turbulent Boundary Layer, ed. by C. R. Smith and D. E. Abbott, AFOSR/Lehigh, p. 507.

9 Clutter, D. W., Smith, A. M. O., and Brazier, J. F. (1961). "Techniques of Flow Visualization Using Water as the Working Medium," Aerospace Engineering, vol. 20, January.

10 Corino, F. R. and Brodkey, R. S. (1969). "A Visual Investigation of the Wall Region in Turbulent Flow," J. Fluid Mech., 37, part 1, 1.

11 Corrsin, S. (1956). First Symposium on Naval Hydrodynamics, National Academy of Sciences - National Research Council, Publication 515, p. 393.

12 Doligalski, T. L. and Walker, J. D. A. (1978). "Shear Layer Breakdown Due to Vortex Motion," in Coherent Structure of Turbulent Boundary Layers, ed. by C. R. Smith and D. E. Abbott, AFOSR/Lehigh.

13 Falco, R. E. (1977). "Coherent Motions in the Outer Region of Turbulent Boundary Layers," Physics of Fluids, 20, 10, part II, S124.

14 Falco, R. E. (1979). "Structural Aspects of Turbulence in Boundary Layer Shear Flows," in Proceedings of the Sixth Biennial Symposium on Turbulence, Oct. 8, Rolla, Missouri.

15 Grass, A. J. (1971). "Structural Features of Turbulent Flow Over Smooth and Rough Boundaries," J. Fluid Mech., 50, part 2, 233.

16 Gupta, A. K., Laufer, J., and Kaplan, R. E. (1971). "Spatial Structure in the Viscous Sublayer," J. Fluid Mech., 50, part 3, 493.

17 Hama, F. R. and Nutant, J. (1963). "Detailed Flow Field Observations in the Transition Process in a Thick Boundary Layer," Proc. 1963 Heat Transfer and Fluid Mechanics Institute, Vo. 77, Stanford University Press.

18 Haritonidis, J. H. (1979). Private Communication.

19 Head, M. R., and Bandyopadhyay, P. (1978). "Combined Flow Visualization and Hot Wire Measurements," in Coherent Structure of Turbulent Boundary Layers, ed. by C. R. Smith and D. E. Abbott, AFOSR/Lehigh.

20 Hebbar, K. S. (1978). "Wall Proximity Corrections for Hot-Wire Readings in Turbulent Flows," in DISA Information, No. 25, Feb., 1980.

21 Kim, H. T., Kline, S. J., and Reynolds, W. C. (1971). "The Production of Turbulence Near a Smooth Wall in a Turbulent Boundary Layer," J. Fluid Mech., 50, part 1, p. 133.

22 Kline, S. J. (1978). "The Role of Visualization in the Study of the Structure of the Turbulent Boundary Layer," in Coherent Structure of Turbulent Boundary Layers, ed. by C. R. Smith and D. E. Abbott, AFOSR/Lehigh.

23 Kline, S. J. and McClintoch, F. A. (1953). "The Description of Uncertainty in Single Sample Experiments," Mechanical Engineering, January.

24 Kline, S. J., Reynolds, W. C., Schraub, F. A., and Runstadler, P. W. (1967). "The Structure of Turbulent Boundary Layers," J. Fluid Mech., 30, part 4, 741.

25 Kline, S. J. and Runstadler, P. W. (1959). J. Applied Mechs., June.

26 Kreplin, H. P. and Eckelmann, H. (1979). "Propagation of Perturbations in the Viscous Sublayer and Adjacent Wall Region." J. Fluid Mech., 95, part 2, 305.

27 Laufer, J. and Narayanan, M. A. B. (1971). "Mean Period of the Turbulent Production Mechanism in a Boundary Layer," Physics of Fluids, 14, 182.

28 Levi, E. (1978). "Eddy Production Inside Wall Layers," Journal of Hydraulic Research, 16, no. 2, 107.

29 Lighthill, M. J. (1963). "Laminar Boundary Layers," Chap. 2, Sec. 3, p. 98 (ed. by L. Rosenhead), Oxford University Press.

30 Liu, C. K., Kline, S. J., and Johnston, J. P. (1966). "An Experimental Study of Turbulent Boundary Layer on Rough Walls," Report MD-15.

31 Loehrke, R. I. and Nagib, H. M. (1975). "Control of Free Stream Turbulence by Means of Honeycombs: A Balance Between Suppression and Generation," ASME 76-FE-2.

32 Lu, S. S. and Willmarth, W. W. (1973a). "Measurements of the Structure of the Reynolds Stress in a Turbulent Boundary Layer," J. Fluid Mech., 60, 481.

33 Magarvey, R. H. and Bishop, R. L. (1961). Canadian Journal of Physics, 39, 1418.

34 Morel, T. (1976). "Design of Two-Dimensional Wind Tunnel Contractions," ASME Publication 76-WA/FE-4.

35 Nychas, S. G., Hershey, H. C., and Brodkey, R. S. (1973). "A Visual Study of Turbulent Shear Flow," J. Fluid Mech., 61, part 3, 513.

36 Offen, G. R. and Kline, S. J. (1975). "A Proposed Model of the Bursting Process in Turbulent Boundary Layers," J. Fluid Mech., 70, part 2, 209.

37 Oldaker, D. K. and Tiederman, W. G. (1977). "Spatial Structure of the Viscous Sublayer in Drag Reducing Flows," Physics of Fluids, 20, 10, part II, S133.

38 Praturi, A. K. and Brodkey, R. S. (1978). "A Stereoscopic Visual Study of Coherent Structures in Turbulent Shear Flow," J. Fluid Mech., 89, 251.

39 Rao, K. N., R. Narasimha, and M. A. Badri Narayanan (1971). J. Fluid Mech., 76, 89.

40 Runstadler, P. W., Kline, S. J., and Reynolds, W. C. (1963). "An Experimental Investigation of the Flow Structure of the Turbulent Boundary Layer," Report MD-8.

41 Schraub, F. A. and Kline, S. J. (1965). "A Study of the Structure of the Turbulent Boundary Layer With and Without Longitudinal Pressure Gradients," Report MD-12.

42 Schraub, F. A., Kline, S. J., Henry, J., Runstadler, P. W., and Littell, A. (1965). "Use of Hydrogen Bubbles for Quantitative Determination of Time-Dependent Velocity Fields in Low-Speed Water Flows," Journal of Basic Engineering, June, 429.

43 Schlichting, H. (1950). Boundary Layer Theory, McGraw-Hill, New York, 6th ed., 1968.

44 Schwartz, S. P. (1980). "Investigation of Vortical Motions in the Inner Region of a Turbulent Boundary Layer," Master's Thesis, Lehigh University.

45 Smith, C. R. (1978). "Visualization of Turbulent Boundary Layer Structure Using a Moving Hydrogen Bubble-Wire Probe," in Coherent Structure of Turbulent Boundary Layers, ed. by C. R. Smith and D. E. Abbott, AFOSR/Lehigh.

46 Townsend, A. A. (1956). The Structure of Turbulent Shear Flow, Cambridge University Press.

47 Utami, T., Ueno, T., Imamoto, H., Ohtoshi, K. (1980). "On the Mechanism of Secondary Flow in Prismatic Open Channel Flow," International Symposium of Flow Visualization (Bochum), p. 476.

48 Walpole, R. E. and Myers, R. H. (1972). Probability and Statistics for Engineers and Scientists, Macmillan, New York.

49 White, F. M. (1974). Viscous Fluid Flow, McGraw-Hill, New York.

50 Willmarth, W. W. (1975). "Structure of Turbulence in Boundary Layers," Advances in Applied Mechanics, ed. C. S. Yih, Academic Press, Vol. 15, p. 159.

51 Willmarth, W. W. and Lu, S. S. (1972). "Structure of the Reynolds Stress Near the Wall,: J. Fluid Mech., 55, part 1, 65.

52 Willmarth, W. W. and Wooldridge, C. E. (1962). "Measurements of the Fluctuating Pressure at the Wall Beneath a Thick Turbulent Boundary Layer," J. Fluid Mech., 14, 187

53 Winant, C. D. and Browand, F. K. (1974). "Vortex Pairing: The Mechanism of Turbulent Mixing Layer Growth at Moderate Reynolds Number," J. Fluid Mech., 63.

54 Zakkay, V., Barra, V., and Wang, C. R. (1978). "Coherent Structure of Turbulence at High Speeds," in Coherent Structure of Turbulent Boundary Layers, ed. by C. R. Smith and D. E. Abbott, AFOSR/Lehigh.

CHAPTER V

APPENDICES

APPENDIX A: ANEMOMETRY RESULTS AND OPERATING PROCEDURE

Hot-film anemometry studies were undertaken to determine the basic parameters of the flows produced in the channel. Mean velocity profiles were obtained for several Reynolds numbers and reduced to extract quantities such as the displacement and momentum thicknesses, and the friction velocity. Unavailable for this investigation was a highly accurate means of determining probe distance from the wall, so the data pairs were plotted with the law of the wall ($\frac{u}{u_\tau} = \frac{1}{.41} \ln \frac{yu_\tau}{\nu} + 5.0$) and the y-values uniformly adjusted to make the data fit the curve. Displacement and momentum thicknesses were then computed from the data by a numerical integration technique using a simple trapezoidal approximation. The friction velocity was calculated by several methods (see Appendix B). Representative values for δ_*, θ, and u_τ as obtained from the best data sets are presented in Table A.1. The accompanying mean velocity profiles are plotted both on a logarithmic scale (Figures A.1a and A.2a), and one normalized on the boundary layer thickness (Figure A.3).

Table A.1. Flow Conditions and Obtained Boundary Layer Parameters for Two Experimental Flows (dP/dx=0)

U_∞ (m/s)	Re_x	x (m)	ν (m^2/s X 10^6)	u (m/s)	δ_*(cm)	θ(cm)	H
.226	.92(10^6)	3.96	.975	.0093	1.40	1.0	1.41
.229	(10^6)	4.27	.975	.0096	1.22	0.84	1.45

Values calculated for the momentum and displacement thicknesses vary 16% and 8% respectively with those obtained from standard empirical correlations (White's [49] equations 6-112 c and d), being larger than the empirical values. The deviation from the empirical values is ascribed to the difficulty had in determining exact y-values for the points at which measurements were taken, relative to the wall. An additional contributing factor was the presence of a persistent drift in the voltage output of the anemometer to lower values. Measures taken to minimize the error due to these causes are discussed shortly.

Two-dimensionality of the mean flow was checked by measuring spanwise profiles of the mean velocity at various distances from the wall, both within and outside the boundary layer (Figure 2.2 in Experimental Apparatus section). Variations of less than 2% were detected for the mean velocity within the 10 cm of spanwise distance traversed, for all profiles taken.

Boundary layer profiles for the longitudinal component of the turbulent velocity were obtained for several cases. The results appear in Figure A.4. Quantitative agreement was found with the data of Klebanoff (1955) appearing in Schlicting [43], the only discrepancy being a peaking of the distribution a small distance farther away from the wall, at $y/\delta = .022$ for the present study vs. $y/\delta = .009$ as measured by Klebanoff.

The main sources of error encountered in the measurement of vertical profiles were (1) the difficulty had in establishing exact probe position relative to the wall, and (2) the presence of a downward drift in the voltage output of the anemometer. One means used to determine as

accurately as possible the location of the probe and its distance from the wall employed the video system. A highly magnified side view picture of the probe element was obtained on the video screen, and a scale factor established that correlated small movements of the micrometer-mounted probe with the resultant displacements on the video screen. Proximity to the wall could then be estimated. A similar but potentially more accurate method would involve the use of feeler gauges (thin strips of a known thickness) to determine probe location. Accurate comparison of the probe height and feeler gauge thickness could be accomplished by using the video system as before to obtain a magnified image.

An additional source of error was a downwards drifting of the anemometer voltage output, due presumably to a buildup on the hot-film element of impurities from the water. A reduced heat transfer rate and consequent loss of calibration was the result. Steps taken to minimize this effect included cleaning the channel thoroughly before performing anemometry measurements, and filling it with fresh water several days in advance to allow de-aeration to occur. No chemicals (sodium sulfate, chlorine, etc.) were added to the water. Even with these precautions some drift still occurred); the remedy was to direct a small jet of water onto the probe element to literally "blow" collected air bubbles and deposits off. This was done using a 3 mm I.D., 1 m long neoprene tube taped to the stem of the probe mount, with its end positioned 3 cm above the element so as to direct a jet of water downwards. A syringe on the other end of the tube created the flow. The hot film element was cleaned in this fashion between each measurement at a given vertical location.

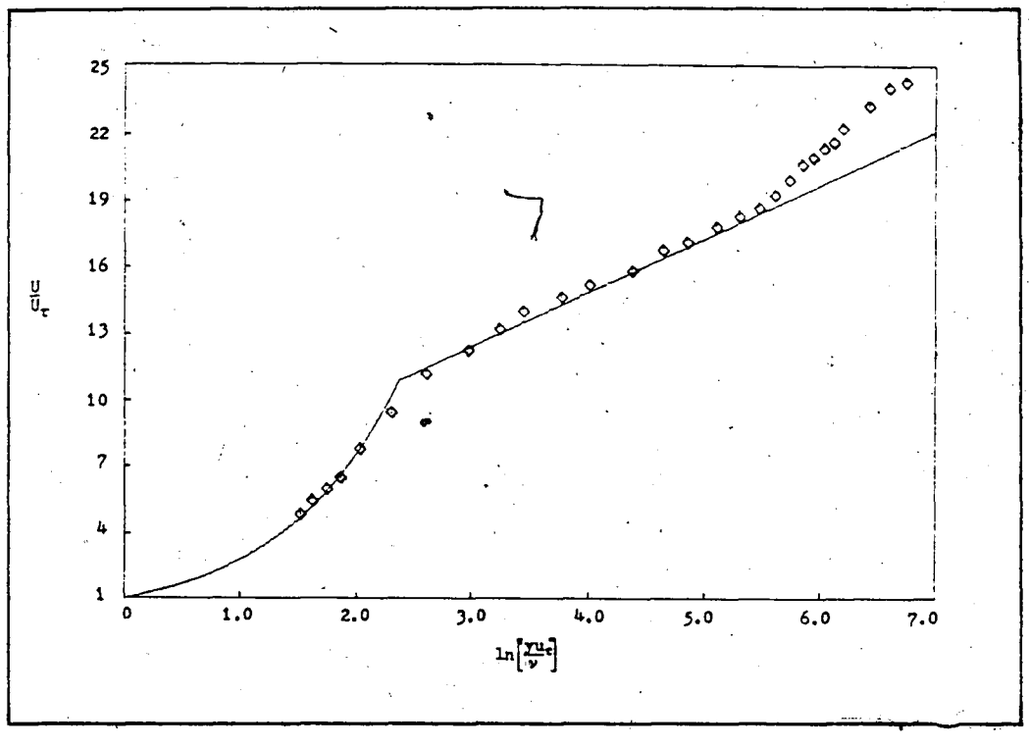

(a)

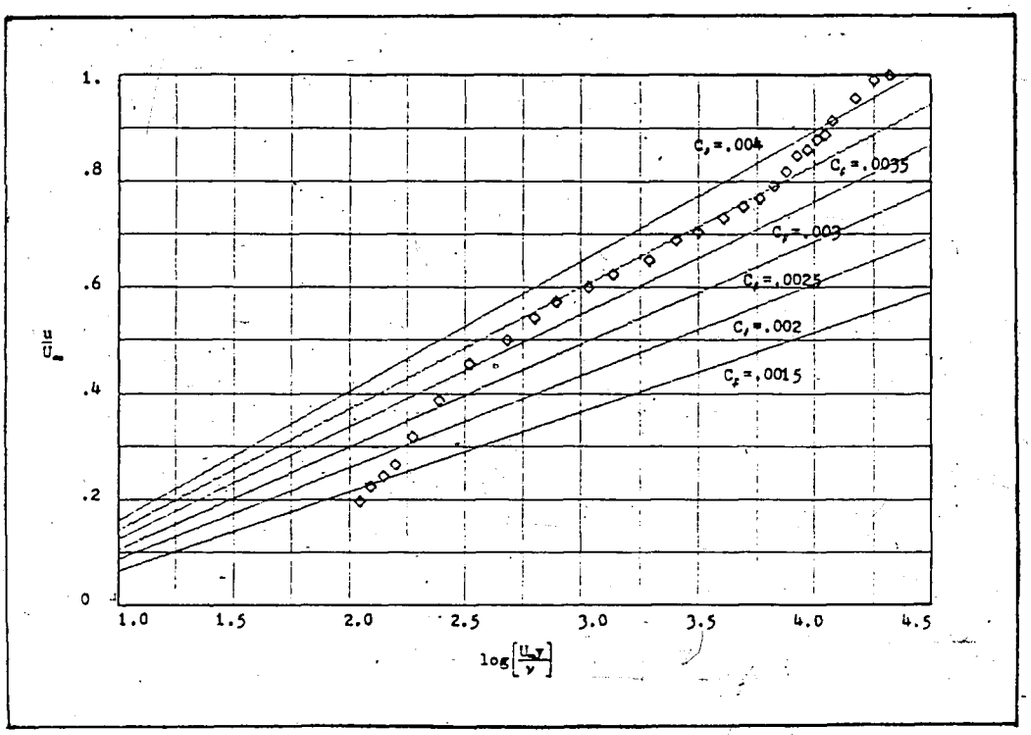

(b)

Figure A.1. $Re_x = .91(10^6)$ (a) Mean Profile Plotted with Law of the Wall
(b) Cross-plot of Mean Profile Data

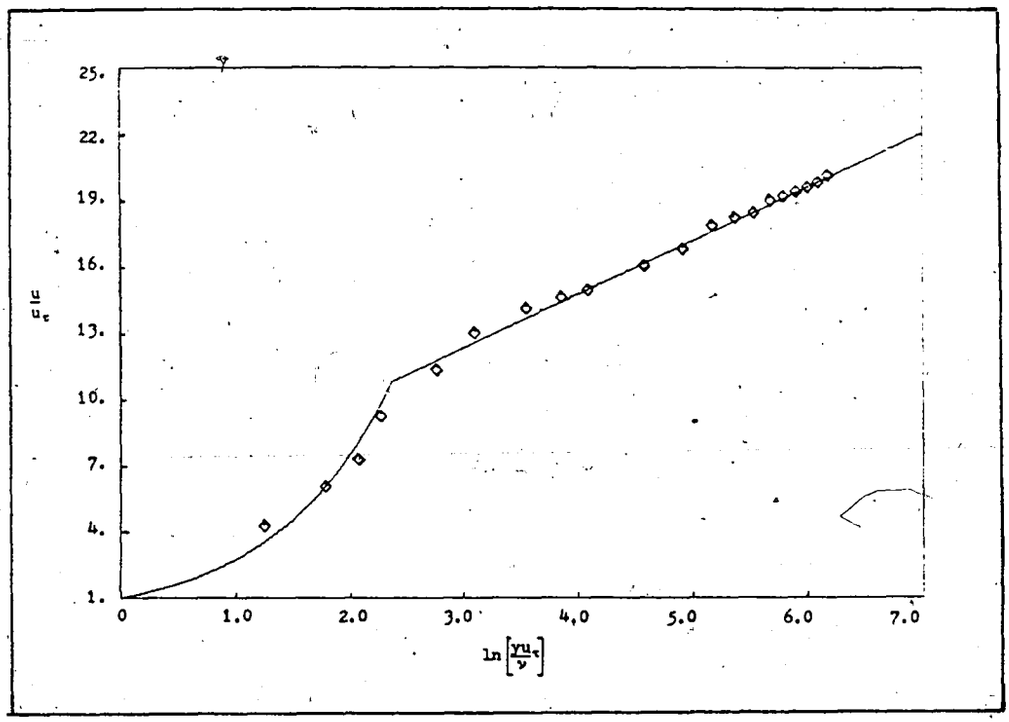

(a)

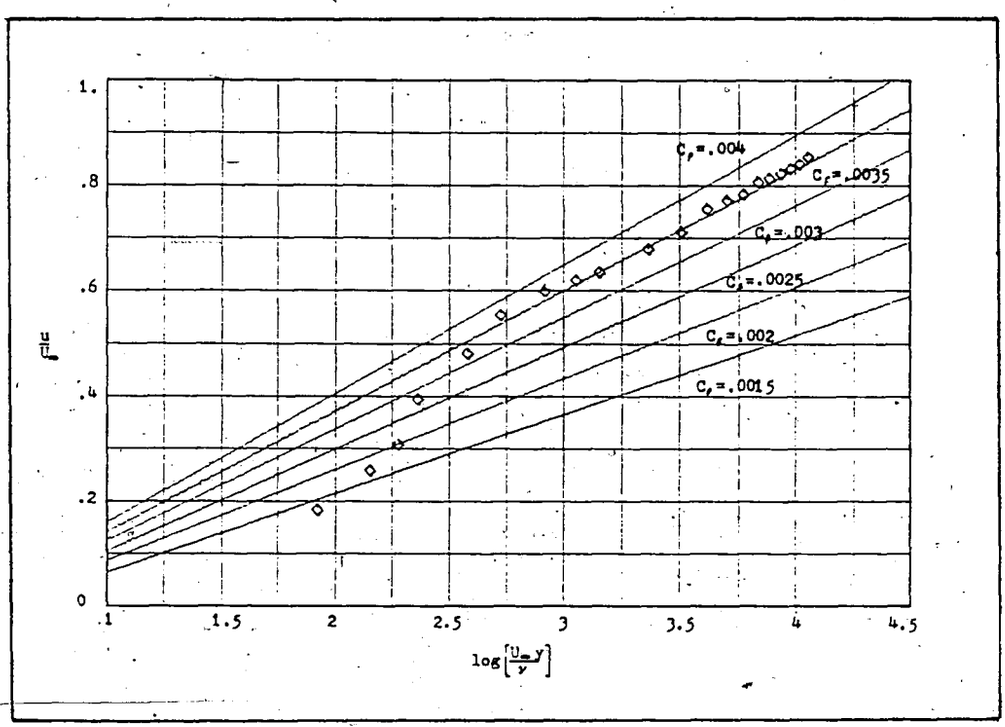

(b)

Figure A.2. $Re_x = (10^6)$ (a) Mean Profile Plotted with Law of the Wall
(b) Cross-plot of Mean Profile Data

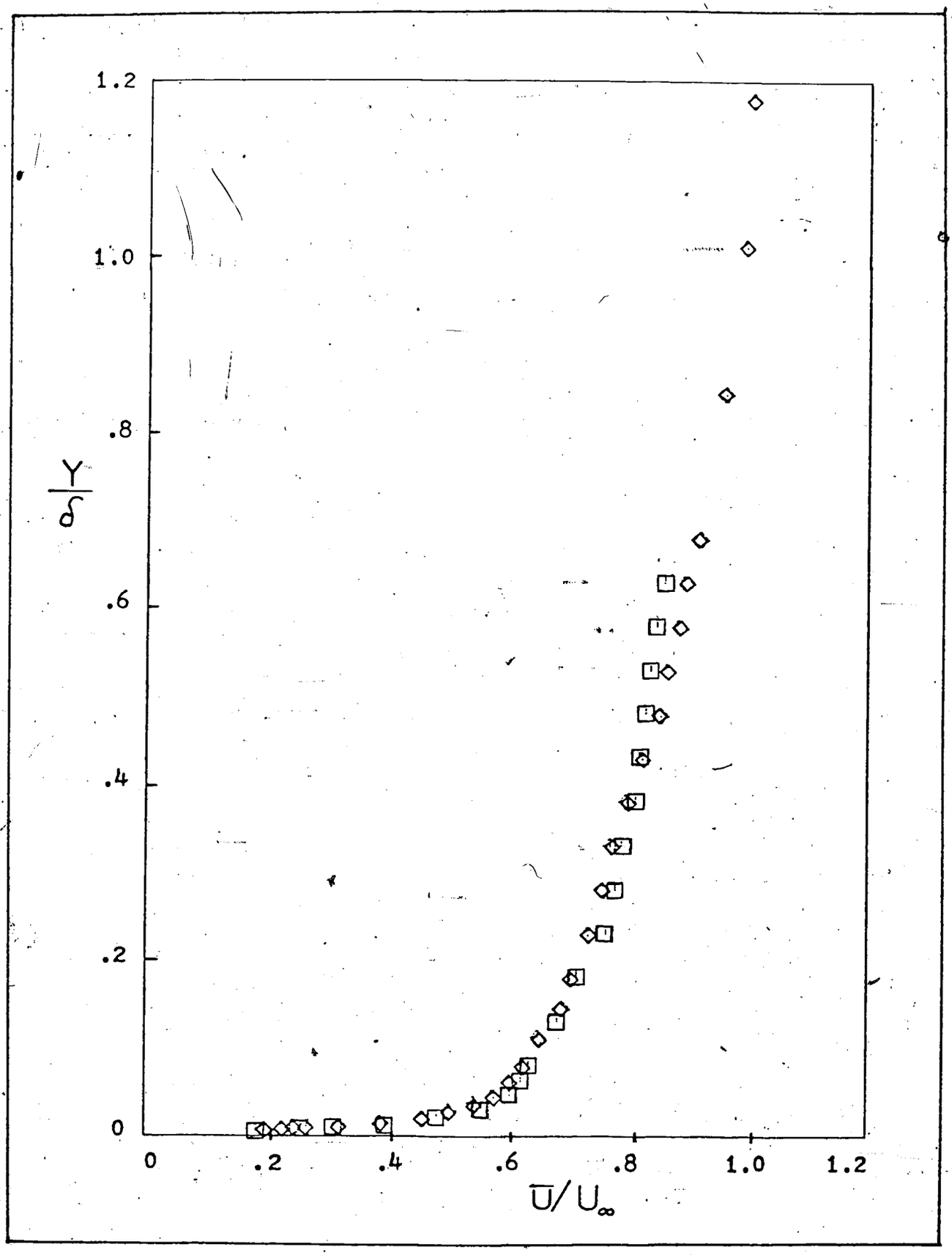

Figure A.3. Experimental Profiles of the Mean Velocity

◇ U_∞=.226 m/s, Re_x=9.2(10^5)

□ U_∞=.229 m/s, Re_x=(10^6)

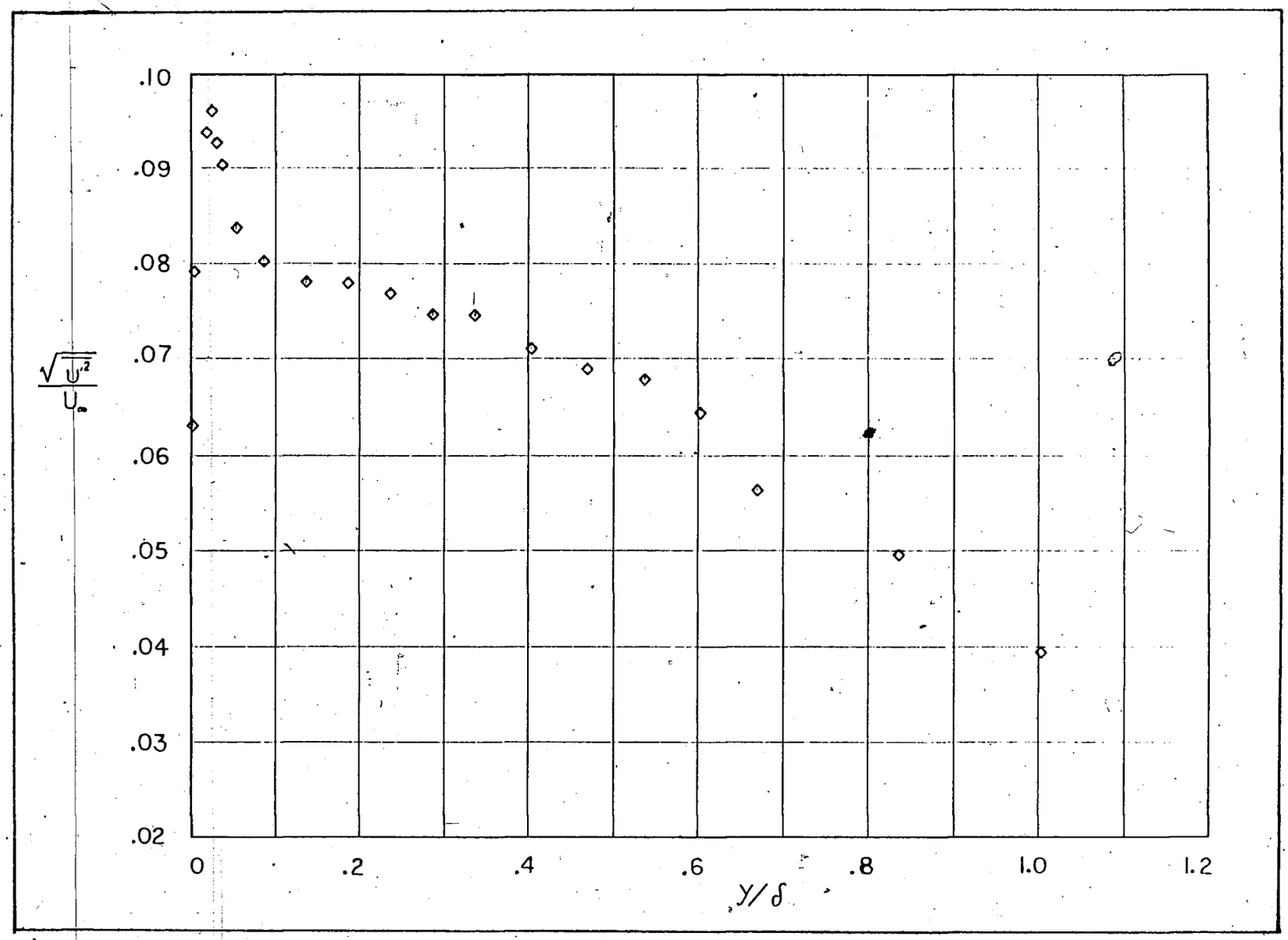

Figure A.4. Distribution of Longitudinal Component of Velocity Fluctuation, $Re_x = 9.3(10^5)$.

A STEP-BY-STEP PROCEDURE FOR OPERATION OF DISA 55 D01 ANEMOMETER UNIT WITH DISA TYPE 55 M25 LINEARIZER

- use clean water, free of chemicals, that has set for several days
- check honeycomb flow straightener for air blockage, check boundary layer trip placement.
- mount the probe micrometer traversing mechanism on the plan view camera mount plate
- slide large probe tube down through traverser, thread probe cable up through it
- tighten end of large probe tube down on probe support tube
- attach probe cable to lead from anemometer unit. (bridge top on anemometer unit attaches to linearizer input, linerizer output goes to voltmeter)
- attach grounding wire (the helical winding on probe support tube) firmly to prove cable/anemometer lead junction - do not tape down syringe tube yet, it would get in the way
- install the shorting probe
- determine cable resistance R_c as per instructions on p. 33 of anemometer instructions and service manual
- mount hot film element, tape syringe tube to probe support so as to direct a jet onto hot-film element
- determine sensor resistance R_c (ZERO OHMS is dismantled; measure $R_o + R_c$ and subtract)
- use 1:20 bridge ratio, overheat a=0.1, and determine (p. 37) operating resistance $R_v = R_c + (1+a)R_o$, set decades to it
- for calibration of linearizer, measure the channel velocity carefully at three different rpm's (say 1000, 2000, 2500), using stopwatch and the displacement/time float
- energize the probe (p. 37), using slow cut-in

- use HF FILTER 2 (may balance the bridge if necessary, p.33)
- ready to linearize: refer to Linearizer Instruction Manual, note p. 3 on control functions
- obtain rough estimate of exponent m using c=.925 as on p. 6, get EXPONENT FACTOR from fig. 3, set it
- from p. 7, set INPUT RANGE, INPUT BALANCE, COMMON OFFSET (set with zero flow)
- follow linearizing procedure as given in manual, for applicable range of measurement (set GAIN HIGH so that .9 ft/s ⇒ 9 Volts, etc)
- run through the pre-measured rpm settings, checking linearity and adjusting controls to get it
- for maximum accuracy, use syringe between each measurement, and when taking a profile go as fast as possible to minimize drift
- measure $V_{freestream}$ before and after profile to check draft, measure V_{rms} in freestream for turbulent intensity
- a high-magnification side view on the video system can help in getting good sublayer measurements without breaking (!) the probe

APPENDIX B: CALCULATIONS OF THE MEAN WALL SHEAR STRESS

Various methods for calculating either c_f or u_τ are given - note the relationship:

$$c_f = \frac{\tau_w}{\frac{1}{2}\rho U_\infty^2} = 2\left(\frac{u_\tau}{U_\infty}\right)^2 \quad \text{where } u_\tau = \sqrt{\frac{\tau_w}{\rho}}$$

(1) Most conveniently, use an empirical correlation (White's [49] equation 6-134 is a good one)

$$c_f = \frac{.455}{\ln^2(.06Re_x)} \qquad u = \frac{.477U_\infty}{\ln(.06Re_x)}$$

---

note: a velocity profile consists of voltage readings at given vertical locations; the relative displacement between readings is known, but their exact position relative to wall is uncertain. May correct the y-values by plotting (QIKPLT) data with curve for law of the wall, assuming that when data fits the curve, y-values and u_τ are correct. Because of logarithmic scaling of the abscissa, outer data points are unaffected by small changes in y; fit them first by adjusting u_τ. (It will be found that the Clauser u_τ value is that which causes the outer data to fit: mathematically this is to be expected.) Lastly, adjust the y-values uniformly so as to cause the data points for $5 \leq y^+ \leq 10$ to fit $u^+ = y^+$. Due to interference between the probe and the wall, the indicated velocity for $y^+ < 5$ is larger than that which actually exists - see Method (4).

---

(2) Clauser Cross-Plot Method: a manipulation of the law of the wall so as to permit the plotting of u/U_∞ versus log of Reynolds number based on y (Re_y), with c_f as an independent parameter.

Generate several such curves for constant c_f and plot the corrected data pairs with them. The derivation proceeds thus:

again: $c_f = \frac{\tau_w}{\frac{1}{2}\rho U_\infty^2} = 2\left(\frac{u_\tau}{U_\infty}\right)^2$ $\qquad u = U_\infty \sqrt{c_f/2} = U_\infty \cdot C_1$

law of the wall:

$$u^+ = \frac{u}{u_\tau} = \frac{1}{K} \ln \frac{y u_\tau}{\nu} + B \qquad (\log_{10} \text{ could be used also})$$

substituting for u_τ:

$$\frac{u}{C_1 U_\infty} = \frac{1}{K} \ln \frac{y C_1 U_\infty}{\nu} + B$$

$$\frac{u}{U_\infty} = \frac{C_1}{K} \ln \frac{y C_1 U_\infty}{\nu} + C_1 B$$

$$\frac{u}{U_\infty} = \frac{C_1}{K} \left[\ln(Re_y) + \ln C_1\right] + C_1 B$$

this is the form:

$$\frac{u}{U_\infty} = A \cdot \ln Re_y + D \qquad [1]$$

where

$$A = \frac{1}{K}\sqrt{c_f/2}$$

$$D = \frac{1}{K}\sqrt{c_f/2} \cdot \ln \sqrt{c_f/2} + B\sqrt{c_f/2}$$

So plot eq. [1] for $1.0 \leq \ln(Re_y) \leq 5.0$ and $.0015 \leq c_f \leq .004$ incrementing c_f by .0005 for each line. Pick line of constant c_f that the data falls on. (Remember that outer data points are impervious to small errors in y-values, and that if they were the first points taken in the profile they are also less affected by drift: give them more weight in the choosing of c_f)

(3) Log-Law Method: utilizes the slope of the data within the logarithmic region to yield an explicit expression for the friction velocity, using the law of the wall: $\frac{u}{u_\tau} = \frac{1}{K} \ln \frac{y u_\tau}{\nu} + B$

and taking the difference between two "typical" data points in the log layer,

$$\frac{1}{u_\tau}(u_2-u_1) = \frac{1}{K}\left[\ln \frac{y_2 u_\tau}{\nu} - \ln \frac{y_1 u_\tau}{\nu}\right] = \frac{1}{K} \ln \left[\frac{y_2}{y_1}\right]$$

solve for u_τ

$$u_\tau = \frac{K(u_2-u_1)}{\ln \left[\frac{y_2}{y_1}\right]}$$

substitute in representative values for points 1 and 2 obtained through a least squares curve-fit of the data (u vs ln y). Data with the y-values corrected as just discussed should be used.

(4) Wall Slope Method: incorporates the linear behavior of the velocity within the sublayer.

note: for points measured at $y^+ < 5$, the close proximity of the wall gives a high reading for the velocity. Therefore, unless the measurements have been corrected using a method such as that given in reference [18], use only data points in the region $5 \leq y^+ \leq 10$. It should be apparent that the data cannot be corrected for wall proximity until the y-values have been adjusted as discussed earlier.

by definition:

$$u_\tau^2 = \frac{\tau_w}{\rho} = \frac{\mu}{\rho}\frac{\partial u}{\partial y} = \nu \frac{\Delta u}{\Delta y}$$

Obtain a value for $\frac{\Delta u}{\Delta y}$ by performing a least squares curve fit upon the data (u vs y).

APPENDIX C: CONSTRUCTION OF A MOVEABLE HYDROGEN BUBBLE-WIRE PROBE

Design Criteria: unobstructed views (side, plan, end-on)
minimal vibration
complete insulation (no spurious bubbles)
straightforward fabrication and maintenance

The present configuration permits clear plan and end-on views of both a vertical (y) and horizontal (z) wire. The side view of a vertical wire is also unobstructed, but for a side view of horizontal wire a slightly oblique positioning of the camera from a small distance downstream of the wire is necessary (see Figure 3.8).

Measures taken to control probe vibration caused by vortex shedding include the use of square stock for probe construction, and the helical winding of all submerged members to break up vortex streets shed from them. These precautions yield a probe that is fairly stable over a wide range of flow velocities, but there is room for improvement.

For insulation, heat-shrink tubing works very well. Red glpt insulating varnish at joints and at the soldered points of attachment of the bubble wire works well for a short time, but is subject to deterioration and a subsequent formation of "extra" bubbles - a better agent should be found.

The probe is constructed of brass because it solders well, is very malleable, and has a high conductivity. The square cross-section, hollow brass stock used is readily available at most hobby shops.

The diagrammed construction of two probe designs is presented, along with a third untried approach that offers potential improvement in vibrational characteristics.

HYDROGEN BUBBLE
SINGLE-WIRE PROBE

(side view)

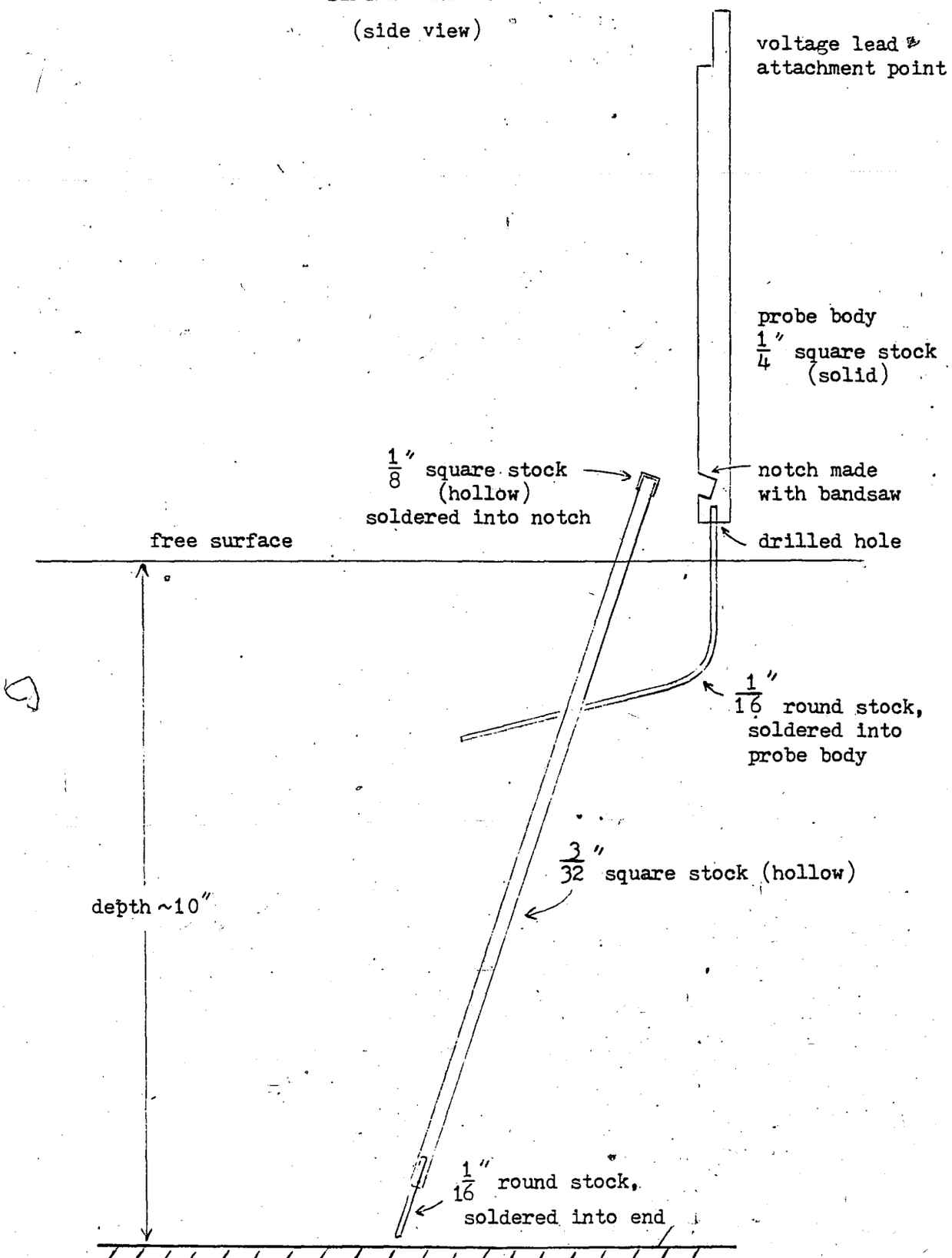

HYDROGEN BUBBLE
SINGLE-WIRE PROBE

(end view)

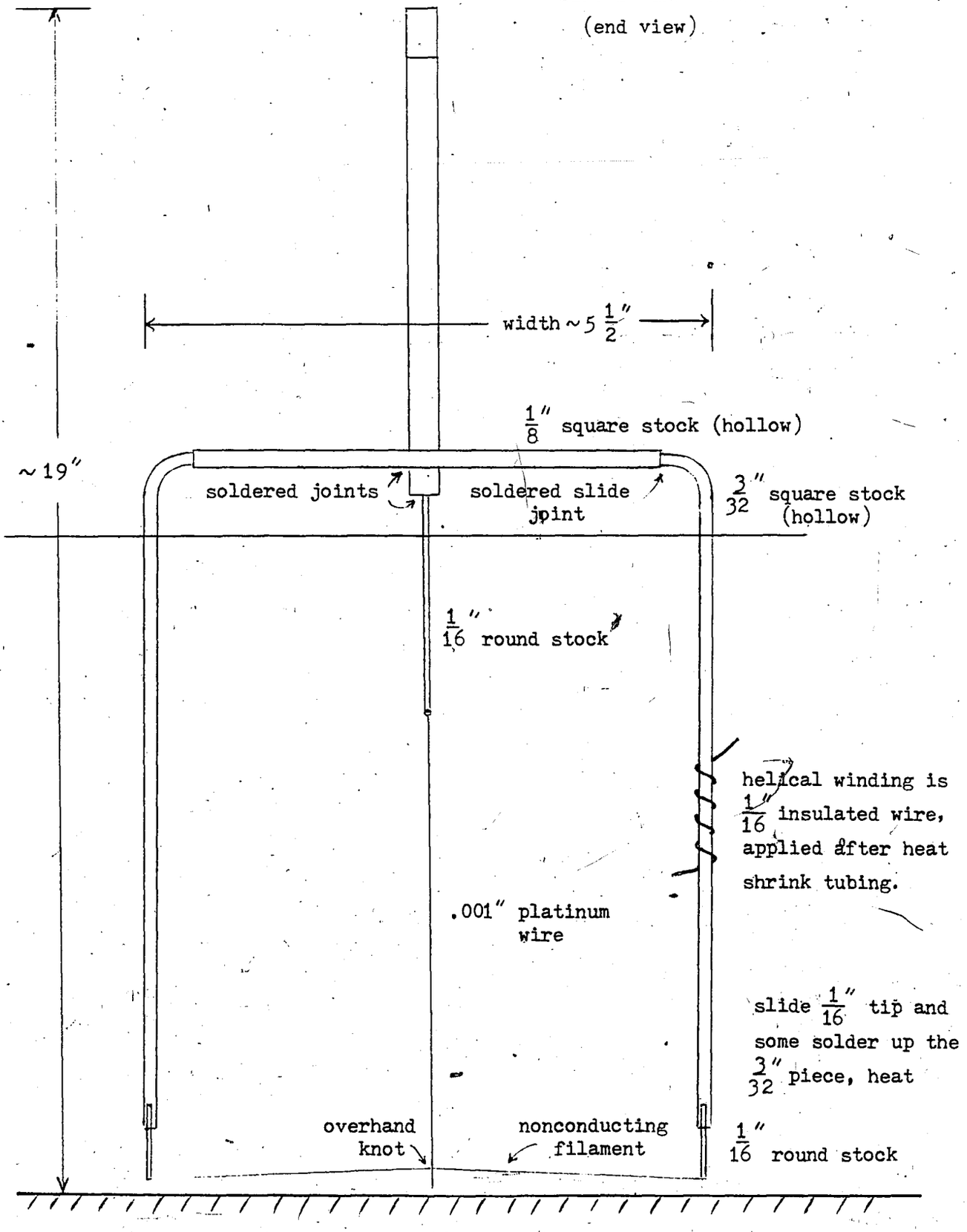

General Construction:

- cut, shape, and drill members
- solder together
- apply heat shrink tubing and insulate the gaps that occur at junctions with red glpt
- wrap helically, spray-paint a dull black for low reflectivity
- a horizontal bubble wire is soldered directly to tips of the legs
- a vertical wire is as pictured: a nonconductive filament (human hair works well) is tied and glued to legs, upper end of bubble wire is soldered, an overhand know in wire secures its lower end

Multiple-Wire Probe

A probe that can simultaneously accommodate both a horizontal and a vertical bubble wire may be constructed in an identical fashion. Instead of a single post set in the end of each leg, use a double prong.

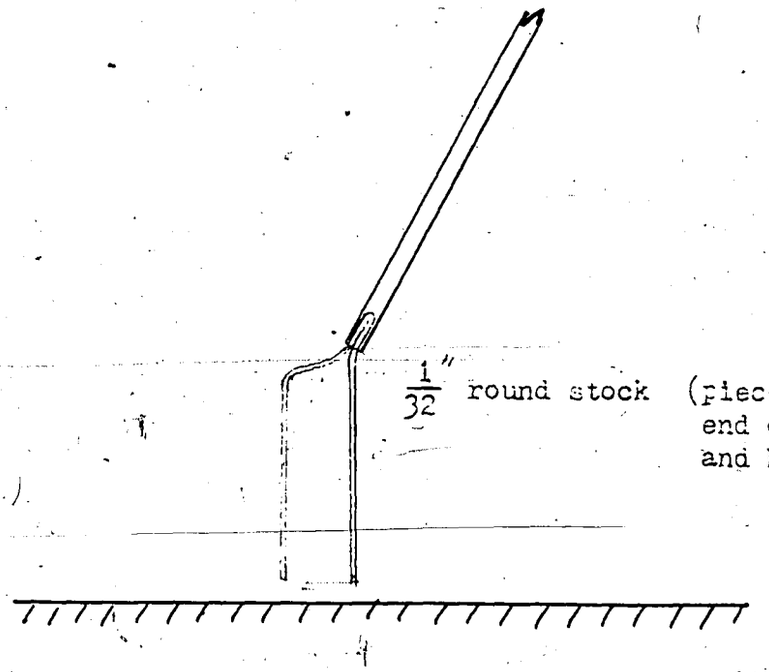

LOW-VIBRATION DESIGN

: similar construction, but with legs of a flat cross-section rather than square

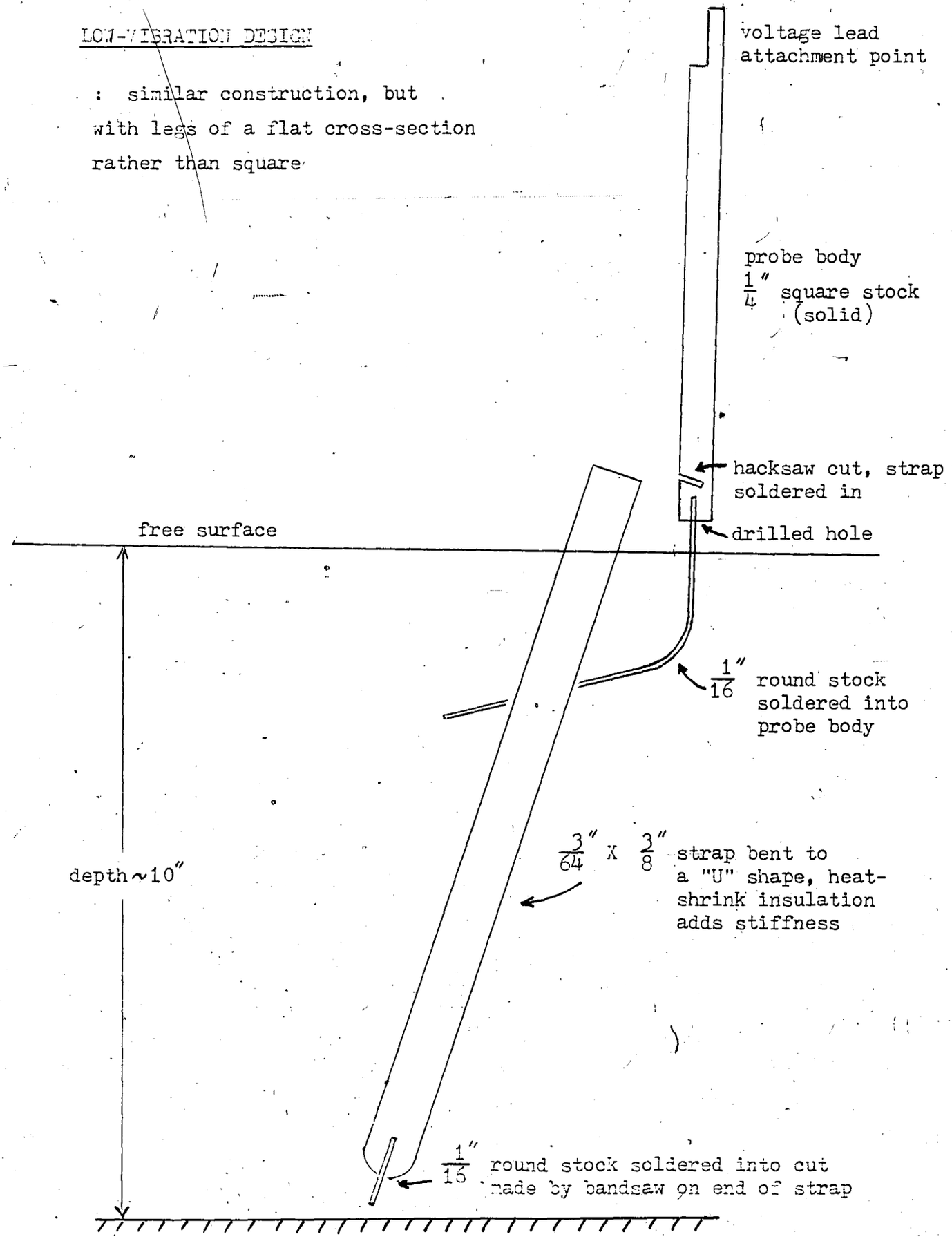

APPENDIX D: UNCERTAINTY ANALYSIS OF RESULTS

A. GENERAL

Uncertainties in numerical quantities obtained experimentally arise both from the finite size of a given sample of results, and from inaccuracies and/or shortcomings in the experimental technique used.

For the former, the difference between the obtained and "true" means of a sample may be calculated at a given level of significance using a standard statistical distribution (Walpole and Myers, 1972 [48]).

Error due to limitations in the experimental approach occurs for samples consisting of one value, such as in the determination of a scale factor from the video screen, or a viscosity. As estimate of the uncertainty involved may be obtained by applying reasonable constraints to the experimental parameters that may not be exact.

The total uncertainty W_R involved in an experimental result $R=R(V_1,V_2,\ldots V_N)$ may be calculated (Kline and McClintoch [23]) by using the expression:*

$$W_R=\left[\left(\frac{\partial R}{\partial V_1}\cdot W_1\right)^2+\left(\frac{\partial R}{\partial V_2}\cdot W_2\right)^2+\ldots\left(\frac{\partial R}{\partial V_N}\cdot W_N\right)^2\right]^{\frac{1}{2}}$$

where $W_1,W_2,\ldots W_N$ are the uncertainty intervals in $V_1,V_2,\ldots V_N$, calculated or estimated at a certain level of significance as just described.

B. MEAN STREAK SPACING

This analysis is carried out for a typical sample (scene 022, tape 6, taken at $y^+=5$ and $Re_x=1.02(10^6)$, for which $\lambda^+=85$ was found from a sample of size N=190.

---

*$V_1,V_2,\ldots V_N$ must be independent and their statistical distributions must have only a single peak. If $V_1,V_2,\ldots V_N$ are normally distributed the expression given is exact.

(1) uncertainty in λ

A standard deviation from the mean $\sigma_\lambda = 3.53$ mm was calculated from a spatial distribution (histogram) of individual streak spacings, using the expression

$$\sigma_\lambda^2 = \frac{\sum (\lambda_i - \bar{\lambda})^2}{N-1}$$

For $\bar{\lambda} = 7.46$ mm, this leads to a statistical uncertainty

$$\frac{W_\lambda}{\lambda} = \frac{z_{\alpha/2}\,\sigma_\lambda}{\sqrt{N}\,\lambda} = \frac{1.96(3.53)}{\sqrt{190}\,(7.46)} = 6.7\% \quad \text{(95\% confidence)}$$

---

(2) uncertainty in u_τ

Although values for the friction velocity were obtained by several methods as outlined in Appendix B, experimentally obtained values were not available for all the Reynolds numbers at which the mean streak spacing was measured. The correlation used was eq. 6-134 from White [49], which yields values for c_f over a wide range of Re_x with a claimed accuracy of +2%. However, since $u_\tau = \sqrt{c_f/2}\, U_\infty$, obtaining an uncertainty for u_τ requires that uncertainty limits be established for U_∞ as well.

:uncertainty in freestream velocity U_∞

$$\frac{W_{U_\infty}}{U_\infty} = \pm 4\% \qquad \text{(t-distribution of displacement/time measurements with the velocity float, 95\% confidence)}$$

Then from [1]

$$\frac{W_{u_\tau}}{u_\tau} = \left[\left(\frac{W_{c_f}}{c_f}\right)^2 + \left(\frac{W_{U_\infty}}{U_\infty}\right)^2\right]^{\frac{1}{2}} = \pm 4.1\%$$

(3) other sources of uncertainty

uncertainty in kinematic viscosity

$$\frac{W_\nu}{\nu} = \pm 1.8\% \qquad \text{(corresponds to a 1°C error in temperature)}$$

:uncertainty in scale factor B

For the present example a scale factor $B = \frac{5.16\ cm}{2.54\ cm}$ was measured from the video screen. The rasters, or scan lines, of the screen are .71mm apart.

$\frac{W_B}{B} = \pm 2.8\%$ (corresponds to an error equal to twice the distance bewteen scan lines)

Combining the foregoing uncertainties yields a total uncertainty for the nondimensionalized mean streak spacing $\frac{W_{\lambda^+}}{\lambda^+} = \pm 9\%$ at 95% confidence.

It should be noted that this analysis does not account for any subjective bias on the part of the observer, and that even with a consistent set of counting rules λ^+ can vary as much as 10% for two counts at a given Re_θ.

C. LOOP CONVECTION VELOCITIES

:statistical uncertainty of time interval for loop passage across screen

$\frac{W_{\Delta t}}{\Delta t} = 6\%$ (t-distribution, 95% confidence)

:uncertainty in scaling factors

Although the horizontal and vertical scaling factors on the video screen should be identical, due to anomalous behavior of the video monitor this was not always the case. Therefore, a scaling factor was measured in both directions across the screen when necessary.

For this experiment $B_{vertical} = \frac{13.5\ cm}{2.54\ cm}$

$\frac{W_{B_v}}{B_v} = \pm 1\%$ (corresponds to an error equal to twice the distance between scan lines)

Because the scan lines are horizontal, determination of a horizontal scale factor B_h is somewhat less accurate; estimate places the error involved as twice that for B_v.

$\frac{W_{B_h}}{B_h} = \frac{2W_{B_v}}{B_v} = \pm 2\%$

combining the uncertainties:

For horizontal convection velocity U_c of a vortex loop

$$\frac{W_{U_c}}{U_c} = 6\% \qquad \text{(95\% confidence)}$$

For vertical convection velocity v' of a loop

$$\frac{W_{v'}}{v'} = 6\% \qquad \text{(95\% confidence)}$$

The error associated with the scaling factors is negligible compared to the statistical uncertainty of the sample. The obtained uncertainty discounts subjectivity on the part of the observer.

D. TIME BETWEEN BURSTS T_B

Bursts consisted of discrete arrays of closely spaced loop vortices. The time between bursts was measured as the time interval between the first loops of two successive arrays.

:stastical uncertainty of time interval

$$\frac{W_{\Delta t}}{\Delta t} = 14\% \qquad \text{(t-distribution, 95\% confidence)}$$

APPENDIX E. BIOGRAPHY

The author was born October 9, 1954 in Chicago, Illinois. He is the son of Dr. David G. and Mrs. Doris K. Metzler. He graduated cum laude from Bridgewater College in May 1977 with a B.S. in Physics. Honors and titles while an undergraduate include the CRC Freshman Chemistry Award, and membership in Lambda Society and Who's Who in American Colleges and Universities. He was accepted as a graduate student at Lehigh University in the Department of Mechanical Engineering, and while there performed research as a Research Assistant under the guidance of Dr. C. R. Smith. Professional background also includes experience as a lab assistant in both Physics and Fortran II, and as an instructor in Fortran IV. He graduated from Lehigh University with an M.S. in Mechanical Engineering January 9, 1981.